MOLECULAR LEVEL INVESTIGATIONS OF COILED-COIL PROTEINS

Daniel Johnson BSc, MSc.

Thesis submitted to the University of Nottingham for the degree of Doctor of Philosophy

September 2005

To see a World in a grain of sand,
And a Heaven in a wild flower,
Hold infinity in the palm of your hand,
And Eternity in an hour.

William Blake, Auguries of Innocence

List of Abbreviations

A	*Alanine*
AFM	*Atomic Force Microscopy*
C	*Cysteine*
CALTECH	*California Institute of Technology*
D	*Apartic acid;*
	Dissipation signal (for QCM-D measurements)
Da	*Daltons*
E	*Glutamic acid*
EPSRC	*Engineering and Physical Sciences Research Council*
F	*Phenylalanine*
f^*	*Modal bond rupture force*
FJC	*Freely Jointed Chain*
f_β	*Force scale*
G	*Glycine*
H	*Histidine*
I	*Isoleucine*
K	*Lysine*
k_BT	*Thermal energy*
L	*Leucine*
LBSA	*Laboratory of Biophysics and Surface Analysis*
L_c	*Contour Length*
M	*Methionine*
MFP	*Molecular Force Probe*
N	*Asparagine*
p	*Persistence length*
P	*Proline*

Q	*Glutamine*
QCM-D	*Quartz Crystal Microbalance with Dissipation Monitoring*
R	*Arginine*
RI	*Refractive index*
S	*Serine*
SPR	*Surface Plasmon Resonance*
T	*Threonine*
V	*Valine*
WLC	*Worm-Like Chain*
Y	*Tyrosine*
Δf	*Frequency Change*

Abstract

The coiled-coil is a very common protein structural motif, consisting of two or more alpha helices intertwined in a supercoil. In biological systems it is found in proteins which fulfil a number of roles, for example in structural proteins such as keratin, as well as a large number of transcription factors and other DNA binding proteins, where it functions as a dimerisation domain. This versatile motif has also been adapted for a number of applications including the production of responsive hydrogels; the construction of self-assembling fibres for tissue engineering applications; as a cross-linking agent in drug delivery applications, as well as in the creation of biosensor surfaces.

In this study two different types of protein containing coiled-coil domains are examined. It is the aim of this work to increase the understanding of how behaviour of this motif at the molecular level relates to those at the macroscopic. The first set of proteins of interest in this thesis form pH-responsive hydrogel systems utilising a variant of the coiled-coil motif, the leucine zipper, as their cross-linking domain. These consist of two or more leucine zippers separated by random coil spacer sections. When the leucine zipper sequences dimerise, they cross-link the proteins forming a gel matrix. As charges within the leucine zippers alter, as the pH of their environment is altered, their relative stability changes causing them to associate or dissociate. This is reflected in a change in the physical characteristics of gels from visco-elastic solids to viscous liquids which is reversible. The bulk properties of these materials is well characterised, but relatively little information is known at the molecular level. Starting at the single molecule level and scaling up to the mesoscale, the behaviour of hydrogel-forming proteins has been probed using a range of techniques, particularly with respect to the interactions of the

coiled-coil forming domains. Studies described in this thesis have concentrated on the change of physical characteristics of these proteins and their assemblies as pH was altered. We have thus been able to connect behaviour of these proteins at the molecular scale to bulk properties of solutions and materials formed from them.

In the final experimental chapter a coiled-coil structure of more complex architecture is examined. This is formed of a ternary complex of three proteins which assemble into a two-stranded leucine zipper domain, designed as a cross-linking motif for nano-particle assemble. Force was used to probe the kinetic stability and mechanical strength of this assembly.

With the increasing use of the coiled-coil motif as a cross-linking domain in the use of biomaterials it is increasingly important to be able to connect the behaviour of such materials to the behaviour of the coiled-coil motif at the molecular scale, to gain further insight into the mechanistics behind their behaviour.

Chapter 1 : Introduction

1.1 The Coiled-Coil Motif

The coiled-coil is a common protein structural motif, consisting of two or more α-helices, usually wound about each other in a left-handed supercoil (see Figure 1-1). It has been estimated to be found in about 2-3% of all naturally occurring protein residues (Burkhard *et al.* 2001) and was first observed in α-keratin in intermediate filaments (MacArthur 1943). It fulfils a number of functional roles in biological systems (Lupas 1996), most notably in structural proteins such as collagen, keratin and myosin, as well as in a large number of DNA-binding proteins, such as transcription factors where the coiled-coil motif acts as a dimerisation domain (Glover and Harrison 1995; Kammerer *et al.* 1998). In recent years this motif has been utilised in a number of applications, where it is used as a reversible dimerisation domain in the development of biosensors, cross-linking agents for drug delivery applications, environmentally responsive hydrogel systems, as well as the creation of fibrous materials for tissue engineering applications. In the work presented in this thesis investigations are carried out at the single molecule and mesoscale levels on a series of proteins utilising coiled-coil linkages for the formation of pH-responsive hydrogels. This was in order to improve the understanding of how properties of the molecules at this level relate to previous observations made of their macroscopic properties.

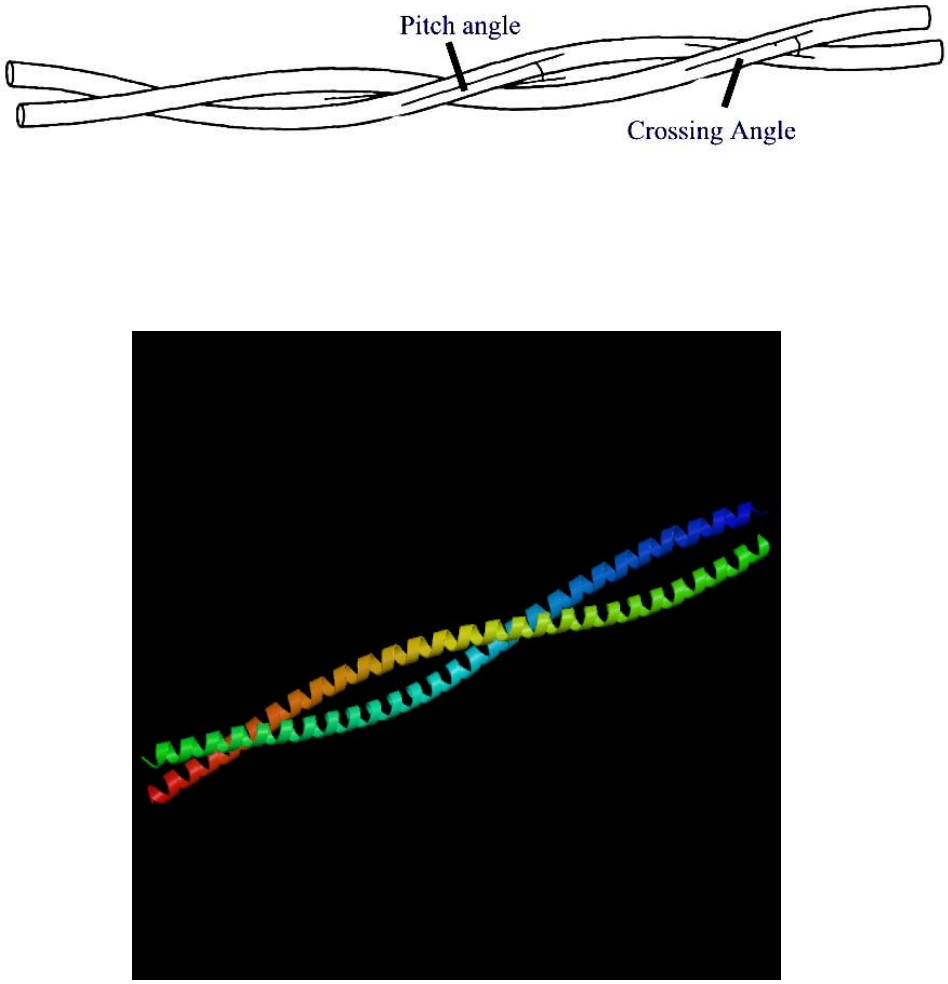

Figure 1-1: Top is an outline diagram of a simple two-stranded coiled-coil indicating both the pitch angle and the crossing angle. Below is a structure of an example of a two-stranded coiled-coil protein domain: the dimerisation domain of the protein cortexillin I obtained from the protein data bank, www.rcsb.org/pdb/cgi, number 1D7M (Burkhard *et al.* 2000).

1.1.1 Structure of Coiled-Coils

The classic feature of coiled-coil domains is a seven residue heptad repeat in their amino acid sequence, with the residues conventionally labelled with the letters *a* through to *g*. The additional twist that the constituent helices undergo to allow them to intertwine is called the supercoil. The axis along the centre of the coiled-coil motif, the supercoil axis, most typically has a left-handed rotation. Coiled-coils have a distinct packing of side chains into a hydrophobic core, often described as "knobs into holes" packing, where a residue from one helix packs into a gap left between residues on the opposing helix. This structural model was first proposed by Crick in the early 1950's from observations of α-keratin crystal structures (Crick 1953; Lupas 1996; DeGrado *et al.* 1999; Burkhard *et al.* 2001). The residues at the *a* and *d* positions are, for the most part hydrophobic amino acids, (commonly leucine). They make up the hydrophobic interface between the helices, forming a 4-3 repeat (i.e. it repeats every four then three residues, with hydrophobic residues in the first and fourth positions), whereas the other residues form the more solvent exposed parts of the assembly. It has been estimated that in naturally occurring coiled-coil domains approximately 80 % of residues in the *a* and *d* positions are hydrophobic (Yu 2002). However, this leaves some of the residues in these positions as polar. Lengthy naturally-occurring coiled-coil structures do not tend to have continuous hydrophobic cores throughout, but rather a number of separate sections with hydrophobic cores (Lu and Hodges 2004).

Core-flanking residues found at positions *e* and *g* are often populated by ionizable residues (Oakley and Hollenbeck 2001), such as lysine or glutamic acid, which may also form salt linkages (Marti *et al.* 2000; Yu 2002). Figure 1-2 displays a 'helical wheel' representation of a coiled-coil structure. In this type of representation, the coiled-coil is viewed as if sighting along the length of the supercoil axis. Each heptad occupies two complete turns of each α-helix, with the *a* and *d* residues arranged into the interface of the coiled-coil.

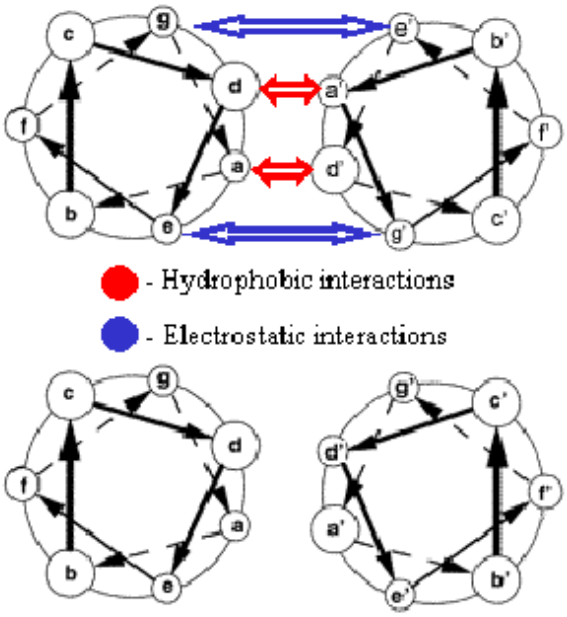

Figure 1-2: Helical wheel representations of two-stranded coiled-coils. Shown here are the parallel (top) and anti-parallel (bottom) orientations. This view is a cross section looking down the axes of the coiled-coils. The hydrophobic residues at positions *a* and *d* form the hydrophobic core.

It is also possible for coiled-coil domains to exist in a right-handed form, where the supercoil winds in the same direction as the constituent α-helices. Such proteins necessarily have to have a different geometry to the more usual left-handed form. Instead of a heptad repeat they consist of an eleven-residue undecad repeat (with residues conventionally labelled *a* to *k*). In coiled-coils such as these, amino acid side-chains are mainly hydrophobic at the *a* and *h* positions and to a much lesser extent at the *d* and *e* positions (Lupas 1996; Yu 2002).

Two-stranded coiled-coils can be found in either a parallel or an anti-parallel orientation, i.e. aligned with the peptide backbone in the same direction (parallel) or in opposite directions (anti-parallel). The differences can be seen in Figure 1-2 by comparing the top and bottom diagrams. Where coiled-coils are parallel, residues at position *a* will tend to pack against *a*' residues on the opposing strand, while *d* residues pack against *d*'. This leads to two distinct layers within the hydrophobic core with geometric requirements that are distinct from one another. In contrast in anti-parallel coiled-coils *a* residues pack against *d*'. This leads to the formation of a single hydrophobic layer in the core (Oakley and Hollenbeck 2001). In both types of coiled-coil the amino acid side chains do not point straight from the helix, but are angled in the direction of the amino terminus. In anti-parallel coiled-coils the optimum interaction between side-chains of opposing helices is obtained when they point in towards each other and the C_α chains are not in register (Lupas 1996).

The α-helices contained within the coiled-coil structure are generally tightly packed, leading to strong packing constraints within the coiled-coils, due to smaller internal cavities being more thermodynamically favourable (Efimov 1999; Yadav *et al.* 2005). Undistorted α-helices have approximately 3.63 residues per turn leading to a pitch of about 140 Å and a crossing angle of 22° for supercoiled helices. The left handed twist in the majority of coiled-coils reduces the number of residues per turn to 3.5 (Lupas 1996), leading to two turns for each heptad, with one residue per turn packing into the core.

A commonly-occurring variant of the coiled-coil dimer is called the leucine zipper. It is so called because it is estimated that approximately 80% of side-chains occurring at the *d* position are leucine residues (Harbury *et al.* 1993). It has been suggested that residues in the *d* position are more important for the stability of the dimer than residues at the *a* position (Skolnick *et al.* 1999).

It is primarily hydrophobic forces which drive the folding during formation of coiled-coil assemblies. Many two-stranded coiled-coils are thought to fold with a two-stage transition between the monomer and dimer species. The monomers may already be partly helical before associating via an unstable and rate limiting transition state. Many of the hydrophobic side-chains that form the core of the protein may already be buried by the transition stage, before formation of the supercoil (Skolnick *et al.* 1999; Bosshard *et al.* 2001; Ibbarra-Molero *et al.* 2001). However, the picture is most likely more complex than this. Studies of the temperature-driven unfolding of coiled-coil domains suggest that there are several transitions during dimer dissociation (Dragan and Privalov 2002). In addition there have been observations of the retention of helical structure of monomers after the dissociation of two-stranded leucine zippers at low pH (Moreau *et al.* 2004).

Many two-stranded coiled-coils, including those found in the proteins GCN4, kinesin and myosin, have been observed to contain a fourteen-residue trigger sequence necessary for coiled-coil formation. For example, removal of the carboxy-terminal end of GCN4 containing this sequence was found to prevent the formation of the coiled-coil. It has been demonstrated that these sequences are autonomous folding units that control chain assembly (Kammerer *et al.* 1998).

The hydrophobicity of the core residues (*a* and *d*) and those at the *e* and *g* positions can determine the number of helices that are present in a coiled-coil assembly. Polar residues buried in the core can lead to the formation of dimers, rather than trimers or tetramers (Akey *et al.* 2001; Oakley and Hollenbeck

2001). This has been demonstrated by substitution of residues at the *a* and *d* positions leading to the formation of dimers, trimers and tetramers, (Harbury *et al.* 1993). Residues in the core-flanking regions can also modulate whether coiled-coil species are hetero- or homomeric. Studies using mixtures of acidic leucine zippers containing pairs of glutamic acid residues, and basic leucine zippers containing pairs of arginine residues at the *g* and *e*' positions, indicated that the specificity of dimerisation appeared to be determined by the repulsion of homodimers and attraction of heterodimers (Krylov *et al.* 1998). It has also been shown that more generally, a single conservative substitution of an apolar residue for another apolar residue within the hydrophobic core of a coiled-coil (in this case a leucine to a valine) can modulate the assembly pathway of the protein (Bravo *et al.* 2001). In addition single, buried polar side-chains can also decide the orientation of a coiled-coil: i.e. whether a two-stranded coiled-coil is parallel or anti-parallel (Efimov 1999).

Mechanisms for polar residues fitting into the core have been suggested, including the filling of cavities with structured water molecules and changes in the parameters of the supercoil, particularly the supercoil radius. For example, in a designed three-helix protein, charged groups in the core were used both to stabilise the predicted structure and to destabilise the formation of alternative structures (Walsh *et al.* 1999).

The specificity of the packing of α-helices can also be governed by ionic interactions at the core-flanking *e* and *g* positions of adjacent helices (Cohen and Parry 1994). In parallel coiled-coils, the residues at the *e* position can be involved in coulombic interactions with *g*' residues. In anti-parallel coiled-coils *g* residues interact with *g*' and *e* interact with *e*' (McClain *et al.* 2001; Oakley and Hollenbeck 2001). The charged side-chains normally found in these positions can impose either attractive or repulsive electrostatic interactions between opposing helices, which can include salt linkages (Marti *et al.* 2000). These charged side-chains can be either fully buried, fully exposed or partly buried depending on their position, with differing degrees of hydrophobicity of the surrounding residues (Kohn *et al.* 1997). Studies of the

pKa of glutamic acid residues on a designed leucine zipper protein suggest that charged residues can contribute unfavourably to the stability of the coiled-coil, leading to the conclusion that the driving force for alignment of residues in a coiled-coil is hydrophobic and not electrostatic in nature (Marti *et al.* 2000). However if residues of opposing charge on opposite strands are oriented to allow them to form salt bridges this can increase the stability of the assembly. Such salt bridges are formed after dimerisation and play no part in the formation of the coiled-coil structures (Ibarra-Molero *et al.* 2004). In another study on a *de novo* designed anti-parallel coiled-coil, the alignment was dictated solely by electrostatic interactions between the core-flanking residues, as repulsive interactions disfavoured formation of parallel coiled-coils (Pagel *et al.* 2005).

Naturally occurring coiled-coils tend to be more stable at low pH values, because acidic residues become protonated and destabilising negative charges are therefore absent (Kohn *et al.* 1997). Conversely at low ionic strength, such as 10mM salt, coiled-coils tend to be much more stable at neutral pH's than at low pH to both thermally and urea-driven unfolding. Above about 100mM of salt coiled-coils become more stable at acid pH. Ion pairs, such as those formed between lysine and glutamic acid, contribute to stability under these conditions (Yu *et al.* 1996). Krylov et al (Krylov *et al.* 1998) observed the coupling energy between several residues at the *g* and *e*' positions on opposing helices in a coiled-coil dimer at varying salt concentrations. Homodimers containing residues of the same charge in these positions were destabilised, whereas heterodimers were stabilised by the presence of opposite pairs. The repulsion between charged glutamic acid residues on opposite strands decreased as the salt concentration was increased, whilst the attraction between oppositely-charged residues also decreased. In addition it was found that residues in the *e* position were more responsive to variations in ionic strength than residues at *g*. This was explained by the greater solvent exposure of position *g* compared with *e*.

1.1.2 Biological Functions of Coiled-Coils

The coiled-coil motif is found in a wide variety of functionally diverse proteins. They can form structural proteins, such as keratin (Kreplat *et al.* 2001), which is a major component of hair, nails and feathers; collagen, a major structural component of skin, bone and connective tissues; muscle proteins such as myosin as well as components of the cytoskeleton, such as intermediate filaments (Lupas 1996). Long coiled-coil strands are ideal for forming such filamentous structures. Coiled-coil motifs, particularly leucine zippers, are also prominent features of some transcription factors and related proteins such as the bZIP transcription factors *fos* and *jun* (Glover and Harrison 1995) and the yeast transcriptional activator GCN4 (Kammerer *et al.* 1998). Such proteins are only functional as dimers and it is the coiled-coil domain that allows dimerisation. In such DNA-binding coiled-coils, the DNA binding region is towards the amino terminal end from the zipper domain (Branden and Tooze 1991; Glover and Harrison 1995). In the case of the bZIP transcription factors different combinations of the subunits are held together by the dimerisation of the coiled-coil subunits (Hu 2000). The dimerisation and binding to the DNA are thought to be simultaneous events, which, to a large extent, are mediated via the formation of a stable coiled-coil structure (Marti *et al.* 2000). Coiled-coils can also be found in a large number of other proteins including the macrophage scavenger receptor, which is observed to undergo a conformational change dependent on the solution pH (Suzuki *et al.* 1999).

1.1.3 Applications of Coiled-Coil-Containing Proteins

The ability to design and manufacture synthetic proteins has made it possible to create new coiled-coil containing proteins tailored for predetermined functions. Such proteins have an emerging number of potential applications. These include:

For the creation of biosensors and affinity chromatography-based systems. In the laboratory of Hodges *et al* (Chao *et al.* 1998) a heterodimeric coiled-coil consisting of two proteins called E and K has been developed to act as a capture and dimerisation domain. Here a surface is first functionalised with the K peptide, before exposing to the E peptide already modified with the ligand of interest (e.g. an antibody). Such a method allows chemical modifications to be carried out away from the biosensor surface. A similar strategy using the same protein system was also used to create an affinity chromatography system for purifying recombinant proteins when modified with the E protein. A similar strategy has been carried out in other laboratories to create to create epitope display systems using coiled-coils as a cross-linking domain (Tang *et al.* 2001). In another study a temperature sensor was creating using the heat sensitive coiled-coil forming protein TlpA when combined with as a fusion protein with green fluorescent protein (GFP) (Naik *et al.* 2001).

For the production of fibres and cross-linking systems for use in tissue engineering applications. Such an approach has been taken by researches in the laboratory of Woolfson utilising the 'sticky-end' assembly of short leucine zipper proteins to self-assemble to produce long fibres (Ryadnov and Woolfson 2003). A variation of the same protein system has produced cross-linking structures for the assembly of nanoparticles (Ryadnov *et al.* 2003). A similar approach has been used utilizing dendrimers displaying leucine zipper domains, which self assemble to form fibrillar macrostructures (Zhou *et al.* 2004).

For the production of reversible cross-linking agents for drug delivery applications (Hodges 1996; Moll *et al.* 2001; Yu 2002). Here the heterodimeric coiled-coil domains are again used as dimerisation domains similar to the approach used above in the creation of biosensors, but instead bring a therapeutic agent, such as a drug, into close proximity to a targeting agent, for instance an antibody. By this method the drug can be concentrated in the tissues of interest.

Coiled-coils can also be used as a cross-linking motif for the production of hydrogels (Petka 1997; Petka *et al.* 1998; Guhr 2000; Tang *et al.* 2001). It is this latter application which is of primary relevance to this study, and will be described in greater detail in the next section.

1.2 Responsive Hydrogels from Coiled-Coil Proteins

The majority of proteins examined in this thesis are proteins designed for the formation of environmentally-responsive hydrogels, utilising coiled-coil assemblies as cross-linking domains between molecules. A hydrogel consists of a polymer matrix that contains a large number of hydrophilic groups, allowing it to absorb a large amount of water relative to its mass (Yang *et al.* 1999; Wang *et al.* 2001). A number of hydrogel systems presently exist, one example being polyacrylamide gels, used in the separation of proteins according to molecular weight by electrophoresis (Dunn 1987). A responsive hydrogel is a hydrogel whose gel-forming ability changes with changes of certain conditions such as temperature, pH or ionic strength. A number of pH- and thermally-responsive hydrogels have been created from polypeptides (Markland *et al.* 1999) and other polymers (Lee and Shieh 1999), which have a range of potential applications, most notably in drug delivery systems.

The proteins of particular interest to this work are ones which form hydrogels utilising the coiled-coil motif as a dimerisation domain. There are several systems which make use of this approach. One notable example is a hybrid hydrogel system assembled from a HPMA copolymer linked to a histidine-tagged protein via metal complexation (Tang *et al.* 2001; Wang *et al.* 2001). Here the protein sections were *de novo* designed to homodimerise to form coiled-coil structures. Melting transitions observed in the hydrogels formed from these assemblies were matched by the melting temperatures observed for the coiled-coil assemblies alone, suggesting that it was the coiled-coil domains which were responsible for the physical properties of the hydrogels.

The proteins examined primarily in this thesis are two related systems of pH-responsive hydrogel proteins, whose cross-linking moiety is based on the dimerisation of leucine zipper sequences (Petka 1997; Petka *et al.* 1998; Guhr 2000). Although they are described in greater detail in the relevant experimental chapters, a general model of their gelation behaviour will be outlined here and illustrated in Figure 1-3. Each hydrogel protein contains two or more leucine zipper sequences separated by a polyelectrolyte spacer. Through the dimerisation of the leucine zipper segments proteins can become cross-linked to form a network which forms the matrix of the hydrogel. Through changes in environmental conditions, such as temperature, pH or the ionic strength of surrounding solution, the stability of these dimers is modulated. Under certain conditions, such as high temperature or a pH regime which causes the formation of a significant amount of repulsive charges, the leucine zipper sections no longer associate significantly, causing the majority of proteins to be dissociated. This causes the gel to undergo a transition from a visco-elastic solid to a viscous fluid. These physical changes are reversible with a return to previous conditions.

1.2.1 The A/B Helix Protein-Based Hydrogel System

The first set of hydrogel-forming proteins examined in this study were designed in the laboratory of D.A. Tirrell (CalTech) (Petka 1997; Petka *et al.* 1998). In essence they consist of leucine zipper sequences which act as cross-linking domains between the proteins, spaced out with long spacer regions, containing many hydrophilic amino acid residues. The spacer regions act as polyelectrolyte sections which increase the water solubility of the proteins, and allow swelling of the gel. They consist of units of the following repeating amino acid sequence, $[(AG)_3PEG]_n$ (McGrath *et al.* 1992), where *n* denotes the number of repeats of this sequence (either 10 or 28).

The leucine zipper domains are based on an original design by McGrath *et al* (McGrath and Kaplan 1993; Petka 1997). The choice of residues in the core

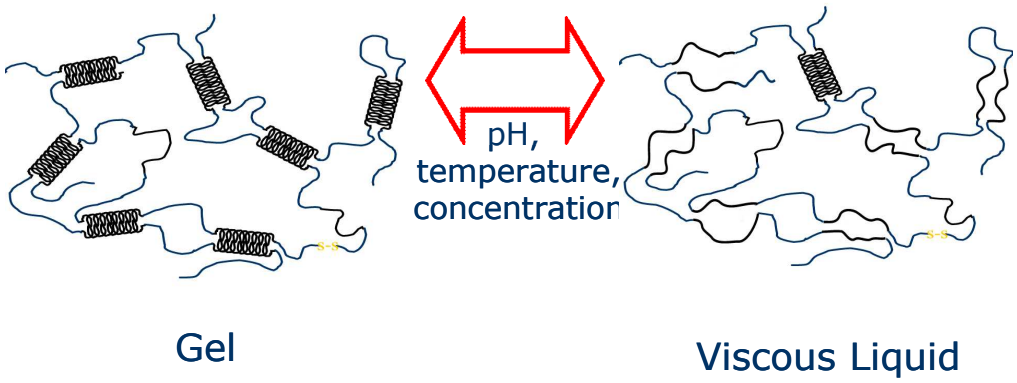

Figure 1-3: Model for gelation of pH-responsive hydrogel proteins. As environment is altered, the stability of leucine zipper dimers becomes altered causing their increased dissociation/association, leading to transitions in the physical properties of gels from visco-elastic solids to viscous liquids. These transitions are reversible.

positions were based upon those found in the *jun* oncogene product, a leucine zipper type protein. They are acidic, A, or basic, B, depending upon the charges that may be adopted by residues in the core-flanking positions. It is worth noting that the only difference between A and B sequences is the sequence of residues in the core-flanking positions, otherwise they are identical. These regions on the A sequence are dominated by acidic glutamic acid residues, whilst on the B sequence they are mainly basic lysine residues. Each consist of 42 amino acids or six heptad repeats, and were designed to assemble with a parallel orientation. Figure 1-4 displays the helical wheel representations for the coiled-coils formed by homodimers of proteins A and B. In Figure 1-5 is a helical wheel diagram of the heterodimeric parallel assembly of A and B.

At ambient room temperature and near physiological pH, mixtures of proteins containing single repeats of the lone A and B helices in solution form heterodimers in preference to homodimers. In solutions of A or B alone weakly-associating homodimers form. The heterodimer conformation is preferred due to oppositely-charged residues in the core-flanking *e* and *g* positions (glutamate in the case of the A helix and lysine in the case of the B helix). In the homodimers the charged groups have a repulsive effect due to having the same ionisation state.

As pH is altered the stability of homodimers formed between sequences of the acidic A sequence is modulated as the charges on the core-flanking residues changes. Glutamic acid side chains have a pK of approximately 4.4 (Stryer 1988). This means that at acidic pH values not all of the glutamic acids in the core-flanking positions on the A helix carry a negative charge, with only approximately 50 % being charged at pH 4.4. As the pH is raised these residues become increasingly de-protonated leading to an increase in repulsion between the opposing helices, destabilising the coiled-coil assembly. This change in stability with pH has been confirmed by thermal melting studies of

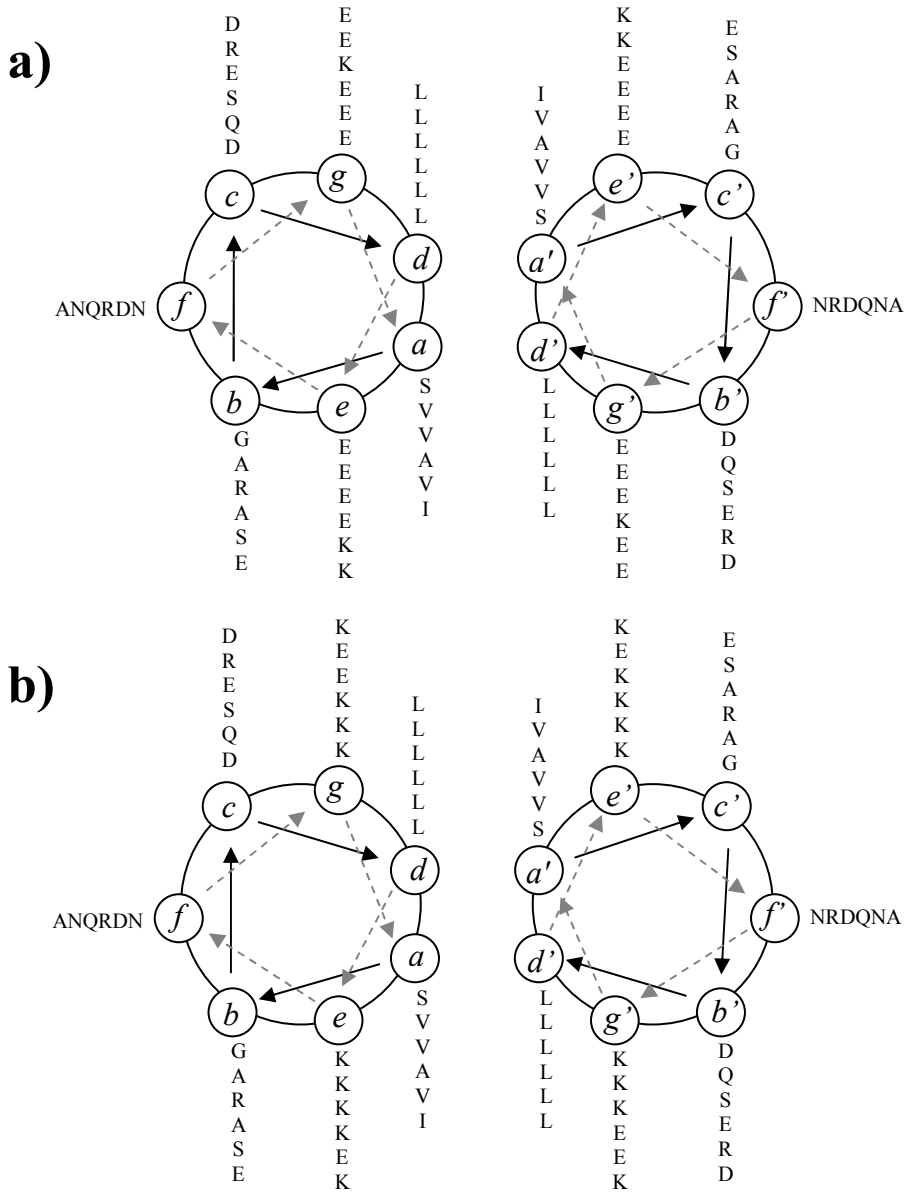

Figure 1-4: Helical wheel representations for parallel homodimer assemblies of a) coiled-coil A; b) coiled-coil B.

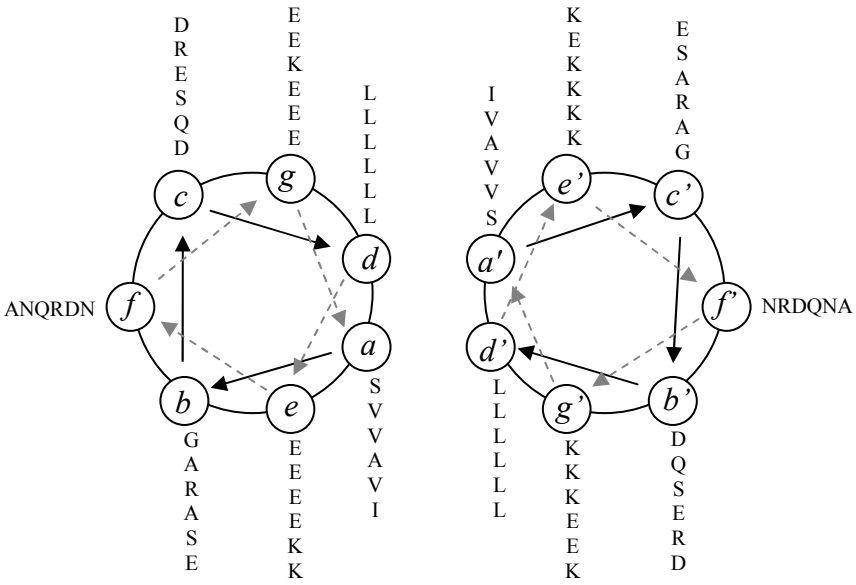

Figure 1-5: Parallel heterodimeric coiled-coil assembly of leucine zipper sequences A (left) and B (right). Note that the two different helices differ only in the sequence of residues in the *e* and *g* positions.

proteins containing the acidic leucine zipper sequence. As the pH was increased a large decrease in thermal stability was observed between pH 6 and 7.5 (Petka 1997; Petka *et al.* 1998). At a pH of 7.5 almost all (>99 %) of the glutamic acid side chains are charged, so it would be expected that any transition based upon changes solely based on glutamic acid would be below this pH. For proteins containing the B zipper with a large proportion of basic lysine side-chains (pK 10.5) in the core-flanking positions the opposite trend was observed (Petka 1997; Petka *et al.* 1998).

As a result of this behaviour, hydrogel proteins containing two of the leucine zipper domains separated by the polyelectrolyte spacer showed physical changes with pH. For proteins with two or more acidic leucine zippers they were found to form a gel at low pH, which changed to a viscous fluid at high pH as coiled-coil domains became destabilised. The converse was true for hydrogel proteins containing two of the basic B sequences. Solutions made from proteins containing both acidic and basic sequences will not be expected to show change in physical properties as pH is altered (Petka 1997).

At the amino-terminal end of each protein is a poly-histidine section, used for purposes of protein purification, and which plays no part in the function of the protein. At the other, carboxy, terminal end of the proteins is a cysteine residue. This residue is useful for the covalent linking of the proteins to other molecules and gold surfaces, and is thus useful for the immobilisation of the protein in experiments described in this thesis. In solution side-chains of these cysteine residues can also form disulphide linkages between proteins serving as a further cross-linking moiety.

The naming convention for these proteins follows the following convention: amino end helix; number of polyelectrolyte sequence repeats; carboxy end helix; cysteine residue. For example, the protein $AC_{10}ACys$ consists of two acidic A helices separated by a spacer containing ten $[(AG)_3PEG]$ repeats. A variety of proteins in this hydrogel system are used throughout this thesis. For

clarity they will not be described in specific terms here but will be described in more detail in the relevant chapters in which they are studied.

1.2.2 A Hydrogel System Based on the F Leucine Zipper Sequence

Another coiled-coil-based protein hydrogel system was created, building on the work of Petka *et al* (Guhr 2000). This system utilises a different leucine zipper design, F, based upon the *fos* oncogene product, as a cross-linking domain and was designed to have a more pronounced pH response than the A and B sequences. A helical wheel representation of a parallel homodimer of F helices is illustrated in Figure 1-6. As can be seen, the F sequence is shorter than A or B and consists of only 35 amino acid residues, comprising five heptad repeats. Coiled-coils formed by F helices are acidic, with a number of glutamic acid residues in the core-flanking regions. This system would be expected to show pH-responsive behaviour similar to the A helix. Hydrogel proteins created by this system have similar architecture to the A/B system – they consist of leucine zipper sequences separated by the same $[(AG)_3PEG]_{10}$ polyelectrolyte domain.

Previously this protein system has been characterised using circular dichroism and viscometry. These experiments demonstrated that the proteins associated in a pH-dependent manner, being more stable at low and neutral pH where they were able to form gels, dissociating to form viscous liquids at high pH (Guhr 2000).

The naming convention for this series of proteins differs from that mentioned previously. It consists of L2F followed by the number of F and polyelectrolyte subunits collectively. For example L2FC3 contains two F coils and one polyelectrolyte spacer; L2FC7 contains four F helices with three spacers.

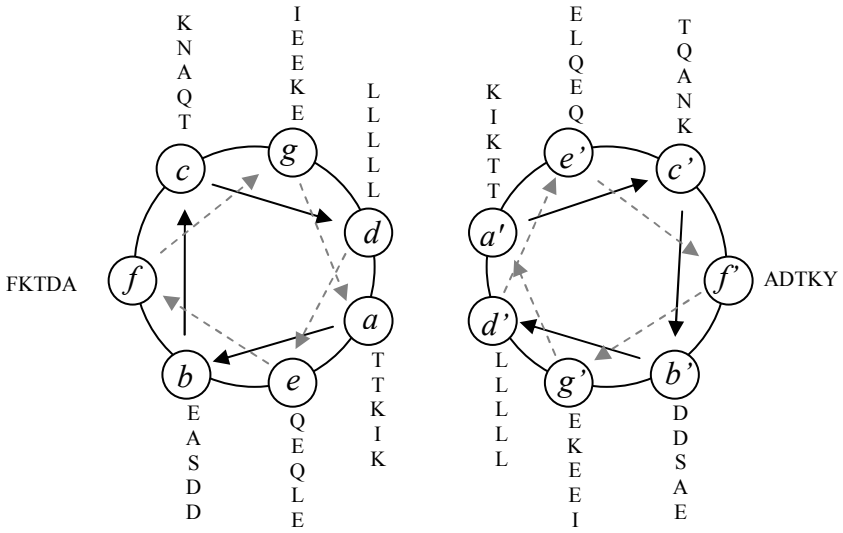

Figure 1-6: Helical wheel representation of parallel homodimer coiled-coil arrangement of helices of the F coil.

1.3 Aims and Objectives

A series of environmentally-responsive protein hydrogel systems have been created, utilising leucine zipper assemblies for cross-linking. These systems undergo reversible transitions in their physical behaviour, switching between viscous liquids and gels, in response to changes in pH, temperature and concentration. The pH-dependent transition is due to the change in ionisation of amino acid side chain in regions flanking the hydrophobic cores of the coiled-coils.

Whilst the bulk properties of these systems are relatively well characterised, little data exists on the molecular scale. It is the primary aim of this work to generate data at the single molecule and mesoscale levels to obtain an increased understanding of how properties at this level relate to those at the macroscopic level. This was undertaken using a range of biophysical techniques, described in greater detail in chapter two. The work included in this thesis builds on preliminary work previously undertaken (Stevens 2001; Kavourides 2003) which established that it was possible to carry out single molecule measurements of these proteins using atomic force microscopy (AFM).

In chapter three studies are presented which represent the most simple experiments in terms of experimental architecture, where hydrogel proteins are mechanically extended under different pH conditions to study any changes in entropic elasticity, using an atomic force microscope (AFM). Changes in the mechanical compliance of these molecules with pH can be related to changes of charge on the molecules. This has implications both for the swelling of hydrogels, and the behaviour of layers of hydrogel proteins attached to surfaces examined in later experiments (chapter 6). Most significantly, before further force experiments can be carried out, an understanding of the changing

stiffness of the proteins with pH needs to be known, to take account of the effect on the loading of force onto biomolecular bonds.

The studies described in chapter four concern the application of dynamic force using AFM to single homodimers of proteins ACys and BCys, which each contain a single A or B leucine zipper sequence. Previous experiments have been undertaken by Stevens to measure forces between homodimers of these proteins (Stevens 2001). However, the response of these systems to force under a range of loading rates has not been studied. In this chapter a dynamic force spectroscopy approach was undertaken to probe changes in behaviour and stability of these homodimers under force. Such an approach can yield data on the dissociation kinetics and reveal aspects of the energy landscape to unfolding, not possible with a static single loading rate approach. In addition this chapter describes a new strategy for the immobilisation of the proteins to the surface. By the co-incubation of proteins with an alcohol thiol molecule it is hoped to reduce the chances of ruptures of multiple proteins complexes, making the observation of single complexes only.

The studies presented in chapter five are on a larger scale than those looked at previously and concern attempts to measure the viscosity of various solutions of hydrogel proteins, at different concentrations and pH values. The resonance response of AFM microcantilevers is sensitive to a number of factors, including the viscosity of the surrounding solution. As such, if other factors remain constant then changes in the resonance frequency of cantilevers will reflect changes in solution viscosity.

In chapter six surfaces were functionalised with layers of proteins L2FC7 and BCys, to create pH-responsive surfaces. The properties of these surfaces were then examined using a variety of techniques, most notably dual polarisation interferometry (DPI) and quartz crystal micro-balance with dissipation monitoring (QCM-D). The intention of this work was to use the optical and mechanical detection capabilities of these two techniques in a complementary manner to gain insight in to the behaviour of these functionalise surfaces. Both

changes in the layers themselves as the surrounding pH was altered and also changes in their ability to associate with protein in solutions of different pH were examined.

Finally in chapter seven a coiled-coil of more complex architecture than previously examined is probed using a single molecule dynamic force spectroscopy approach, similar to that used in chapter four. This system consists of three proteins, which together form a two-stranded leucine zipper assembly. These proteins were designed for the cross-linking of nano-particles in the formation of biomaterials. The aim of the work detailed in this chapter is to probe the stability of the assembly under increasing force, to allow the inference of some of the assemblies' physical properties, such as dissociation kinetics. Also as any biomaterial which may be made using these proteins is likely to be exposed to external forces, probing their stability by mechanical means is especially relevant.

Chapter 2 : Instrumental Techniques and General Methods

Within this chapter the general instrumental techniques used throughout this thesis are described. However, the specific experimental methods used for each study are described within the methods sections of the relevant chapter.

2.1 General Methods

Unless otherwise indicated all chemicals and reagents used were obtained from Sigma-Aldrich Ltd. (Gillingham, Kent). All aqueous buffers and solutions were prepared using high purity de-ionised water purified on an Elga water system (resistivity 18.2 MΩ cm), and filtered with a 0.2 μm syringe filter prior to use.

2.1.1 Template-stripped Gold

In experiments where the functionalisation strategy employed required gold (Au) surfaces, the template-stripped gold method (Hegner *et al.* 1993) was used to create a clean gold surface that is atomically flat. A mica sheet (Agar Scientific, Stansted, Essex) was cleaved down the centre to reveal a clean and atomically flat surface. Under vacuum, gold was evaporated onto this surface at 315 °C at a pressure of 10^{-6} mbar, before being allowed to anneal at 390 °C for 24 hours. The annealing step allows islands of epitaxial gold created on the

mica surface during evaporation to grow at the expense of smaller islands leading to the creation of a more even layer. The gold surface was then glued to a glass coverslip using two part epoxy-resin which was baked until hard for 2 hours at a temperature of 200°C. When the gold surface was required the sandwich was immersed in the solvent tetrahydro-furan for approximately 5 minutes allowing the mica to be peeled away in one piece. This exposed the gold surface which had previously been pressed against the mica. The coverslip carrying the gold was then rinsed with 100% ethanol and high purity de-ionised water before drying under a stream of N_2.

2.2 Atomic Force Microscopy

The atomic force microscope (AFM) was first described in 1986 by Binnig and colleagues as a new technique for imaging the topology of surfaces to a high resolution (Binnig *et al.* 1986). Since then AFM has enjoyed an increasingly ubiquitous role in the study of biological systems, both as an imaging and surface characterisation technique, and also as a means of probing interactions and properties of single biomolecules by the application of force to these systems. It is this latter approach which is relevant to the experimental work described in this thesis. Hence only the operation of the AFM for the obtaining of force data will be described here and not modes used for imaging applications.

2.2.1 AFM Apparatus

In Figure 2-1 the basic set-up of a typical AFM is shown. A cantilever, which may be either V-shaped, as shown, or a rectangular 'diving board' shape cantilever, attached to a chip has mounted upon its free end a pyramidal tip which acts as the probe of surface forces. The probes are most commonly made of silicon nitride (Si_3N_4) or silicon (Si). Typically the upper surface of

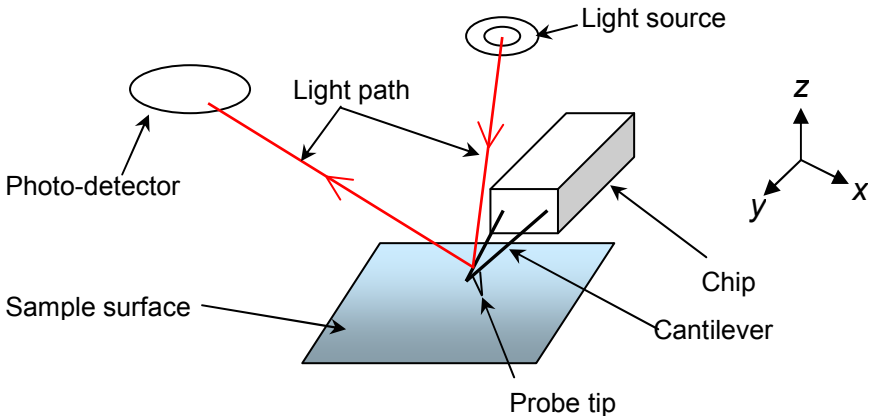

Figure 2-1 : Basic set-up up the AFM. A pyramidal tip is mounted on the end of a flexible Si_3N_4 cantilever, itself attached to a chip attached to a piezo crystal. Deflection of the cantilever is monitored by the change in the path of a beam of laser light deflected from the upper side of the end of the cantilever by a photodetector. As the tip is brought into contact with the sample surface, by movement of the piezo, its deflection is monitored.

the cantilever, opposite to the tip, is coated with a thin reflective surface of either gold or aluminium (Al).

The probe is brought into and out of contact with the sample surface by the use of a piezo crystal, upon which either the cantilever chip or the surface itself is mounted. A beam of laser light is reflected from the reverse (uppermost) side of the cantilever onto a position sensitive photodetector. When the tip of the cantilever becomes deflected the path traced by the light changes position on the photodetector and as a consequence the magnitude of deflection of the cantilever can then be deduced using by the instrumentation software.

2.2.2 Use of AFM as a Force Sensor

Within certain limits the cantilever behaves as a linear, 'Hookean', spring. As a result the magnitude of the deflection of the cantilever can be used to calculate the force being exerted on the end of the cantilever using Hooke's law:

$$F = -kd \qquad \textit{Equation 2-1}$$

Where F is force (N), d is the deflection of the cantilever (m) and k is the spring (or force) constant of the cantilever (N m^{-1}), which essentially represents the stiffness of the cantilever.

As the tip of the cantilever is brought into and out of contact with a surface a force curve is generated. A sketch of a typical force curve is shown in Figure 2-2. The deflection of the cantilever is shown as a function of the z-displacement of the cantilever by the piezo. As the cantilever begins its approach (described by the blue trace) it is away from the surface and hence there is no net change in force detected (point 1. in the figure) – the cantilever is said to be at its free level. When the cantilever makes contact with the surface it is deflected upwards and a positive force is observed (point 2.). The cantilever is then retracted (red trace) and initially follows the path of the

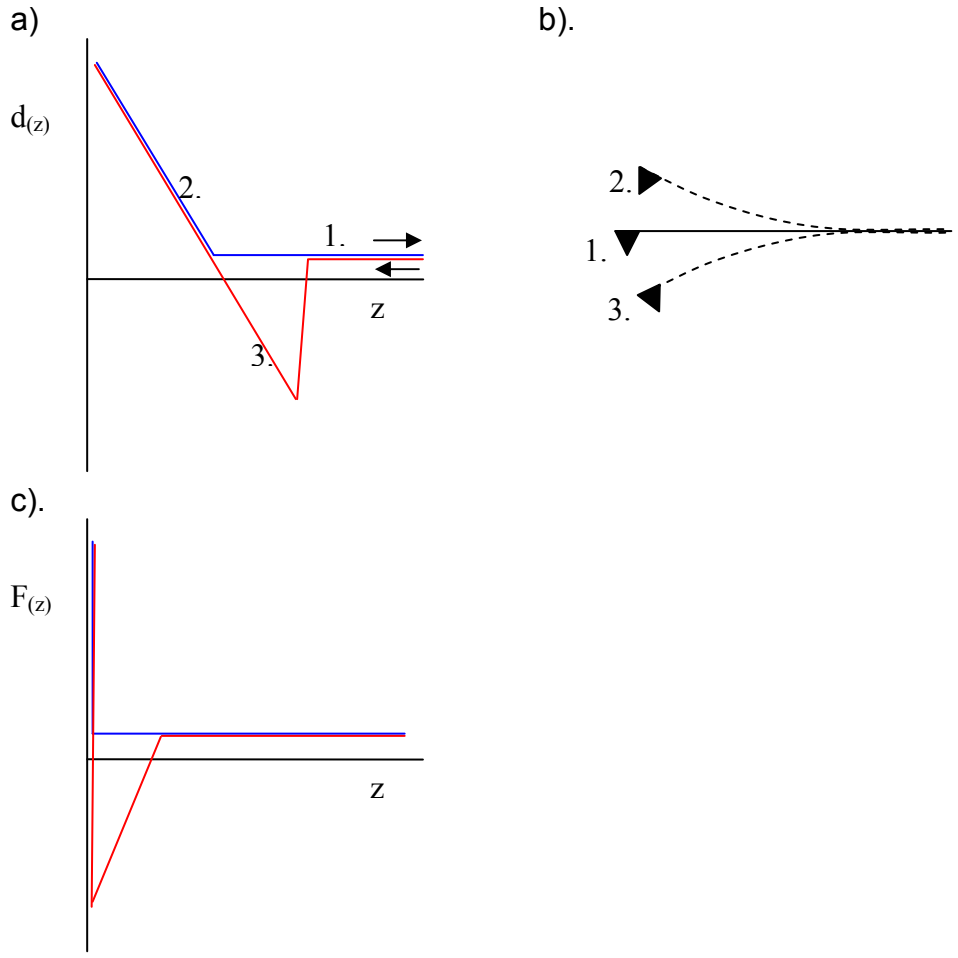

Figure 2-2: Representation of a typical force curve generated upon contact of AFM cantilever tip with a hard surface. The force curve illustrated in a) shows cantilever deflection (with repulsive forces here represented as positive) against piezo displacement. Cantilever movement is shown in b), with numbered labels referring to the deflection of the cantilever at various points in the curve. In c) a force curve is shown corrected to show force against actual tip movement. Note that the attractive surface interaction ruptures while the cantilever is still in contact with the surface (z=0).

approach trace in the contact region. The cantilever often remains attached to the surface by attractive forces which results in a downwards deflection of the cantilever (point 3.) as the probe and surface are separated. Eventually the separation force becomes sufficient to overcome the attraction between the cantilever tip and the surface and the cantilever returns to its initial free level position. The force exerted by the cantilever can then be calculated using Hooke's law (equation 2-1) using the deflection of the cantilever and its spring constant.

There are several methods by which the spring constant can be calculated, each with their own advantages and disadvantages. These include the addition of known masses to the free end of the cantilever and observing resonant frequency change (Cleveland *et al.* 1993); pressing a cantilever against another reference cantilever of known spring constant (Gibson *et al.* 1996); calculating the spring constant from the ambient thermal excitation spectra of the cantilever (Hutter and Bechhoefer 1993); and calculating a theoretical spring constant from the geometry and material properties of the cantilever (Sader 1995; Sader *et al.* 1995; Sader 1998; Sader *et al.* 1999; Sader 2002) amongst others. For its accuracy, convenience of use and its non-destructive nature the thermal excitation method, developed by Hutter and Bechhoefer (Hutter and Bechhoefer 1993; Levy and Maaloum 2002) was used throughout this work.

Here the area of the fundamental resonant peak of the cantilever under ambient thermal excitation is used to directly calculate the spring constant of the cantilever. A correction must be made to take into account the optical set-up of the system i.e. how the laser and photo-detector are aligned with the cantilever, changes in which can produce significant errors in spring constant measurement. To do this the cantilever is driven into a hard surface to produce a force curve (signal amplitude verses piezo displacement) and the slope of the contact region of this curve is used as a correction factor in the spring constant calculation. Multiplying the cantilever deflection by its spring constant will then allow the conversion of the graph in Figure 2-2 into one which shows force versus piezo displacement. To get a graph of force versus the actual

movement of the cantilever tip the deflection is then subtracted from the z-displacement on the x axis.

2.2.3 Instrumentation

All force measurements were carried out on an MFP-1D force molecular force probe (Asylum Research, Santa Barbera, USA), using IGOR Pro (Wavemetrics Inc., Lake Oswego OR. USA) as a software interface. For force measurements a variety of cantilevers were used throughout this work; these were NP type cantilevers (Veeco, Santa Barbera, CA), with nominal spring constants of approximately 60 pN nm^{-1}, 'Park' type cantilevers with nominal spring constants of 20 to 120 pN nm^{-1} (Veeco, Santa Barbera, CA), and Olympus 'diving board' shaped cantilevers with spring constants of 6 and 30 pN nm^{-1}.

2.3 Quartz Crystal Microbalance

In chapter 6 experiments are described using a modified version of the quartz crystal microbalance (termed QCM-D) to determine changes in the physical properties of monolayers of pH-responsive proteins immobilised on surfaces. Described here is the theoretical background to the operation of the instrument and also how the instrument used was set-up during experiments.

2.3.1 Theoretical Background

The quartz crystal microbalance (QCM) has long been established as a method for the monitoring of film thickness changes in coating applications and for the analysis of adsorption of gases to surfaces via the monitoring of changes to the resonant frequency, *f*, of the quartz crystal (Sauerbray 1959).

The sensor in a QCM consists of a quartz crystal disc through which is passed an AC current via electrodes mounted on the opposing surfaces of the disc (see

Figure 2-3). This causes the disc to oscillate laterally at a frequency related to the mass of the disc and the current being passed through it. As an increase in mass is applied to the disc the frequency, *f*, of the disc and its harmonics decrease proportionately. If the adsorbed film has a very small thickness and a small mass relative to the sensor crystal, does not slip on the sensor, and is sufficiently rigid to have negligible internal friction, then a change in the mass on the sensor can be calculated based on the change in resonant frequency of the sensor using the Sauerbray relationship (Sauerbray 1959):

$$\Delta m = -\frac{C}{n}\Delta f \qquad \textit{Equation 2-2}$$

where Δm is the change in mass, C is the mass sensitivity constant (equal to 17.7 ng cm^{-2} Hz^{-1} for f = 5 MHz) and n is the number of the overtone being measured (Höök *et al.* 2001).

More recently an extended version of the technique, QCM-D has been developed which monitors the dissipation signal, D, in parallel to the *f* signal. Power to the crystal is applied in pulses, rather than constantly and the decay of the oscillations is measured between pulses. D is a dimensionless quantity, having no units, and constitutes the sum of all mechanisms by which energy is dissipated from the crystal. This may originate from interactions between the adsorbed film and either the liquid overlayer or the underlying surface, or from interactions between constituent molecules of the film itself (Rodahl and Kasemo 1996; Rodahl *et al.* 1997; Voinova *et al.* 1999; Höök *et al.* 2002). As a result it can give information on the dissipative properties of layers adsorbed to the sensor. This allows information about the mechanical properties of monolayers or thin films to be assessed.

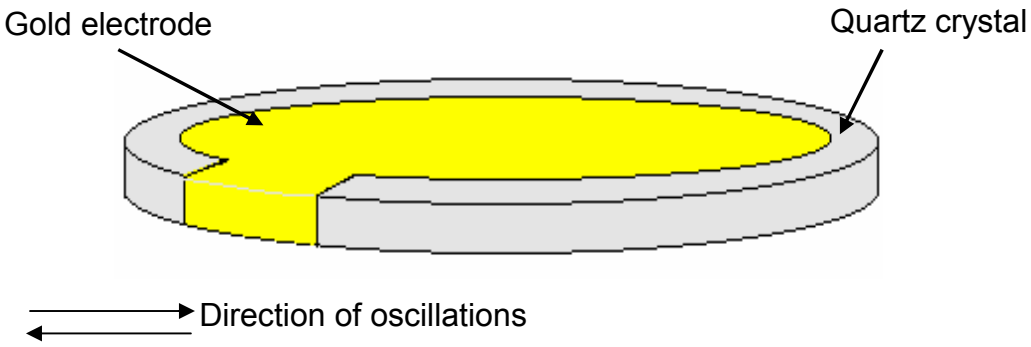

Figure 2-3: Schematic of the QCM-D sensor crystal. The upper surface is largely covered by the upper of two gold electrodes and constitutes the sensor surface. When an AC current is applied between the electrodes the crystal oscillates laterally at approximately 5MHz.

2.3.2 Instrumentation

For experiments outlined in chapter 6 a D300 model QCM-D was utilised, (Q-Sense, Gothenburg, Sweden), with simultaneous frequency and dissipation monitoring. The sample chamber has a total volume of 80 µl. Before samples reach the sample chamber, they first have to pass through a T-loop embedded in a temperature controlled block to equilibrate the sample solution temperature with that of the sample chamber. This is essential as temperature variations can have a profound effect on both the f and D signals. The employed sensor crystals consisted of 1cm diameter quartz discs fitted with gold electrodes. The gold electrode on the upper surface constituted the surface onto which samples were introduced.

Standard gold-coated quartz sensor crystals (Q-Sense AB, Sweden) were used for all experiments and had fundamental resonant frequencies of 4.9 MHz and mass sensitivities of 5 ng/cm^3 in a liquid environment (manufacturers quoted values). Changes in resonant frequency (Δf) and dissipation (D) were measured simultaneously at the third, fifth and seventh overtones. All samples were introduced in a volume of approximately 2.0 ml via an axial flow chamber, which included the T-loop, where the sample was thermally equilibrated at 23.0 $^{\circ}$C for at least two minutes before injection of 0.5 ml into the sample chamber.

2.4 Dual Polarization Interferometry

2.4.1 Theoretical Background

The instrument used for the technique of dual polarisation interferometry (DPI) consists of a pair of wave-guides through which light, polarised in two planes perpendicular to each other, is passed (Figure 2-4). The light waves exiting the waveguides interact with each other to produce an interference pattern. The

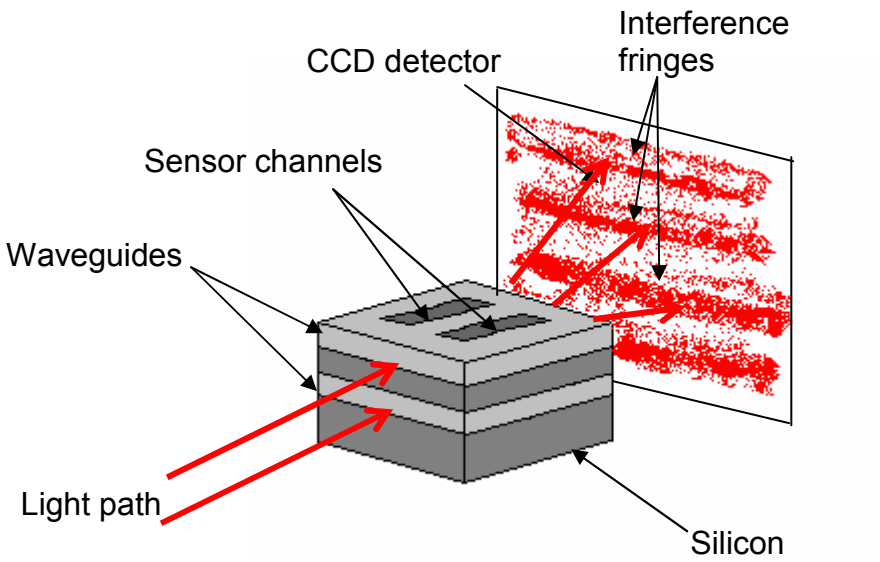

Figure 2-4: Schematic of the of the waveguide set-up during DPI experiments. Light polarized in two directions perpendicular to each other is shone through two waveguides. As they exit the waveguides an interference pattern is formed. As adsorbed molecules interact with the evanescent field of the upper waveguide a change in the phase of the light travelling through this waveguide occurs causing a shift in the resultant interference pattern. This then allows calculation of film thickness and refractive index.

appearance of this interference pattern depends upon the relative phase of the light passing through the waveguides, which is affected by the refractive indices of the waveguides. The surface of the uppermost wave-guide constitutes the sensor surface, and as biomolecules are deposited upon this surface or immobilised molecules change their physical characteristics, such as density, the resultant change in refractive index of the waveguide causes a change in the interference between the light passing through the waveguides. By monitoring the resultant shift in the interference pattern, film thickness and refractive index can be directly measured (Cross and Ren 1999; Cross *et al.* 2003; Cross *et al.* 2004). Layer density can also be calculated from changes in the refractive index, using the relationship:

$$\rho_L = \frac{\rho_p \times (RI - RI_b)}{(RI_P - RI_b)} \qquad \text{Equation 2-3}$$

Where ρ_L is the layer density, ρ_p is the density for a tightly packed layer of protein (0.7100 g/cm^3), RI_p is the refractive index associated with such a tightly packed protein (1.456) and RI_b is the refractive index of the bulk solution, obtained during instrument calibration. The layer mass was obtained by multiplying the calculated density with layer thickness.

2.4.2 Instrumentation

Experiments in chapter 6 using DPI were carried out on an Ana Light Bio200 dual polarization interferometer kindly loaned to our laboratories by Farfield Sensors Ltd. (Salford, UK), with an amine-functionalised FAR-100 chip (Farfield Sensors Ltd., Salford, UK). Within the instrument the sample chamber consists of a continuous flow cell attached to a syringe pump. For all experiments the flow rate was set at 100 µl minute^{-1} unless otherwise stated. The sample chamber was kept at a constant temperature of 20.0 °C throughout all measurements.

2.5 Surface Plasmon Resonance

2.5.1 Theoretical Background

The total internal reflection of light travelling through a glass prism is attained when the light encounters the interface of the glass with a substance of much lower refractive index, such as a gas or liquid. When this happens evanescent waves, which are an electromagnetic component of the light, penetrates a short distance into the medium of lower refractive index. When the surface of the prism is coated with a thin layer of a heavy metal such as gold the evanescent wave causes a resonant effect with the electrons in the metal layer. This causes an attenuation of the light reflected at a specific angle (the resonance angle) which is a function of the refractive index of the materials through which the light passes. The adsorption or desorption of molecules to or from the metal interface will affect the refractive index and cause a shift in the resonance angle. In this way the surface plasmon resonance (SPR) can be used to monitor changes in adsorption to metal films or layers of biomolecules attached to metal films (Höök *et al.* 2001; Kapoor *et al.* 2003).

A typical SPR apparatus is illustrated in Figure 2-5. Light is shone from a light source, through the prism coupler and then detected by a CCD detector. The entire sensor surface is sealed into a liquid cell, with analytes and macromolecules being allowed to flow over the gold surface at a predetermined rate and constant temperature.

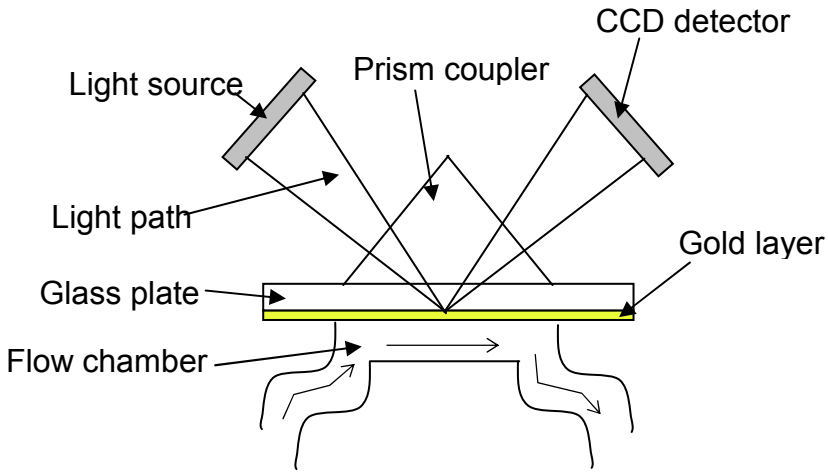

Figure 2-5: Schematic of a typical SPR set-up. As biomolecules bind to the gold surface, interaction with the evanescent field causes a shift in the SPR angle, which can be related to change in adsorbed mass.

2.5.2 Instrumentation

Experiments using SPR were carried out on a Biacore3000 instrument (Biacore, Uppsala, Sweden). Unless otherwise stated flow rates were set at 5 µl min^{-1}. For protein immobilisation studies plain unfunctionalised gold-coated sensor chips (Au, Biacore) were used.

Chapter 3 : Mechanical Extension of Single Protein Molecules

3.1 Introduction

Whilst the hydrogel-forming proteins studied in this thesis have their pH-responsive association mediated by their leucine zipper regions, they also contain large random coil polyelectrolyte sections. The behaviour of these latter sections may possibly affect their properties in bulk solution. In addition the mechanical compliance of the proteins under investigation may affect the analysis of force measurements described in later chapters. It is therefore of interest to investigate whether the hydrogel-forming proteins undergo any such change in their properties as a response to pH. This chapter details a series of experiments designed to assess whether changes in environmental pH affect the intra-mechanical properties of single molecules of two related proteins, termed AC_{10}ACys and AC_{28}ACys, which are ordinarily pH-responsive in their functions. This was carried out using AFM-based force spectroscopic techniques to extend single molecules of these proteins, before fitting an appropriate mathematical model for the behaviour of polymers under force to the resultant force curves.

3.1.1 Mechanical Extension Experiments

The atomic force microscope has, amongst other applications, become a useful tool for studying the mechanical properties of single biopolymeric molecules.

The types of molecules which lend themselves well to mechanical extension experiments tend to be long biomolecules or polymers, such as DNA (Rivetti *et al.* 1998; Anselmetti *et al.* 2000; Bustamante *et al.* 2000; Zhang and Zhang 2003), long chain proteins (Rief *et al.* 1997; Rief *et al.* 1999; Zhou 2001; Ikai *et al.* 2002), complex carbohydrates (Camesano and Wilkinson 2001; Xu *et al.* 2001), and polypeptide chains (Lee and Vilgis 2002a), as well as other polymers, such as poly(methacrylic acid) (Ortiz and Hadziioannou 1999). These experiments have been carried out using a number of different techniques, including those based on atomic force microscopy (AFM), optical tweezers (OT) and the biomembrane force probe (BFP).

With regard to proteins, a large amount of work has been done on the giant muscle protein titin (also called connectin) (Rief *et al.* 1997). Titin consists of a long chain of tandem immunoglobulin (Ig) like repeats, as well as a small quantity of sequences rich in the amino-acids proline, glutamic acid, valine and lysine (termed the PEVK region). Extension of titin using mechanical force typically gives a 'saw-tooth'-shaped force-distance curve (Rief *et al.* 1997) (Rief and Grubmuller 2002), where steep gradients in the curve respond to unfolding events in the Ig-like domains, and longer curved slopes represent the stretching of the extended polypeptide chain. Similar mechanical stretching experiments performed on titin using optical tweezers techniques (Tskhovrebova *et al.* 1997) were found to generate similar results, confirming that this observation was not an artefact generated by the AFM. Force extension experiments of the long protein spectrin, which contains many triple-helical coiled-coil repeats, yielded a similar pattern to that observed with titin (Rief *et al.* 1999). In more recent work (Lee *et al.* 2002; Lee and Vilgis 2002a; Lee and Vilgis 2002b) 'protein-like' copolymer chains with arbitrary sequences have been extended under force. It was found that the shape of the force-extension curve was caused by the unfolding of domains from a globular to an open-string conformation. The force relating to the transition from one domain to another was characterised as a plateau in the curves. When long-range interactions between the domains were present the sharp transitions due to unfolding of domains became smoothed out.

A range of different mathematical models have been developed to interpret data obtained from the extension of macromolecules, most notably including the free-jointed chain model (Rivetti *et al.* 1998), which models the polymer as a series of statistical segments with orientational independence (Kuhn segments), the length of which is a direct measure of chain stiffness, and the worm-like chain model (WLC). In the literature the WLC model describes the behaviour of polypeptide chains under mechanical extension well (Rief *et al.* 1997; Rivetti *et al.* 1998; Rief and Grubmuller 2002; Clarke and Williams 2005), and as such will be used for analysis of force curves generated during this work.

3.1.2 The Worm-Like Chain

The worm-like chain is a mathematical model which can be applied in the interpretation of the entropic elasticity of polymers and biomacromolecules. It has particularly been applied to the situation where a tethered polymer or long biomolecule has been extended by the application of an external force. In the WLC model the polymer is treated as a homogenous semi-flexible rod, with a contour length, which represents the end to end length of the rod if in a straight line, that undergoes changes in curvature due to thermal fluctuations. A simple representation of this model is shown in Figure 3-1. At very low applied forces the conformation of a polymer chain can be described by a self-avoiding random walk. Force applied to the ends of the chain causes it to become more extended leading to the formation of an elastic restoring force resulting from the reduction in the number of possible configurations. The WLC predicts that as the extension begins to approach the contour length the molecule will

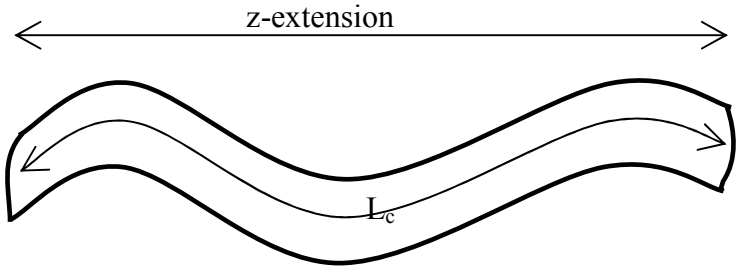

Figure 3-1: A simple representation of a polymer chain modelled as a flexible rod with an end to end distance, z and a contour length, L_c, representing the total length of the rod.

become stiffer (Ortiz and Hadziioannou 1999; Makarov and Wang 2002). The interpolation formula for the worm-like chain is shown in equation 3-1 (Bustamante *et al.* 1994):

$$F = \frac{k_B T}{p}\left(\frac{1}{4\left(1-\frac{z}{L_c}\right)^2} - \frac{1}{4} + \frac{z}{L_c}\right) \qquad \text{Equation 3-1}$$

where F is the force used to extend the polymer in Newtons; k_B is Boltzmann's constant (1.38 $x10^{-23}$ J K^{-1}); T is the absolute temperature (K); z is the extension of the polymer (nm), i.e. the end to end distance of the polymer; L_c is the contour length (nm) and *p* is the persistence length (nm). In essence the persistence length represents the entropic stiffness or flexibility of the polymer. More precisely it can be described as the length of the polymer over which the memory of a previous orientation of the molecule persists after stretching (Rivetti *et al.* 1998). The stiffer the polymer chain the longer the persistence length of that chain (Bustamante *et al.* 2000). Typical *p* values obtained for peptides as quoted in the literature are of the order of around 0.3 and 0.4 nm (Rief *et al.* 1997; Zhou 2001), which can be approximated to the length of a single peptide unit (0.38 nm). However, this can be affected by environmental factors such as solution salt concentration (Bouchiat *et al.* 1999), where ions in solution are able to shield charges on the polymer chain, such as amino-acid side-chains in a protein, from interacting with each other.

3.1.3 Proteins $AC_{10}ACys$ and $AC_{28}ACys$

The proteins used in this chapter, termed $AC_{10}ACys$ and $AC_{28}ACys$, are proteins which contain leucine zipper-based coiled-coil-forming domains. These domains can become associated in solution causing the proteins to

aggregate in to networks forming pH-responsive hydrogels, as described in chapter 1. The overall amino acid sequences of these proteins are shown in Figure 3-2. Both have a helix-loop-helix structure, where two leucine zipper domains are separated by a polyelectrolyte region consisting of repeats of an alanyl-glycine rich sequence: $((AG)_3PEG)_n$, where n is 10 for $AC_{10}ACys$ and 28 for $AC_{28}ACys$. This linker in solution is designed to have a random coil conformation. The purpose of this region is to increase the overall water solubility of the proteins as well as to link the coiled-coil domains. The protein $AC_{10}ACys$ consists of a total of 230 residues, of which 84 contribute to the helical domains and 90 form the polyelectrolyte linking region between the helices. This gives a maximum theoretical contour length for this protein of 87.4 nm, assuming that each residue contributes 0.38 nm to the length of the protein when extended (the length of a peptide unit). This is the length that would be obtained if the protein is stretched end to end into a straight line with no secondary structures present. With $AC_{28}ACys$ there are 392 residues; again 84 make up the leucine zipper regions, with 252 residues forming the linking region. The maximum theoretical contour length for this protein is expected to be 150.0 nm if fully extended.

Both leucine zipper domains in each protein are the acidic A sequence as described in chapter 1. As pH is increased the concomitant increase in the number of negatively-charged glutamic acid residues within the leucine zippers increases causing an increased repulsion between adjacent helices in any coiled-coil structures present, and hence destabilising the coiled-coil. As a result of this at low pH, solutions of $AC_{10}ACys$ and $AC_{28}ACys$ of sufficiently high concentration will form a gel due to the cross-linking by the leucine zipper regions, whereas at high pH, where dimers are unstable and less populous they will instead form viscous liquids.

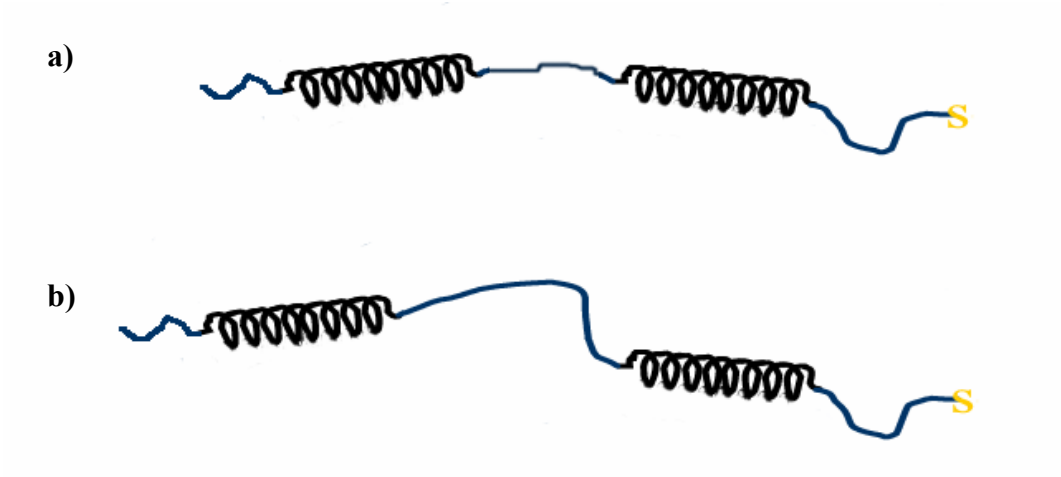

Amino acid Sequence:

MRGSHHHHHHGSDDDDKWA – *Helix* – IGKHVAPRDTSYRDPMG – [AG$_3$PEG]$_n$ – ARMPTGD – *Helix* – IGDHVAPRDTSMGGC

Figure 3-2: Shown above is an illustration of the proteins AC$_{10}$ACys and AC$_{28}$ACys. Below is the amino-acid sequence or the proteins AC$_{10}$ACys and AC$_{28}$ACys. The sequence [AG$_3$PEG]$_n$ is an alanine and glycine rich region repeated n times. In the case of AC$_{10}$ACys n = 10 and for AC$_{28}$ACys n = 28. Adapted from (Petka 1997; Petka *et al.* 1998).

3.1.4 Experimental Aims

In this chapter, proteins $AC_{10}ACys$ and $AC_{28}ACys$ were mechanically extended using an atomic force microscope (AFM) and force extension curves were obtained. The intention was to assess whether changes in the charges carried by amino acid residues within the proteins would cause an alteration of the mechanical properties of individual protein molecules. This would also help to determine whether changes in the stiffness of the proteins would need to be taken into account in further experiments where force is applied to coiled-coil dimers in chapter 4. In addition it will help us to understand whether changes in the properties of protein chains of these or similar hydrogel proteins will have to be taken into account when looking at their behaviour both in bulk solution or in immobilised monolayers, as described in later chapters.

3.2 Materials and Methods

Measurements were carried out on a MFP-1D (Asylum Research) as described in chapter 2. Solutions of proteins were produced by allowing protein to dissolve in pH 7.4 solutions of 10 mM sodium phosphate and 150 mM sodium chloride to a final protein concentration of 1 μM. The 1 μM solution of protein was then allowed to incubate with a ready-prepared surface of template-stripped gold (see chapter 2) overnight, to allow attachment of protein to the gold by thiolate attachments via the cysteine residues located at the carboxy terminal ends of the proteins. After incubation the surface was rinsed several times with pH 11.2 buffer. This was to dissociate and hence wash away any protein not directly attached to the gold surface. The alkaline pH of this buffer causes the large number of glutamic acid residues to become negatively charged, causing repulsion between adjacent proteins and dissociation of coiled-coil complexes.

For the experiments described in this chapter NP-type AFM cantilevers (Veeco) were used, having nominal spring constants of approximately 60 pN nm^{-1}. Before use, to remove any contaminants, cantilevers were cleaned by exposure for at least ten minutes to UV-light This causes the breakdown of any contaminants from packaging materials etc on the surface of the cantilevers, by direct action of the UV itself and also by the chemical action of ozone produced by reactions of oxygen in the air with UV light. Cantilevers were left otherwise untreated.

Prior to making force measurements the cantilevers were calibrated using their thermal excitation spectra to determine their spring constants as described in chapter 2. Force curves were produced by allowing the cantilever to come into contact with the sample surface to allow interaction between the probe tip and proteins on the surface. The cantilever was then retracted away from the surface to allow mechanical stretching of protein chains adhering to the probe. Raw data was collected as deflection versus z-displacement of the piezo, and subsequently converted to graphs of force versus tip movement as described in chapter 2. A minimum of 1000 force curves were produced for each condition and with each protein. Force curves were initially analysed using an Igor Pro software interface (Wavemetrics), to determine extension forces and distances. Observation of the forces at which the protein became disengaged from the probe at each pH allowed the assessment of whether the attachment was changing with pH. Curves which showed clear single molecule stretches with a single rupture event, with minimal non-specific interactions were then selected for further analysis. Curves which contained large non-specific interactions arising from the interaction between underlying surfaces can obscure part of any specific event, due to the time needed for the cantilever to snap back into position. Raw data for each selected curve was then exported as delimited text into an Excel spreadsheet to allow further analysis. Curves from the same protein and condition were normalised by adjusting the scaling on the distance axis so that they could be overlaid. This was to take account of the fact that the picking up of a protein chain on the cantilever tip is a non-specific event where

the protein may become attached at any point along its length. Scaling of the force curves allowed comparison between curves obtained in identical conditions. Each individual curve then had the WLC model fitted to it. This was carried out by adjusting the persistence length and contour length parameters until the sum of the squares of the differences between model and experimental force values were at a minimum.

3.3 Results and Discussion

3.3.1 AC_{10}ACys Extension Measurements

The AFM cantilever probe was repeatedly brought into and out of contact with the gold surface, with resultant force curves measured and corrected by the methods outlined in chapter 2. At the start of experiments force curves were taken on the gold surface prior to functionalisation with the AC_{10}ACys protein to serve as negative controls. With these measurements no specific force curves were observed. Example of single specific interactions are shown in Figure 3-3a. A specific interaction caused when a biomolecule is stretched typically has a curved profile and extends away from the surface. In these control measurements the approximately 90% of curves had no interaction between the surface and the probe, while the remaining curves displayed adhesion events typical of 'non-specific' surface interactions. A non-specific interaction which occurs between the underlying surfaces is typified by an adhesion event which is linear with the contact region of the force curve and does not extend away from the surface prior to detachment (Burnham and Colton 1989). An example non-specific interaction is illustrated in Figure 3-3b. This demonstrates that the surface, probe tip and buffer solutions were free of contaminants, such as polymers from packaging materials for the cantilevers, which may have given rise to the incorrect identification of specific force curves.

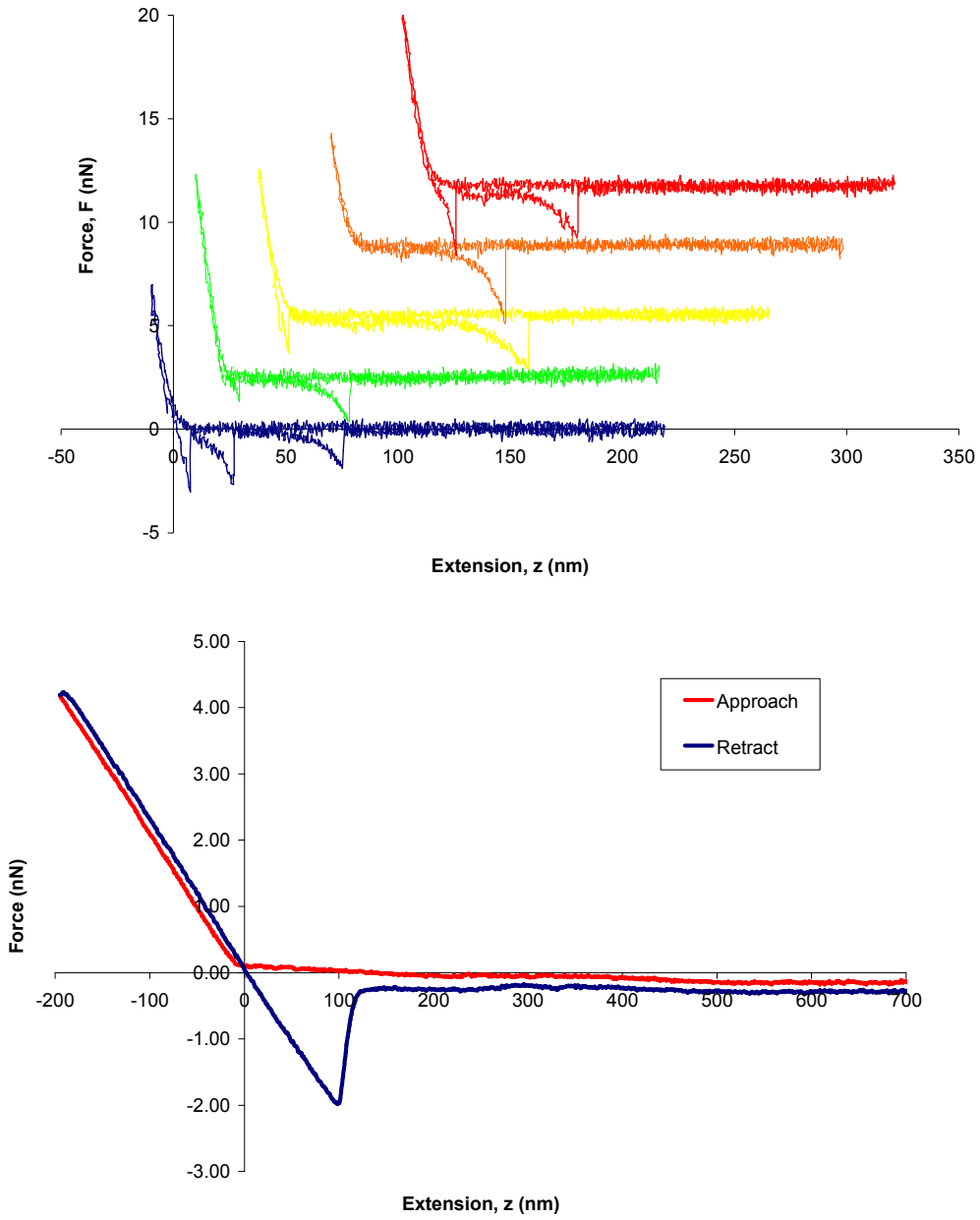

Figure 3-3: a) A series of example force extension curves obtained with $AC_{10}ACys$. As the protein is extended there is initially little resistance. As the protein becomes increasingly extended the force increases in a non-linear manner until the protein becomes dissociated from the tip with a rupture event. **b)** An example non-specific interaction between the tip and an underlying surface. Note that the negative force region is linear with the contact, indicating that it is adhesion at the surface.

After the surface was functionalised with the $AC_{10}ACys$ protein, measurements were taken in three different pH environments (pH 4.5, pH 7.4 and pH 11.2). The environmental pH was varied by using sodium phosphate solutions adjusted to different pH values using NaOH. During each experiment a minimum of one thousand measurements were taken for each pH condition. An example force extension curve representing the stretching of a single molecule taken from a surface functionalised with $AC_{10}ACys$ is shown in Figure 3-3. For clarity, only the retract trace is shown. As the cantilever tip leaves the surface (z extension is zero) there is no net force on the cantilever. As the protein becomes increasingly extended its resistance to further extension increases and results in a non-linear increase in force. This results in the characteristic curved appearance of the force curves. Eventually the protein becomes disengaged from the tip resulting in a sudden change from the maximum force reached to a net force on the cantilever of zero as it returns to its free level, at an extension of approximately 60 nm. As the carboxy-terminal end of the protein is anchored to the gold surface by a covalent thiol linkage, the rupture event is likely to always result from the parting of the protein chain from the tip and not the surface, as the protein is only attached to the tip by non-specific physisorption. Figure 3-4 shows histograms displaying the maximum force and extension length obtained for the observed specific interactions for one such experiment performed on $AC_{10}ACys$. In general it can be seen that the distributions for force have similar appearances for each pH, suggesting that the interactions between the probe and the protein is not altering with pH. The cantilever tip may interact with the protein at any point along its length, giving rise to the range of extension lengths observed. The majority of extensions fall well within the expected maximum contour length of 87.4 nm for $AC_{10}ACys$ calculated from a peptide bond length of 0.38 nm multiplied by the number of amino acid residues present in the protein. However, there are a small number of extensions above this value. It is possible that these may be due to adhesion events with proteins attached to raised features on the surface or possibly higher order assemblies of proteins. It

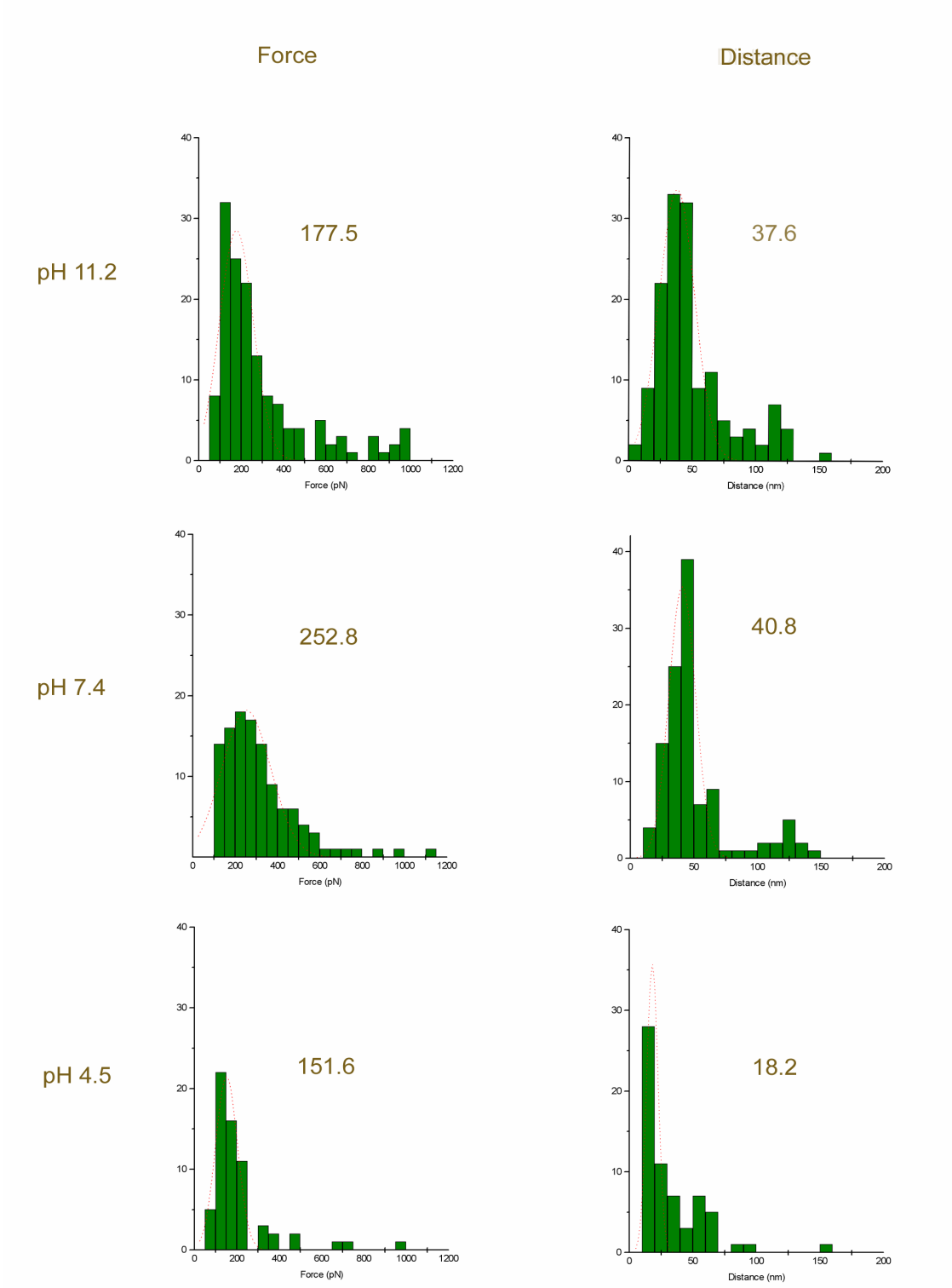

Figure 3-4: Histograms showing maximum forces (left) and distances (right) obtained from specific stretches of $AC_{10}ACys$ molecules with the AFM probe under different environmental pH regimes. The modal (peak) forces and extensions are indicated next to each histogram. Peak values were obtained by Gaussian fits, superimposed over each histogram.

is also apparent that the extension distances recorded at pH 4.5 seem to be considerably shorter than at the other pHs, with a mean distance of 18 nm compared with mean extensions of around 40 nm for pH 11.2 and 7.4. The protein contains a large number of acidic glutamic acid residues, both in the polyelectrolyte spacer region and in the leucine zipper sequences. At a pH of 4.5 only approximately 50 % will carry a negative charge, whereas at pH 7.4 over 99 % will be ionised. The electrostatic repulsion between these residues may be expected to cause the protein to adopt a more open and extended conformation, and hence for the same force applied a longer extension may be reached than for an uncharged protein chain. Such an increase in the extension would be expected to be reflected by an increase in *p* (Li and Witten 1995).

In previous intra-mechanical measurements carried out on $AC_{10}ACys$ chains (Stevens 2001; Stevens *et al.* 2002) small adhesion events were noted close to the surface, before mechanical stretching of single $AC_{10}ACys$ curves. It was conjectured that this represents the separation of the two leucine zipper regions as tension is applied to the molecule. In this study adhesion events were observed close to the surface, but were relatively large and inconsistent in size, varying both in length and in force between a few tens of piconewtons and up to one nanonewton. An example of such a curve is illustrated in Figure 3-5. Such adhesion events observed in this study are most probably due to adhesion between the tip and the protein-coated surface. This could consist of multiple attachments both directly to the tip and between the proteins being extended and other proteins on the surface.

The worm-like chain model (WLC) was fitted to all the selected curves by adjusting values of p and L_c until the sum of the squares of the differences between the model and the experimental data reached a minimum. A typical WLC model fit to a single experimental curve is shown in Figure 3-6.

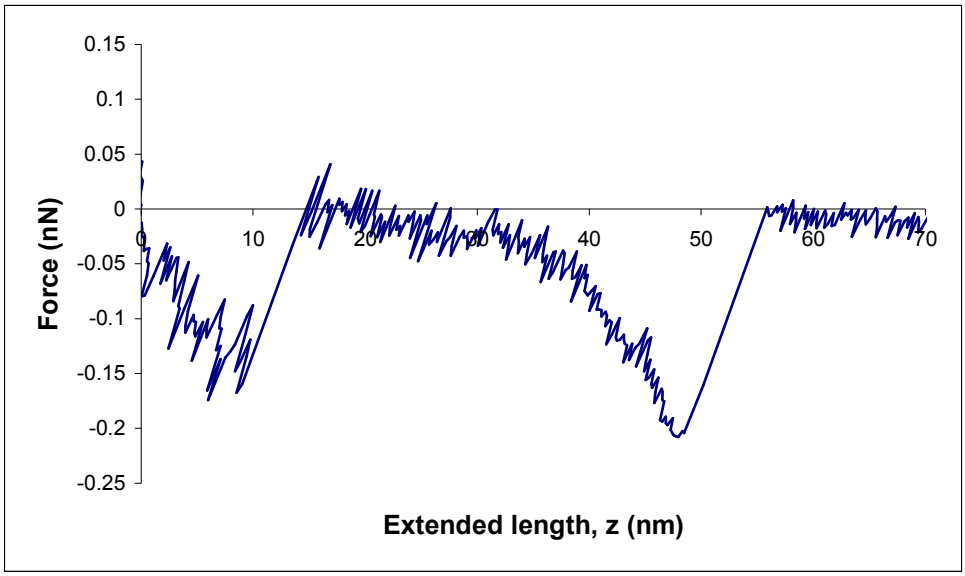

Figure 3-5: Example force extension curve showing adhesion close to the surface.

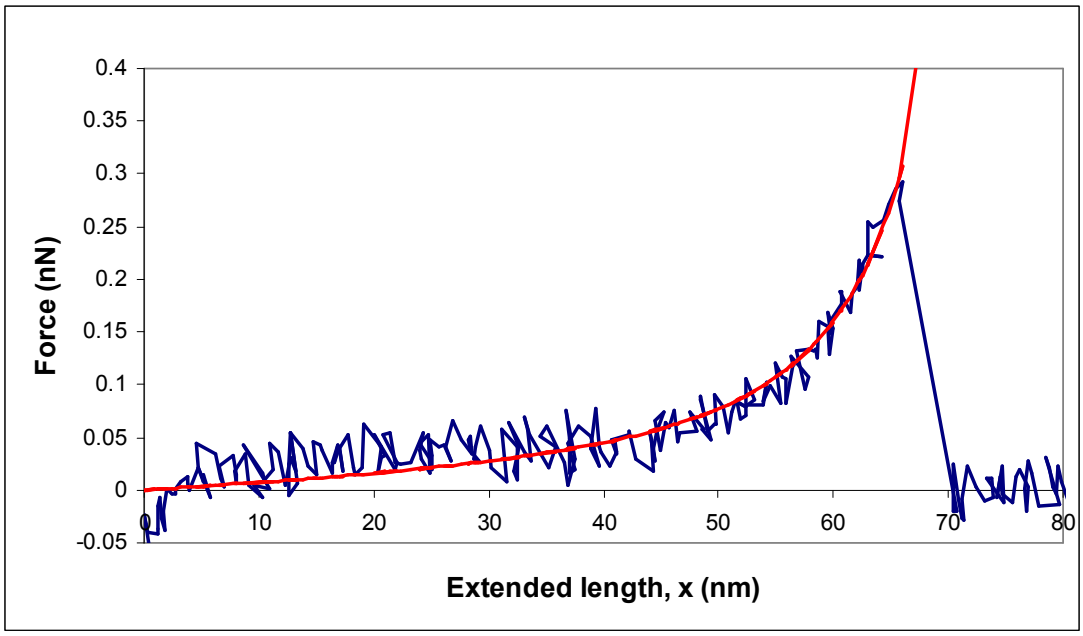

Figure 3-6: An example of a fit of the WLC model (red) to experimental data (blue). This particular fit has a persistence length of 0.11 nm.

Before applying WLC fits to force curve data, curves had to be selected for suitability according to the following criteria. They had to have single specific rupture events, indicating that only single proteins had been extended, and also have extensions within the maximum theoretical extension length of 87.4 nm. Finally, to ensure good fits, curves with rupture events of only 50 pN and greater were selected for further analysis. This was to ensure that the majority of the curve rose above the noise generated by the ambient thermal excitation of the cantilever (approximately 20 pN rms amplitude for the type of cantilevers used in these experiments). Selected curves were then overlaid upon each other by normalising them to the same contour length to take account that different lengths of the protein being stretched each time. To do this the extension lengths appearing on the x-axis were adjusted so that all the curves coincided at a force of 50 pN. This allowed the WLC model to be fitted to an ensemble of all the curves obtained for each pH. This has the advantage of increasing the number of data points that the model is fitted to, and thus increasing the reliability of any numbers obtained. Before this was carried out, WLC fits were also made to individual curves both before and after normalising, to ensure that persistence length values obtained were not affected by the scaling of the force curves. A comparison of the data from these two sets is shown in Figure 3-7. The data points are extended in a line originating at the abscissa, indicating that there is no difference between the data points. This gives a clear indication that the normalising procedure does not cause changes to the p values obtained when fitting the WLC to normalised curves.

An example of an ensemble of normalised and overlaid curves is shown in Figure 3-8. The ability to superimpose the curves in this way demonstrates that the curves are reproducible suggesting that the same type of stretching event is being observed each time, i.e. that they all result from the stretching of single polypeptide chains rather than resulting from stretches of varying numbers of polypeptide chains (Rief *et al.* 1997).

The persistence length data generated by the fits to the experimental data for the three different pHs is shown in Figure 3-9. The error bars indicated on the

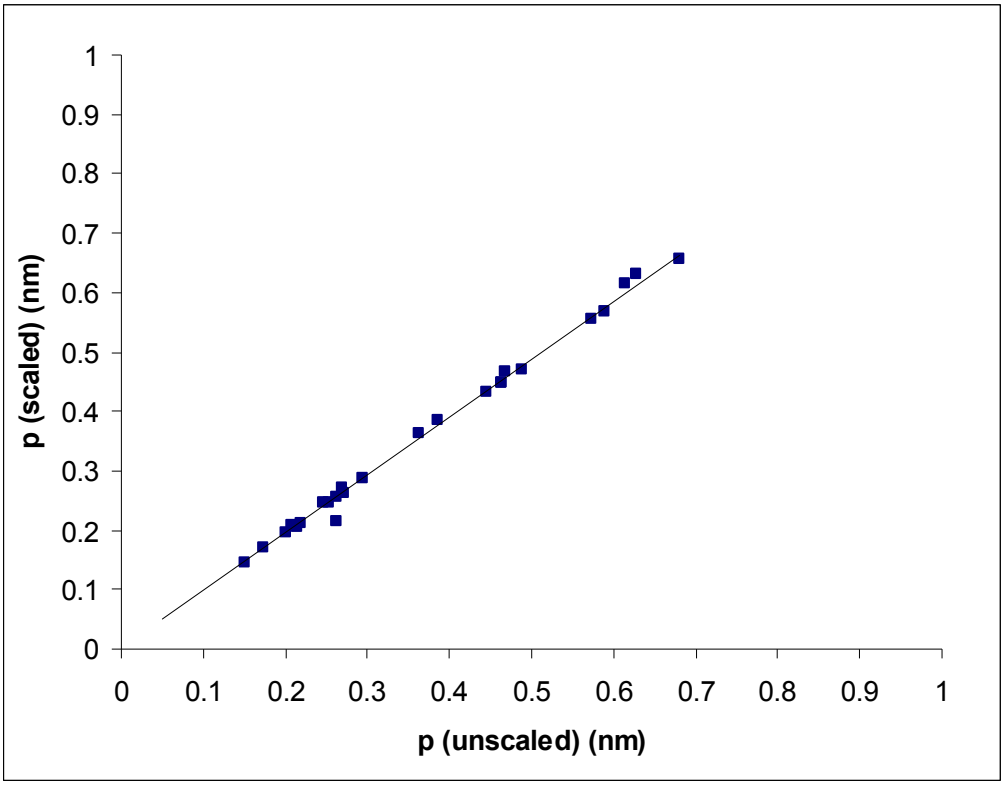

Figure 3-7: Comparison of persistence lengths generated by fits to the normalised and unscaled individual force curves. The diagonal line originating from the zero point of both axes indicates that there is no overall difference. The occasional slight divergence from this line is probably due to small errors generated during curve fitting.

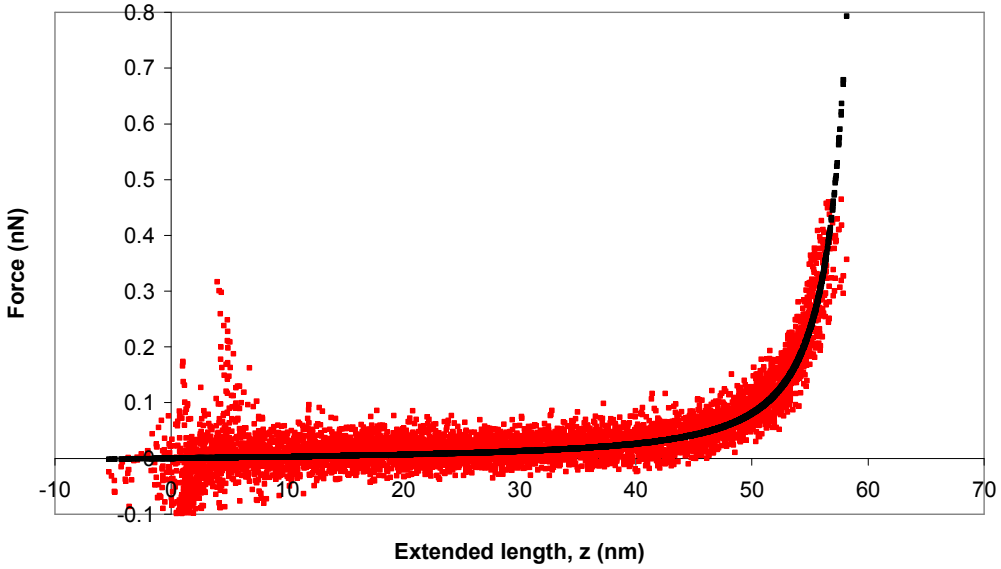

Figure 3-8: A series of force curves generated by the extension of single chains of $AC_{10}ACys$ overlaid by scaling to the same contour length, before fitting them to the WLC simultaneously. The data shown here are the force curves obtained at pH 11.2.

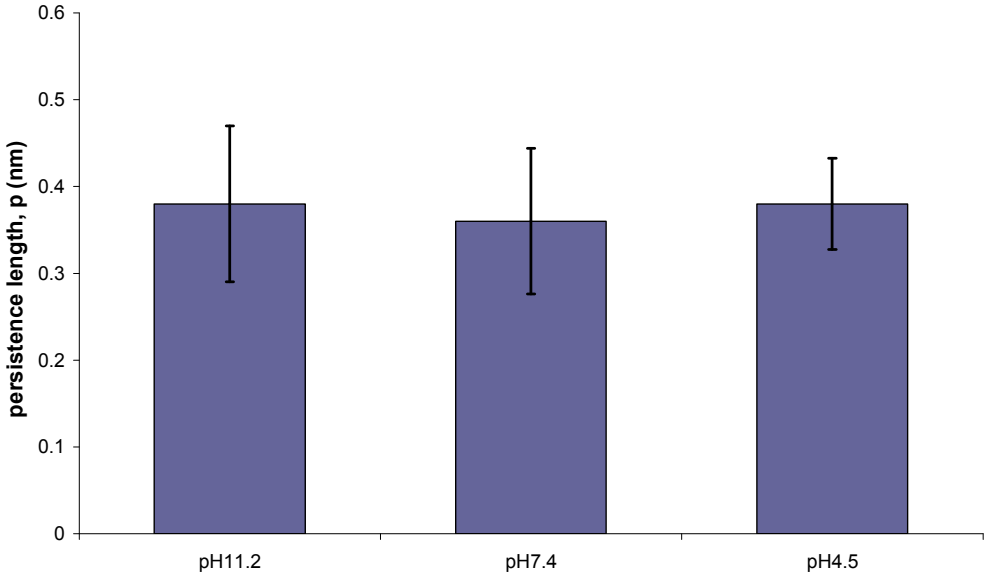

Figure 3-9: Persistence lengths for $AC_{10}ACys$ generated by fitting of the WLC model to ensembles of force curves. Bars represent standard deviation of the mean obtained from fits to the individual force curves.

graph are the standard deviations of the mean obtained from the fits to individual curves. Values calculated for *p* are approximately 0.38, a value in agreement with values quoted in the literature of 0.4 for proteins in a random coil conformation (Rief *et al.* 1997). No significant observable difference was observed in *p* with pH. Given the difference in average maximum extension length between the pH values studied, it would have been expected that an increase in *p* with an increase in pH would occur. However, it is possible that such a change was too subtle to be observed by the methods used here.

Due to the size of the surface adhesion events mentioned previously, combined with the strict criteria for selecting force curves suitable for further analysis using the WLC there was a high attrition rate with the number of curves suitable for analysis. From a total of two thousand force curves generated for each pH only a very small proportion were suitable for fitting of the WLC especially at low pH (n = 26 for pH11.2; n = 18 for pH7.4; and n = 8 for pH 4.5). It was decided to repeat these experiments using the longer protein AC_{28}ACys. The longer contour length of this protein was expected to generate longer stretches, which would make any initial adhesion at the surface interfere with a smaller proportion of the force curve. Also the longer extensions would provide force curves containing a greater amount of data points, allowing for a greater accuracy when fitting the WLC. In addition it might indicate whether the change in the maximum extension length previously observed for AC_{10}ACys would have an effect on the observed mechanical properties of the protein.

3.3.2 AC_{28}ACys Extension Measurements

The AC_{28}ACys protein is similar to the already examined AC_{10}ACys protein, but with a spacer region consisting of 28 repeating units instead of 10. This will have no affect on the macroscopic properties of the molecule, as there is

no change to the cross-linking leucine zipper regions. However, the change in length may effect its mechanical response to applied force.

Experiments were carried out according to the same methodology as with $AC_{10}ACys$ in section 3.3.1. Before the commencement of each experiment approximately fifty force curves were taken with the cleaned sample surface prior to functionalisation with the $AC_{28}ACys$ protein. No curves were obtained that had evidence of any specific stretching events, showing that the surface, cantilever tips and buffer solutions were free from contaminants that could produce force curves that could be confused with those obtained from $AC_{28}ACys$. Curves obtained from the bare surface showed either no interaction or only non-specific interactions with the underlying surface.

After surfaces were functionalised with the $AC_{28}ACys$ protein, surfaces were immersed in phosphate buffers of pH 11.2, 7.4 or 4.5. Force measurements were taken at each pH and the resultant force curves as well as the maximum force and extension distances were recorded. Figure 3-10 shows histograms generated for maximum extension and detachment forces for each of the measured pH values. As would be expected from a protein with a longer contour length, on average longer stretches were observed here than were observed with the $AC_{10}ACys$ protein, but remain within the maximum theoretical contour length of 150 nm for $AC_{28}ACys$. In addition the average extension distances seem to alter with pH in the same manner. At pH 4.5 a mean maximum extension distance of about 33 nm is observed, at pH 7.4 it is at 59 nm and pH 11.2 has a mean maximum extension of 82 nm. This is similar to the observation made with the $AC_{10}ACys$ protein. Also the distributions appear to be much broader at pH 7.4 and pH 11.2 than at pH 4.5, indicating a greater variance in extension distances for these pHs.

Curves suitable for fitting the WLC model to were selected according to the same criteria as for $AC_{10}ACys$. Again curves were scaled to the same contour length and were found to overlay well with each other, showing that they represented the same type of stretching event, i.e. that of single molecules of

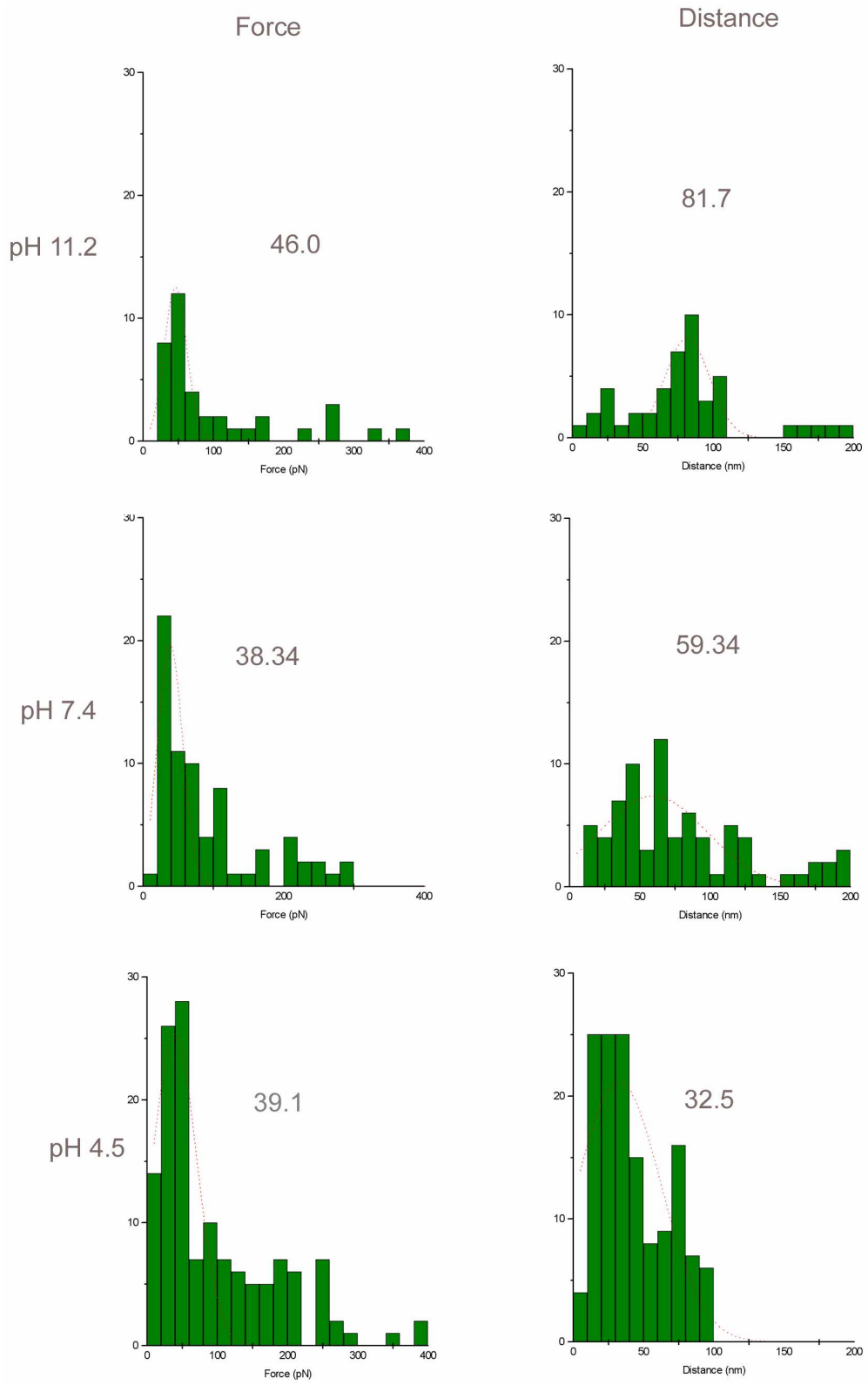

Figure 3-10: Histograms of maximum force and extension length generated by stretches of single $AC_{28}ACys$ molecules at different environmental pH. The peak force and extension are indicated next to each histogram.

$AC_{28}ACys$. An example of overlaid curves taken from measurements of $AC_{28}ACys$ at the same pH is shown in

Figure **3-11**. The WLC model was fitted to the curves according to the same procedure as with $AC_{10}ACys$ and the resultant data is shown in Figure 3-12. The *p* values were again calculated at 0.38 nm, as observed for $AC_{10}ACys$, suggesting that the increased length of the polyelectrolyte spacer region did not affect observations. In addition the persistence length was not altered by pH.

3.3.3 General Discussion

Both $AC_{10}ACys$ and $AC_{28}ACys$ showed an apparent decrease in the average maximum extended length at pH 4.5 when compared with pH 7.4 and 11.2. This is unlikely to be due to a change in the adhesion of the proteins to the probe as there appears to be no change in the appearance of the force distribution with pH. In addition the majority of maximum extension lengths suggest that the majority of probe-protein interactions occurred in the polyelectrolyte region for all pH values studied. It is therefore unlikely that the probe was interacting with the protein in a different way at each pH. A possible explanation is the change in charge of amino acid residues along its length. The $AC_{10}ACys$ and $AC_{28}ACys$ proteins contain a large number of residues which can carry a charge, most notably a preponderance of glutamic acid residues, both in the leucine zipper regions and in the central spacer region. In the absence of screening by ionic species in the water the presence of an overall charge on a polymer can cause it to become elongated due to repulsion effects (Li and Witten 1995). Glutamic acid side chains have a pK of 4.4 (Stryer 1988). At pH 4.5 only approximately 50 % of glutamic acid residues will be de-protonated and carry a negative charge, whereas at a pH of 7.4 and above almost all will be de-protonated. Therefore at high pH there will be a greater amount of repulsion between these residues than at low pH. As a result

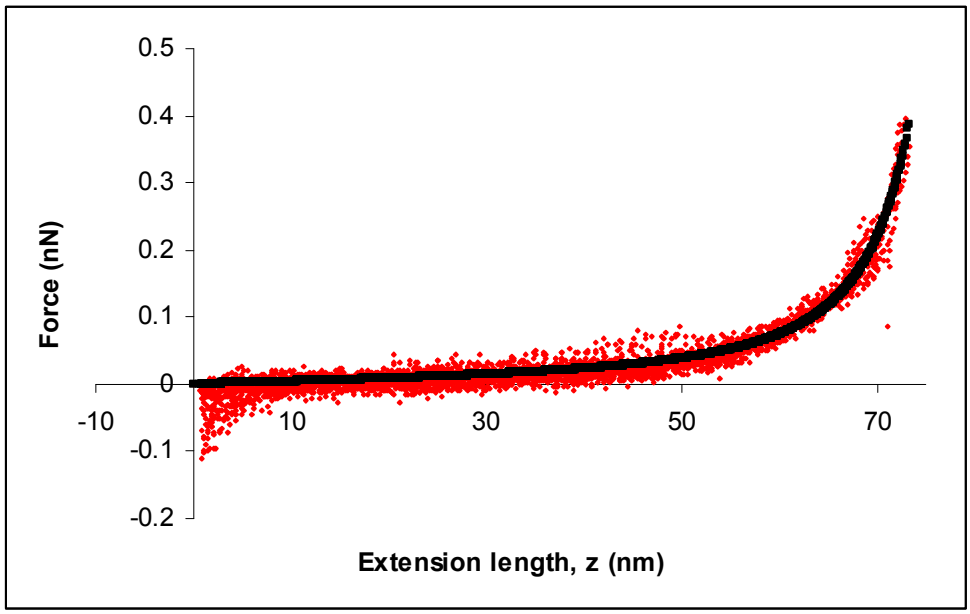

Figure 3-11: Force distance curves obtained from extension of $AC_{28}ACys$ protein scaled to the same contour length and overlaid. Superimposed (black) is the WLC fit to this data.

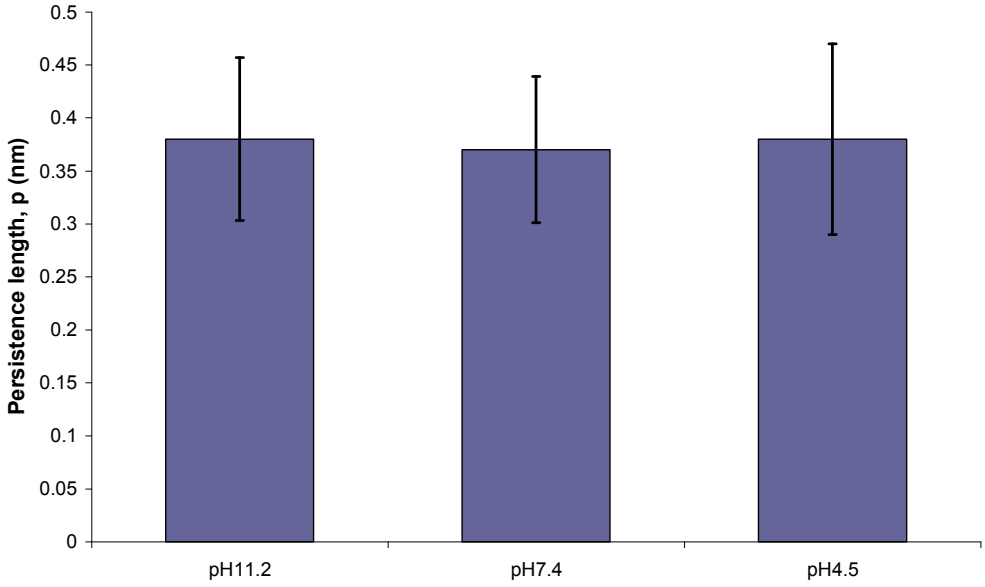

Figure 3-12: Persistence length values obtained from WLC model fits to force curves of the protein $AC_{28}ACys$.

it would be expected that any change in the flexibility of these proteins would be observed as pH changes between acid and neutral ranges, which is what is observed with the change in the average maximum extension lengths. This makes it likely that the behaviour observed is due to the repulsion between glutamic acid side chains along the length of the proteins causing them to become elongated. However, if this was the case then we would expect there to be a simultaneous alteration in the stiffness of the proteins, leading to changes in persistence length with pH, but this was not observed.

3.4 Conclusions

The entropic elasticity of two similar proteins in random coil configurations has been probed at three different pH regimes by the application of a mechanical extension. Measured values of *p* were comparable with values quoted in the literature of 0.4 nm for protein chains in a random coil conformation.

It was also observed in both proteins that the average maximum extension lengths were shorter at pH 4.5 than at both pH 7.4 and pH 11.2. This could also be caused by repulsive forces present between the negatively charged glutamic acid residues causing the proteins to more readily accept an elongated conformation. However, if this was the case it would be expected that there would be a concurrent increase in *p,* which was not observed. It is possible that any changes in *p* caused by changes in the charge of the proteins may be too subtle an effect to have been observed by the methods utilised here.

The information generated by the work described in this chapter has implications of two sorts. The observed elongation of the hydrogel proteins is consistent with an observed swelling of hydrogels as pH is increased (Petka 1997). Secondly it had implications for experiments described in later chapters where force is applied to biomolecular bonds. The compliance of proteins to a

mechanical force has implications to the rate at which force can be applied to biomolecular bonds within the proteins. This is discussed further in chapter 4.

Chapter 4 : Probing the Interaction Between Single Coiled-Coil Dimers using Force

4.1 Introduction

In this chapter a series of experiments are described to determine the behaviour of single coiled-coil dimers as environmental pH is varied, using the application of force to probe pH-related changes in their stability. The application of force to single biomolecular bonds is a subtle approach to probing the behaviour, particularly the kinetics, of long-lived non-covalent bonds. Many biological bonds have very long lifetimes, making the measurement of dissociation kinetics problematic. The application of force to these bonds serves to accelerate the dissociation kinetics, shortening the lifetime of these bonds.

Two coiled-coil forming proteins are examined by this approach, ACys and BCys. The intention of the work presented in this chapter was to probe changes in the stability of homodimers of these proteins, using force. In addition a new immobilisation strategy is employed using the co-functionalisation of surfaces with both protein and alcohol thiol molecules to cause proteins to be diluted on the surfaces and hence limit occurrence of multiple interactions. Dimers formed by the acidic protein ACys was expected to have greater stability at low pH than at high pH, with the converse true for homodimers of BCys. At all velocities examined ACys dimers dissociated at greater forces at pH 4.5 and

7.4 than at pH 11.2, demonstrating greater mechanical stability. At the single retract velocity at which BCys dimers were probed, dimers dissociated at a lower force at pH 4.5 than at the other two pH values, although the differences were less pronounced than for ACys.

By taking a dynamic approach and applying force at a range of rates, it was possible to extrapolate back to the zero force state to predict the natural dissociation rate of the bond. Before describing experiments it is necessary to present a summary of the theory behind this dynamic force technique.

4.1.1 Dynamic Force Spectroscopy

A range of instruments have been utilised in the application of force to biomolecular bonds, most notably the atomic force microscope (AFM) (Allen *et al.* 1997; Rief *et al.* 1997; Rief *et al.* 1999; Clausen-Schaumann *et al.* 2000; Allison *et al.* 2002), optical tweezers or laser optical traps (LOT) (Tskhovrebova *et al.* 1997), magnetic tweezers (MT) (Gosse and Croquette 2002; Danilowicz *et al.* 2003; Trepat *et al.* 2003) and the biomembrane force probe (BFP) (Evans and Ritchie 1997; Merkel *et al.* 1999; Nguyen-Duong *et al.* 2003). While the instruments used in each of these techniques at first appear to be very different to each other, they all apply force in a very similar manner. The biomolecular bond of interest is linked either by direct covalent attachment or via a polymer linker to a spring of some kind which acts as a transducing mechanism allow measurement of the response of the bond to force. In the case of AFM this is the silicon microcantilever; for LOT this is a potential well caused by the interaction of beams of coherent laser light, in which a bead is trapped; whilst with the BFP, a membrane capsule, such as a red blood cell, is used. In all cases a ramp of increasing force can be applied to the bond of interest via this transducing mechanism.

Application of force to probe the strength of biomolecular bonds has required the development of an analytical approach to evaluate the experimental data fully in order to generate meaningful information, such as dissociation kinetics.

This was pioneered by Evans and colleagues (Evans and Ritchie 1997) to encompass a dynamic approach where the force required to break chemical bonds is a function of the rate at which the force is applied. The groundwork for the analysis of the dynamic force spectra of single molecular bonds was laid by the theoretical work of Kramers (Kramers 1940) in the 1940's, which examined the behaviour of chemical bonds under thermal excitation in a harmonic well. By the application of force at a range of rates of loading of force several orders of magnitude apart it is possible to extrapolate back to the zero force regime and gain insight into the kinetics of the unloaded system. In addition information can be obtained which describes the energy landscapes for dissociation of bonds by the unmasking of previously hidden barriers and transition states.

4.1.1.1 Dissociation of Molecular Bonds Under Applied Force

All biomolecular interactions occur in a fluid environment and are thus subject to the Brownian motion that results from the thermal fluctuations of the surrounding solvent molecules. Collisions with the surrounding water molecules serve to provide energy allowing bonds to make attempts at escaping from a potential well. As a result the kinetics for dissociation of the bond are dominated by the viscous damping of the system (Kramers 1940; Evans 2001). The simplest situation that can be considered is escape from confinement by a single sharp energy barrier. Escape from the bound state can be conceptualised by a movement along a reaction coordinate from an energy minimum over a barrier via a saddle point in the energy surface (Evans and Ritchie 1997; Evans 1998). This is illustrated diagrammatically in Figure 4-1a. The energy minimum on the left hand side of the landscape represents the situation in the bound state. Movement to the right represents a progression towards an unbound state, but requires the negotiation of the energy barrier, E_b. Here E_0 represents the difference in energy between the bound and unbound states and ΔE_b is the difference between E_0 and E_b. As an external force is applied to the bond the energy landscape is tilted (Figure 4-1b) by a

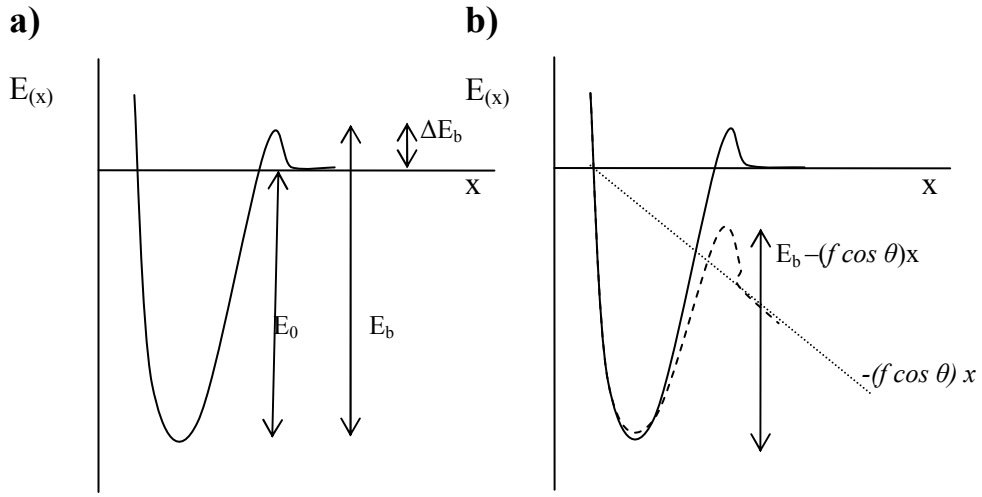

Figure 4-1: Notional energy landscape for a bond confined by a single sharp activation barrier along a scalar reaction coordinate, x. b) An external force applied to the bond, at an angle θ, has the effect of tilting the energy landscape by –f *cos θ* x and thus lowering the energy of the confining barrier.

mechanical potential – f cos θ x. This causes an exponential decrease in the energy barrier, E_b, which can have a dramatic effect on the kinetics of unbonding. The rate of unbonding (or off-rate) increases in an exponential manner with relation to an increase in applied force as first postulated by Bell (Bell 1978; Evans 2001). This leads to the following rate equation:

$$v_u(f) = v_0 \exp\left(\frac{fx_\beta}{k_B T}\right) = v_0 \exp\left(\frac{f}{f_\beta}\right) \qquad \textit{Equation 4-1}$$

Here v_0 is the rate of unbinding at zero force; f is force. k_B is Boltzmann's constant and T is absolute temperature, where the term k_bT represent the thermal energy in the system. Also included, f_β is the force scale, a measure of a resistance to force of a bond, and which can be directly related to the distance to the energy barrier along the reaction coordinate from the bound state, x_β, by the following relationship: $f_\beta = k_BT/x_\beta$ (Clarke and Williams 2005).

However, this single barrier model of a dissociation event is a simplified picture of what actually occurs in the majority of situations. Most biomolecular interactions consist of a large number of small interactions rather than one simple discreet bond, and it would thus follow that energy landscapes are much more rugged and complex than that described by a single barrier. In Figure 4-2 is sketched a notional energy landscape which contains two energy barriers of different heights. Under no force the second energy barrier is higher and thus dominates unbonding. Applied force will tilt the energy landscape, until eventually a force will be reached above which it is the first smaller inner barrier that becomes the dominant energy barrier. It can be predicted that the unbonding rate constant will rise in a force dependent stepwise manner, with the rate of transition increasing less and less with each increase, as subsequent barriers are overcome (Evans 1998).

For most experiments which employ force to accelerate the dissociation of chemical bonds, including those described in this thesis, the force applied is not constant, but rather a ramp of increasing force is applied to the bond. This

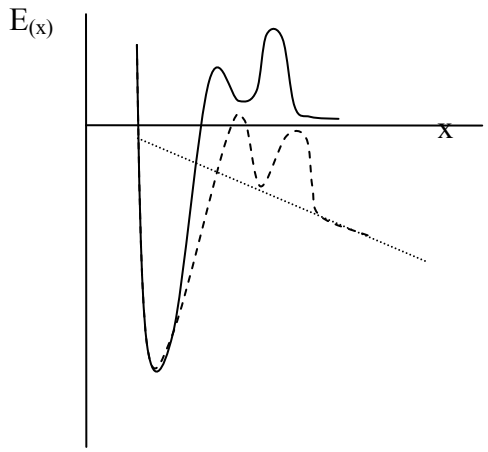

Figure 4-2: Energy landscape for a bond confined by two energy barriers. With no force present the second energy barrier is higher and thus is the dominant barrier to unbonding. As the energy landscape becomes tilted under an applied force the relative heights of the barriers change until eventually the first energy barrier becomes more prominent.

is a direct consequence of force being applied via a transducing mechanism. The rate with which force is applied to the bond, i.e. the loading rate, R_f, needs therefore to be considered. The loading rate consists of the stiffness of the system mediating the application of force, k (its 'spring constant'), multiplied by the velocity, v, with which the force is applied (for AFM measurements, this is simply the speed with which the probe is retracted), i.e. $R_f = kv$ (if ignoring the contribution of polymer linkers to the compliance of the system – see section 4.1.1.2 for further discussion). Retract velocities for AFM instruments can vary from about 10 nm s^{-1} to around 10 000 nm s^{-1} in principle. However in practical terms this is limited further. At high retract speeds hydrodynamic drag on the cantilever can cause it to become deflected, resulting in erroneous force values. In addition limitations of the instruments sampling speed leading to force curves consisting of relatively few data points, giving a practical upper velocity of approximately 5 000 nm s^{-1} at best. At the slower end of the scale, very low retract rates mean that the time taken to make a single force curve makes data acquisition very time-consuming, as well as increasing the likelihood that background interference, such as noise and unwanted vibrations. may disrupt the appearance of the curve, making measurement at velocities of less than 50 – 100 nm s^{-1} problematic. This, combined with the range of available spring constants for cantilevers suitable for force measurements of about 10 to 100 pN nm^{-1} give a range of possible loading rates of about 1000 to 500 000 pN s^{-1}, or about three orders of magnitude at best.

The time frame for the thermal oscillations of the biomolecules of interest is many orders of magnitude greater than the time frame over which force can be applied during an experiment. This means that during the application of force to a biomolecular bond a ligand can undergo very many attempts at escape. The probability of a bond surviving over the time frame with which force is applied is therefore not a simple function of time with a constant off-rate. The chances of a given bond becoming detached is a 1^{st} order kinetic process with a rate of dissociation dependent upon the time over which force is applied in addition to the size of the force (Evans and Ritchie 1997). As a result the

probability of bond failure within a short time interval can be described by the following equation:

$$p(t,f) = v(f)\exp\left\{-\int_{0\to t} v[f(t')]\cdot dt'\right\} \qquad \textit{Equation 4-2}$$

Where the exponential part of this equation describes the likelihood of the bond surviving for a time, t. As it is a ramp of increasing force that is being applied, where force increases in direct relation to time, force can be viewed as the independent variable instead of time. The probability density for unbonding as force is increased is given by (Evans 1998):

$$p(f) = (1/R_f)v_0(f)\exp\left[-(1/R_f)\int_{0\to f} v_0(f')df'\right] \qquad \textit{Equation 4-3}$$

Here we now have the probability of rupture related directly to both force and loading rate. These distributions of bond rupture probabilities results in a stochastic nature of bond rupture by force, where there is not a single force associated with the rupture of a bond at a particular loading rate, but rather a distribution of forces spread around a single maximum. This means that during experiments, even if there is negligible experimental error, a variety of forces will be measured for a particular condition, necessitating the acquisition of a large number of observations. The distribution of measured rupture forces is the result of the interaction of two phenomena: the exponential increase in failure of a bond as time, and hence force, increases and a sudden decline in bond survival as force further increases. As a result the strength of a bond, under a given rate of loading of force, is best described by the peak or most frequent (or modal) rupture force, f^* (Evans and Ritchie 1997; Evans 2001). With the aid of a few assumptions including that of a linear loading rate and the presence of a single sharp energy barrier an equation describing f^* in terms of loading rate can be used (Evans and Ritchie 1997; Clarke and Williams 2005):

$$f^* = f_\beta \left[\ln(R_f) - \ln(f_\beta v_0)\right] = \frac{k_B T}{x_\beta} \ln\left[\frac{R_f x_\beta}{k_B T v_0}\right] \qquad \textit{Equation 4-4}$$

From equation 4-4 it can be seen that a plot of f^* against the natural logarithm of R_f will yield a straight line with a slope of f_β. Extrapolation to the intercept on the x-axis where f^* is zero will allow the determination of the unloaded unbinding rate v_0 as at this point $R_f = f_\beta v_0$.

For the situation where there is more than one energy barrier in the energy landscape there will be several linear regimes on a plot of f^* versus the natural log of the loading rate. As crossover is achieved from one energy barrier being dominant to another, x_β and hence f_β will shift, leading to a visible alteration in the gradient of the slope (Evans 1998).

4.1.1.2 Application of Force Under Non-Linear Loading Conditions

For most experiments carried out using AFM, the assumption of a linear loading rate is not necessarily valid. The force is not mediated only through the linear spring of the cantilever, but also through the biomolecule itself, plus any polymer linkers used to attach them. Protein chains and polymer linkers are characteristically non-linear when it comes to describing their mechanical properties. As force is increased, their stiffness also increases. It is this non-linear behaviour that gives the typically curved force trace obtained when pulling on biomolecules or polymers. For the loading rate to be constant throughout a measurement the loading rate would have to be dominated by the stiffness of the cantilever. When springs are connected in series the stiffness of the resultant system as a whole can be described by the following relationship:

$$\frac{1}{k_t} = \frac{1}{k_1} + \frac{1}{k_2} \ldots \frac{1}{k_n} \qquad \textit{Equation 4-5}$$

for 1 to n springs arranged in series, where k_t is the force 'constant' of the total system. If a protein chain or polymer linker attaching the bond to the cantilever is similar in stiffness to or softer than the cantilever then the loading of force will be described to a large extent by the non-linear behaviour of the molecules. If the stiffness of the linkers is much less than the stiffness of the cantilever then the loading due to the cantilever will be insignificant, and loading will only be described by the changing stiffness of the linkers. From the literature and the work described in chapter 3 of this thesis, protein chains are known to be well described by the worm-like chain model (Rief *et al.* 1997), WLC (see chapter 3 and equation 3-1). From the WLC an approximation for the stiffness at a given force can be made (Clarke and Williams 2005):

$$k_{WLC} \approx 4\frac{k_B T}{pL_p}\left(\frac{pF}{k_B T}\right)^{3/2} \qquad \textit{Equation 4-6}$$

Where p is the persistence length and L_p is the contour length of the protein. So for a WLC polymer with L_p of 100 nm and a p of 0.4 nm at a typical force of around 50 pN the 'spring constant', or stiffness, of the protein chain is about 4.4 pN nm^{-1}. Using equation 4-5 for attachment of this protein in series with a cantilever of spring constant 50 pN nm^{-1} will give a system with a stiffness at this force of 4.0 pN nm^{-1}. Thus, for such a situation where the biomolecular bond of interest is connected to the cantilever by a protein or soft polymer linker the loading dynamics will be dominated by the behaviour of the protein. In short to understand the dynamic behaviour of a bond in response to force applied through such a system account needs to be taken of the non-linear loading of force.

One simple approximation that can be made is to use equation 4-6 to estimate the stiffness of the linker and cantilever system at the point of rupture for each force curve. This can then be used to estimate a more accurate loading rate than obtained from calculations using the cantilever stiffness alone. However, this is a relatively crude approximation, which only gives the maximum loading rate at the point of rupture, and does not take account of the changing aspect of the loading rate (Friedsam *et al.* 2003; Clarke and Williams 2005). An alternative description of f^* as force is applied by a WLC linker based upon the retract velocity is:

$$f^* \approx f_\beta \left[\ln\left(\frac{v_r}{v_\beta}\right) + \ln\left(\frac{f^*}{f_\beta} - \frac{3}{2}\right) + \frac{1}{2}\ln\left(\frac{f^*}{f_\beta}\right) \right] \qquad \textit{Equation 4-7}$$

$$v_\beta = \frac{L v_0}{4}\left(\frac{x_\beta}{p}\right)^{1/2} \qquad \textit{Equation 4-8}$$

Where v_r is the retract velocity. By altering f_β and v_β until the difference of theoretical values of f^* for a given v_0 to experimental values is minimised, it is possible to gain the true v_0 value, as long as persistence length and contour length values are known.

4.1.2 Proteins ACys and BCys

The proteins examined in the experiments in this chapter, ACys and BCys, are truncated versions of the hydrogel-forming proteins discussed in the introduction and in chapter 3. Both consist of a single leucine zipper region, with the sequence of residues in the core forming *a* and *d* positions based on the *jun* oncogene product (Petka 1997). Each leucine zipper region contains a total of 42 amino acids in length, consisting of 6 heptad repeats. The total

number of amino acid residues in each protein is 76. Both proteins contain a 6 nm long random coil configuration 'tail' towards the carboxy-terminal end of the leucine zipper, which is terminated by a cysteine residue. For the purposes of force measurements this tail makes a convenient linker, allowing conformational flexibility, with the cysteine residue acting as a convenient anchoring point for bonding to gold surfaces. In the case of ACys the leucine zipper is the acidic A helix whereas BCys contains the basic B helix.

4.1.3 Experimental Aims

Previously experiments have been carried out to use force to probe single interactions between homodimers of both ACys and BCys (Stevens 2001). However, no attempt was made to study the dynamic properties of these systems under applied force. In addition these experiments employed monolayers of these proteins, which may give rise to the formation of multiple coiled-coil interactions. Any situation where multiple interactions are being recorded is best avoided as this makes analysis of data extremely complex. The aim of the work described in this chapter was therefore to use a dynamic force spectroscopy approach to probe the change in behaviour of single homodimers as environmental pH was altered. It is through the pH-responsive interaction of the leucine zipper sequences of the hydrogel proteins that determines their macroscopic behaviour. It was envisaged that the probing of their behaviour on the individual level would shed light on how this behaviour was modulated.

In addition a new strategy was developed for the immobilisation of these proteins onto the surfaces by the co-incubation with a spacer molecule, to distribute the proteins on the surfaces more sparingly. This was in an attempt to limit the amount of interactions that could occur, making any that are observed more likely to be representative of single interactions only, by making measurements of specific interactions rare events.

4.2 Materials and Methods

Proteins ACys and BCys were produced in the laboratory of Prof. D. Tirrell (Division of Chemistry and Chemical Engineering, California Institute of Technology) by bacterial expression of novel genetic sequences (Petka 1997; Petka *et al.* 1998). Different pH environments were achieved by using solutions of 10 mM sodium phosphate, 150 mM sodium chloride, with pH adjusted using 5 M NaOH to a final pH of 4.5, 7.4 or 11.2.

Sample surfaces consisted of freshly prepared template-stripped gold surfaces. Ordinary cantilevers were first cleaned by exposure to ultraviolet light for 10 minutes to remove any contaminants coating their surfaces, before being coated in approximately a 30 nm thickness of gold using a sputter coater. To minimise the number of interactions observed and thus ensuring that measured force curves represented only single interactions, protein was diluted down on the sample surface and probe by the co-incubation of mercapto-undecanol as a hydrophilic spacer molecule at a ratio of protein to mercapto-undecanol of 1:100. Incubation solution was made up of the following: 200 µl of ACys solution (20 µM in pH 7.4 solution), 300 µl de-ionised H_2O, and 100 µl mercapto-undecanol solution (4 mM) in ethanol. This was made up to 2 ml by the addition of 100% ethanol, to give final concentrations of 2 µM ACys, 200 µM mercapto-undecanol in 75% v/v ethanol. Ethanol was required to be present in these concentrations to prevent the mercapto-undecanol from precipitating out of solution. The sample surfaces and gold-coated cantilevers were then immersed in the incubation solution overnight, to allow attachment to the surface via thiol bonds between sulfhydryl groups in the proteins and mercapto undecanol. Surfaces and cantilevers were then rinsed with several washes of de-ionised H_2O and pH 11.2 buffer to remove any molecules not covalently bound to the surface, to ensure a coating of a single monolayer only. An diagram illustrating the experimental set-up is shown in Figure 4-3.

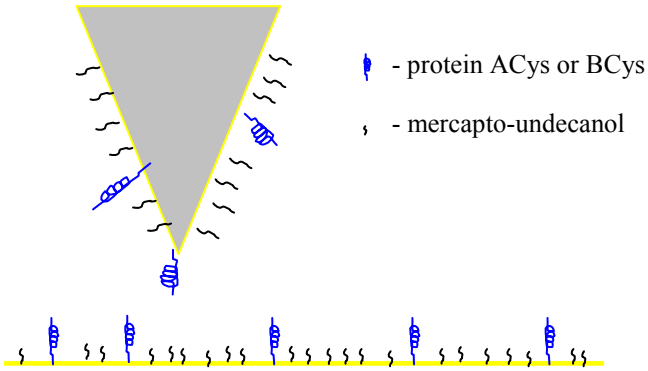

Figure 4-3: Diagram of experimental set-up. Protein (either ACys or BCys) is immobilised onto a gold-coated AFM probe or surface along with a hydrophilic spacer molecule (mercapto-undecanol) to dilute protein coverage and hence reduce likelihood of multiple interactions occurring.

AFM cantilevers were calibrated and their spring constants calculated from their thermal excitation spectrum (Hutter and Bechhoefer 1993). All force measurements were undertaken using an MFP-1D (Asylum Research) as detailed in Chapter 2, in a liquid environment. After correcting force curves to display force versus probe surface separation the maximum (rupture) force and maximum extensions for each curve were measured.

4.4 Results and Discussion

Force measurements were obtained between homodimers of both ACys and BCys. In the case of ACys the measurements were carried out dynamically at a range of pulling speeds to access changes in the kinetic stability of single dimers when subjected to forces under different loading rate conditions, and in environments of different pH. Measurements have been made previously of interactions between surfaces and probes coated in monolayers of ACys at different pH (Stevens 2001) but no attempt has previously been made to access the extra information that can be obtained through a dynamic approach.

To ensure that forces measured were specific forces between the proteins of interest and not interactions between protein and the underlying surface, protein and mercapto-undecanol or interactions between mercapto-undecanol molecules a series of control measurements were carried out. These consisted of measurements between a tip functionalised with protein plus mercapto-undecanol and a surface coated with a monolayer of mercapto-undecanol alone. Typically when protein was present on both the surface and the probe between 7 and 10 % of approach-retract cycles yielded a force trace which was considered to be a specific interaction, i.e. the retract region of the trace contained a section where the cantilever was deflected towards the surface in a non-linear manner before a sharp rupture event. An example specific force curve, obtained from the rupture of an ACys homodimer, is shown in Figure 4-4 with point at which measurements are taken indicated. On the other hand

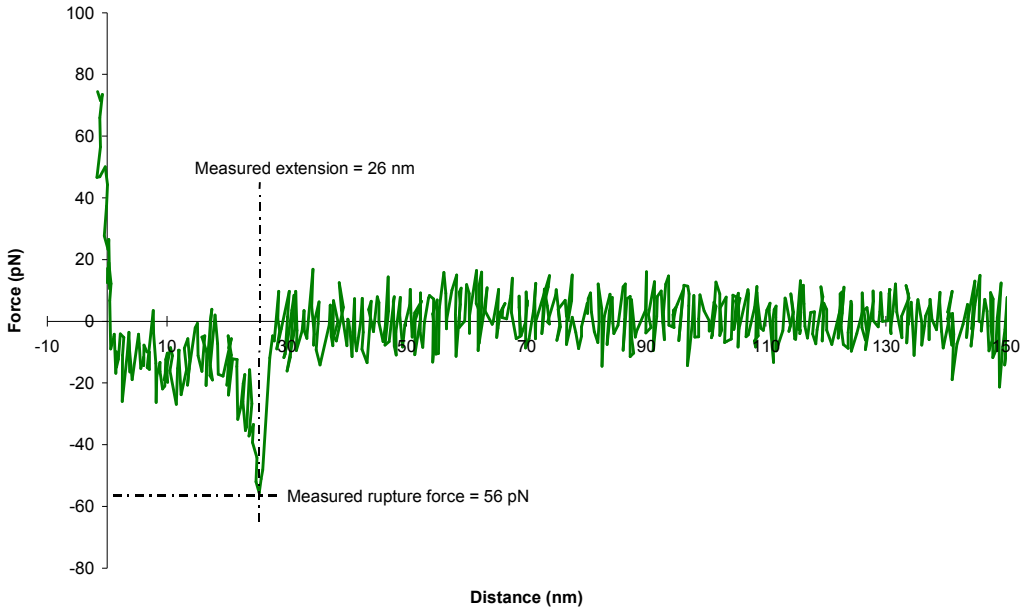

Figure 4-4: An example of a specific force extension curve generated between ACys homodimers, corrected to show force against actual tip-sample separation. Dotted lines cross at point at which measurements are taken from. Here a maximum, rupture, force is measured at 56 pN with an extension distance of 26 nm.

when the surface was coated with mercapto-undecanol alone specific force curves were a rare event, comprising less than 0.2 % of force curves obtained. This demonstrates that of the curves considered few are the products of an interaction that was not the protein-protein interaction intended to be measured. With regard to the few interactions that were seen in the control conditions there are a number of possible explanations that may account for them. Firstly there could be interaction between protein on the cantilever probe and the mercapto-undecanol on the surface. This could be between hydrophobic groups on the protein (such as leucine side-chains) and the hydrophobic chains of the mercapto-undecanol. It is also possible for the protein on the probe to be pressed into the surface with sufficient force to push it through the monolayer of mercapto-undecanol and allow it to interact with the surface in a non-specific manner. However, the small proportion of undesirable interactions measured suggest that they have no significant effect on the data.

For this type of experiment it is important to ensure that only single interactions occur. The measurement of multiple simultaneous bond rupture events complicates the situation somewhat and makes any analysis problematic (Williams 2003). While only force curves that visibly demonstrated a single detachment were analysed, a method of verifying that only single attachments are occurring is to obtain a low frequency of stretch-rupture events. If a proportion of only 1 in 10 approach-retract cycles results in the generation of a specific stretch-rupture event then the probability that an event will be representative of a single rupture is greater than 0.9 (Evans *et al.* 2001). If greater than 10 % of touches on the surface result in a specific event, then the chances of multiple attachments occurring increases significantly. To ensure that only a small proportion of attachment events occurred, protein was co-incubated on the surface with mercapto-undecanol at a ratio of 1:100 protein : undecanol, to dilute the concentration of protein on the surface. As none of the experiments undertaken in this work generated a proportion of stretch-rupture events greater than 10 % (in most experiments the value was closer to 7 %), it

is safe to conclude that the majority of measured events were the result of the dissociation of a single coiled-coil dimer.

4.4.1 Force Measurements Between ACys Homodimers

Rupture forces and maximum extension lengths for each force curve obtained with ACys homodimers were measured at a range of different probe retract velocities. As the speed with which the probe approaches the surface does not play a part in interactions it was kept constant throughout experiments at 2000 nm s^{1}. Distributions of rupture forces for each condition are presented as histograms in Figure 4-5 (for pH 7.4 data), Figure 4-6 (pH 4.5) and Figure 4-7 (pH 11.2). In previous studies undertaken by Stevens (Stevens 2001), interactions between cantilevers and surfaces coated with ACys were undertaken at a single retract velocity of 1000 nm s^{-1}. As pH was increased in that study the adhesive forces also decreased, accompanied by a decrease in width of force distributions. In this work the same trend is noticed with comparable forces. This demonstrates that using the different surface preparation approach in this study has not negatively affected the observed relationship between force and pH.

In these experiments at pH 7.4 and pH 4.5 the peak of the histograms moves to the left as the retract velocity decreases. At pH 11.2, for the range of retract rates measured, the forces were clearly much lower than for pH 7.4 and 4.5. This made it difficult to obtain data as the forces measured were close to the lower measurement limit for the type of cantilevers used (approximately 20 pN) due to thermal fluctuations of the cantilever. For this reason at pH 11.2 further measurements were carried out using a 'Park' type cantilever (MCLT-AUHW, Veeco, Santa Barbera, CA.), which has both a much lower spring constant (with a nominal value of 12 pN nm^{-1}) and less noise (~ 15 pN). In Figure 4-8 are histograms of the rupture forces measured between homodimers

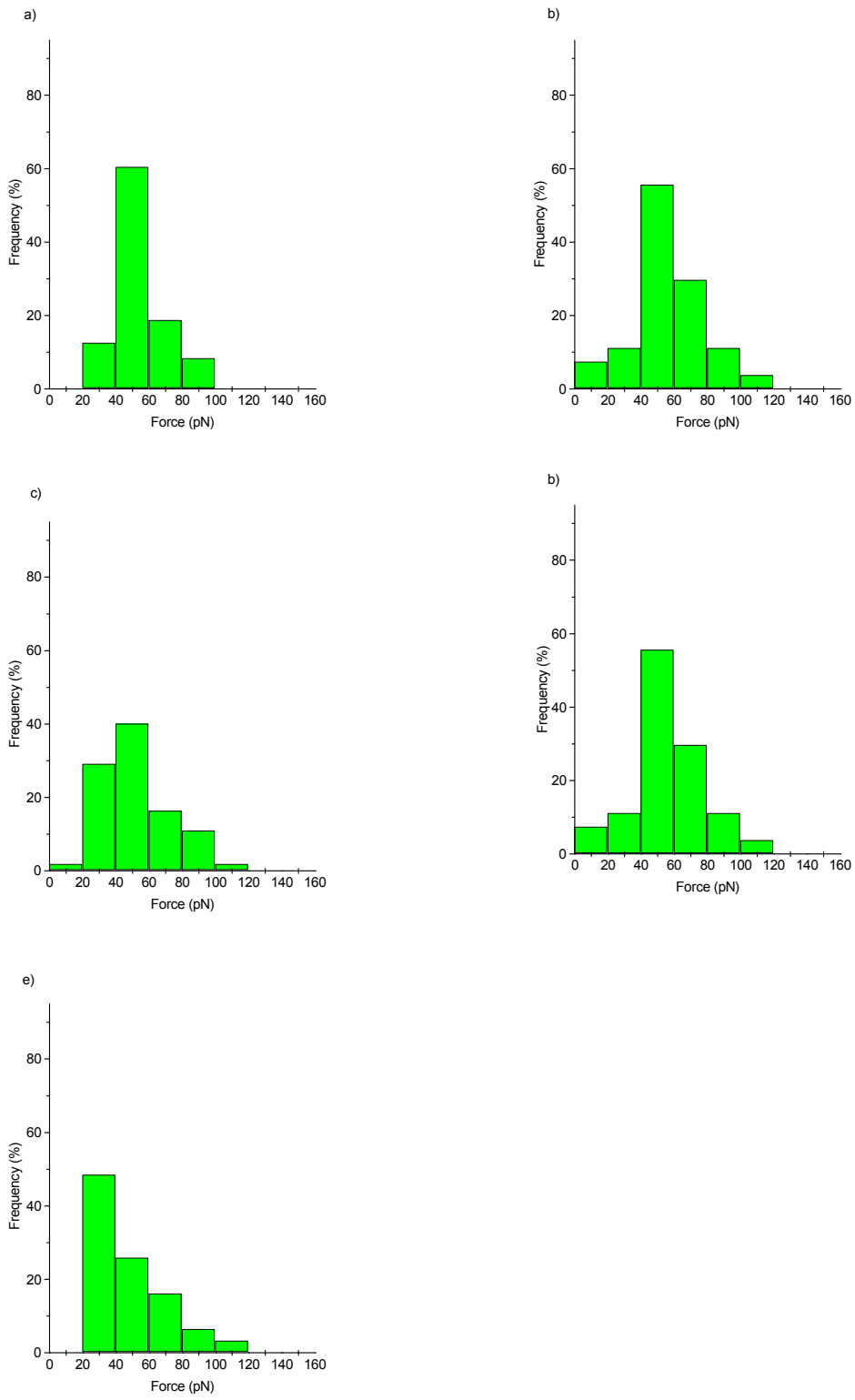

Figure 4-5: Histograms of rupture forces obtained for interactions of dimers of ACys at pH 7.4. Superimposed over the individual histograms are Gaussian fits to the data. Retract velocities are: a), b) 2000 nm s^{-1}; c) 500 nm s^{-1}; d) 400 nm s^{-1}; e) 100 nm s^{-1}.

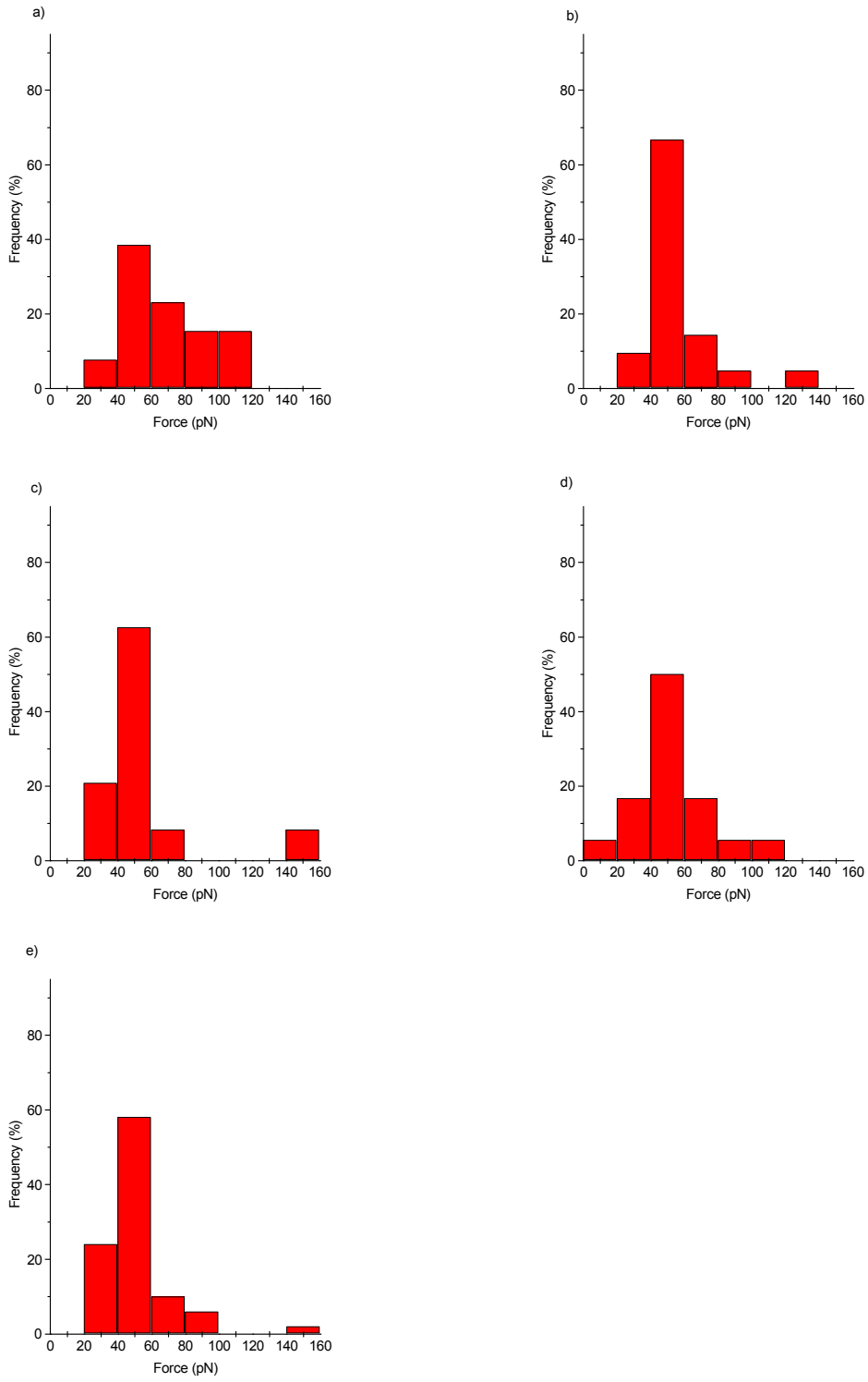

Figure 4-6: Histograms of rupture forces obtained between homodimers of ACys at pH 4.5. Curves superimposed over the histograms are Gaussian fits to the data. The retract velocities are: a) 5000 nm s^{-1}; b),c) 2000nm s^{-1}; d) 500 nm s^{-1}; e) 400 nm s^{-1}.

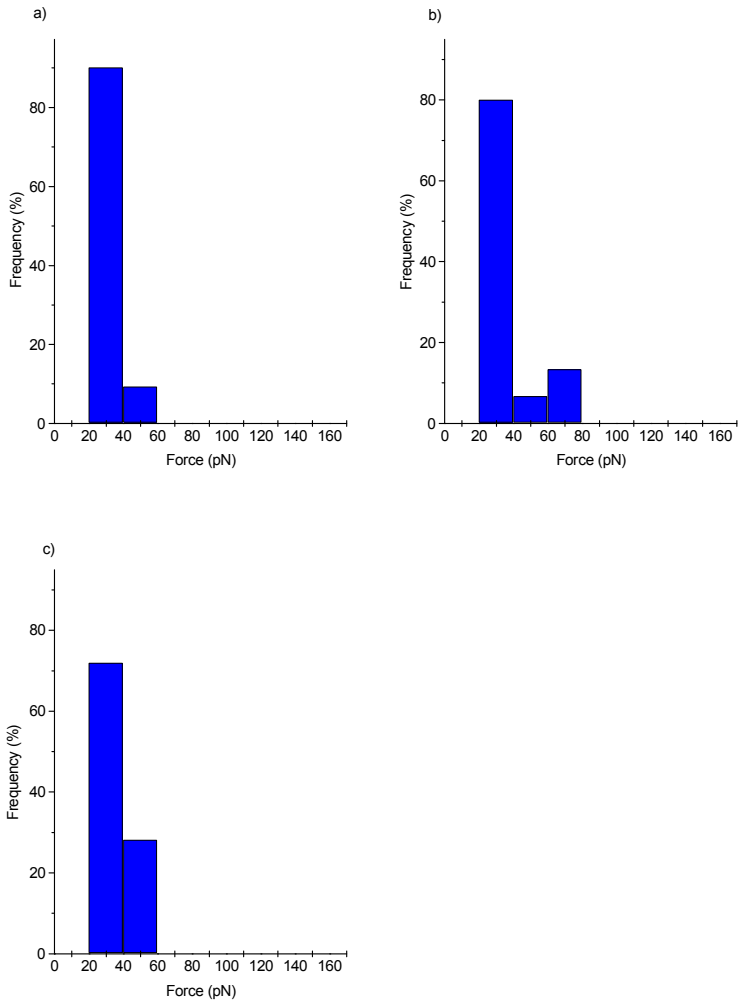

Figure 4-7: Histograms of rupture force data measured between dimers of ACys molecules at pH 11.2, using 'NP' type cantilevers. Many of the measurements made at this pH are close to the lower measurement limit for this type of cantilever due to thermal fluctuations at approximately 20 pN. Retract velocities are a) 5000 nm s^{-1}, b) 2000 nm s^{-1} and c) 1000 nm s^{-1}.

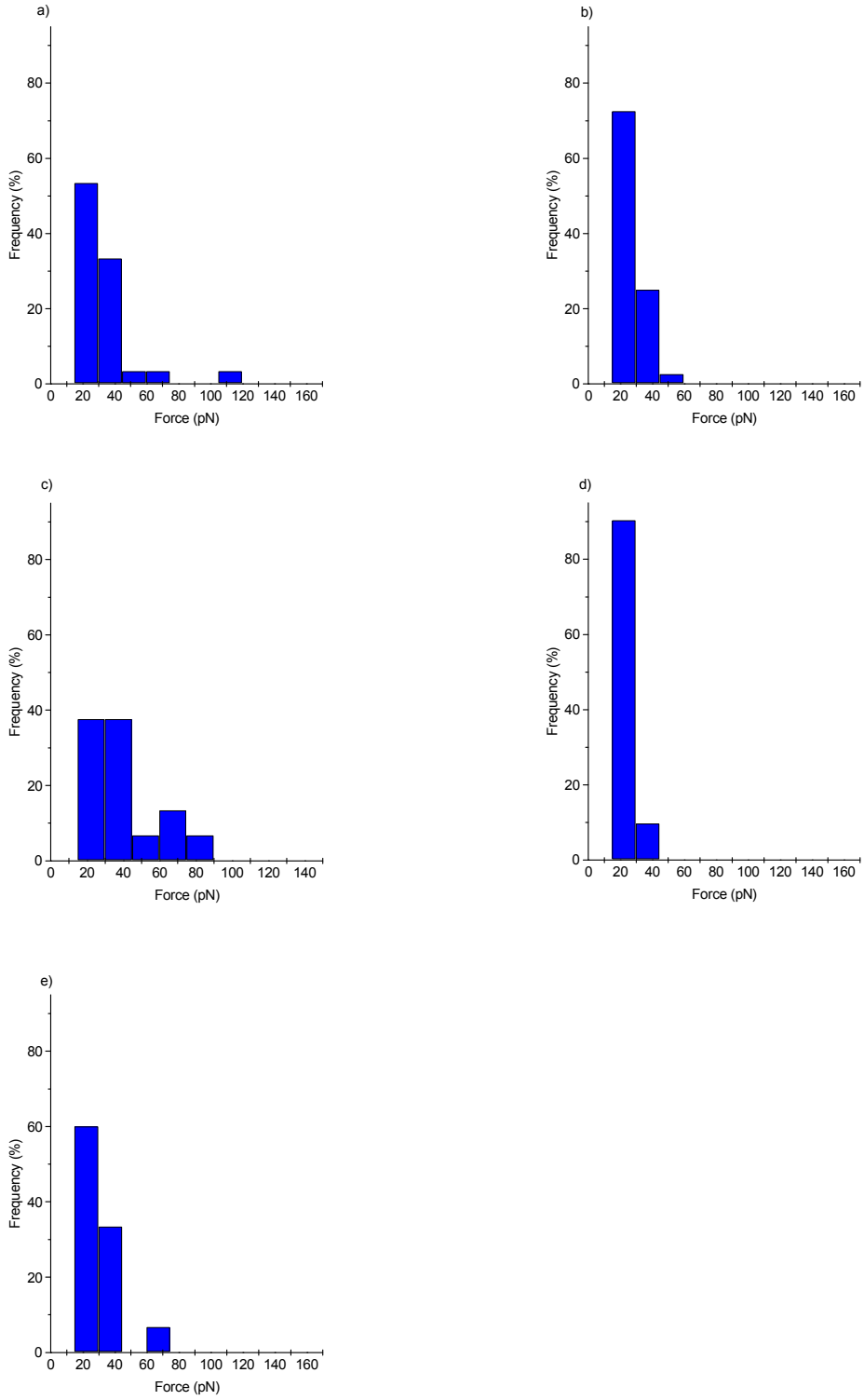

Figure 4-8: Histograms of rupture forces measured between ACys homodimers at pH 11.2. Velocities for each histogram are: a) 5000nm s^{-1}; b) 2000 nm s^{-1}; c) 500 nm s^{-1}; d) 100 nm s^{-1}; e) 50 nm s^{-1}. Bin sizes used here are 15 pN, to reflect the lower noise of this type of cantilever.

of ACys at pH 11.2 using this softer cantilever. In all cases the bin size for the histograms was the approximate value for the cantilever noise (20 pN for NP cantilevers, 15 pN for MCLT-AUHW cantilevers).

In order to determine the most frequent (modal) rupture force for each set of measurements the Gaussian distributions based upon the distributions of the histograms cannot be relied upon, as small changes to the arbitrary binning size can give large changes in the modal values obtained. Instead software developed by P.M. Williams (LBSA, University of Nottingham) was used (FDist) which assumes that each force measured is at the centre of a Gaussian distribution with a width equal to that of the cantilever noise. Gaussians for all forces measured are then summed and the mode force where the value of the sum is at its greatest is acquired (Clarke and Williams 2005).

In Figure 4-9 the modal rupture forces for measurements made at all three pH values are plotted versus retract velocity. For all of the retract velocities examined modal rupture forces are higher at pH 7.4 and 4.5 than for pH 11.2, suggesting that at these retract rates the coiled-coil dimers are more stable and resistant to force. At pH 7.4 as the retract velocity is increased, the force needed to rupture the coiled-coil dimers also increases. This behaviour is closely imitated at pH 4.5. The dependence of the observed rupture forces upon the retract velocity (and hence loading rate) suggests that at these two pH values the separation of the dimers by force is in accordance with the theory outlined in section 4.1.1. In other words it appears that we are observing force-induced dissociation across a single energy barrier.

As the short 6 nm random coil protein sequence tethering each ACys molecule to the surface will act as a non-linear spring, the static loading rate approach described by equation 4-4 was not considered appropriate to obtain values for the off rate and force scale for these experiments. To obtain these values software developed by Williams (LBSA, University of Nottingham) was used. The software fitted equation 4-7 to the experimental data by the adjustment of the v_β and f_β parameters for each v_r value obtained until the square of the difference

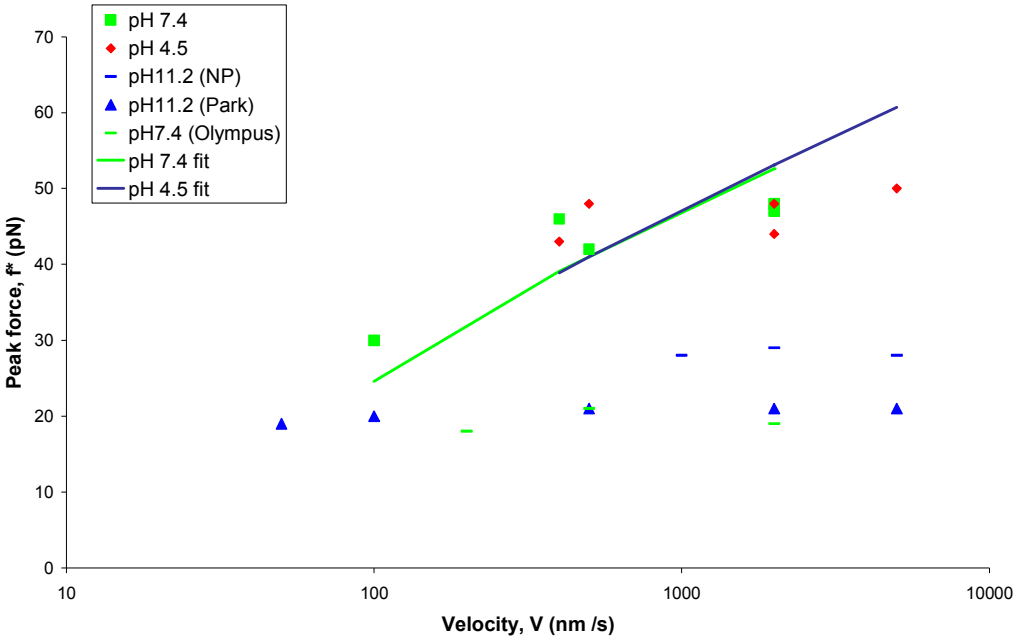

Figure 4-9: Plot of most common rupture force (f*) versus cantilever retract velocity for each pH measured. As the measurements at pH 11.2 using the 'NP' cantilever are relatively close to the lower measurement limit due to noise (approx. 20 pN) measurements for this pH were repeated using a softer 'Park' type cantilever with a lower noise threshold (approx. 15 pN).

between the experimental and theoretical values of f^* were minimised. This process generated f_β values for the pH 4.5 and 7.4 dissociation under force of 5 pN (standard deviation +/-0.6) and 6 pN (+/- 0.4) respectively. Using the relationship $x_\beta = k_BT/f_\beta$ the x_β values were calculated as 0.8 nm (+/- 0.07 nm) and 0.7 nm (+/- 0.04 nm) for pH 4.5 and pH 7.4 respectively. This suggests that the slopes of the force spectrum and distances along the energy landscape to the main barrier to dissociation are comparable at both pH 4.5 and pH 7.4, with a barrier to dissociation at 0.7 to 0.8 nm along the dissociation coordinates from the energy minima of the bound state.

To calculate the natural off rate under zero force (v_0) for the energy barrier being probed, further analysis was required, taking into account the non-linear WLC loading of force. Using equation 4-8, v_0 for the dimers could be calculated. This required the L_c and p values for the protein. For L_c a value of 12 nm was used, which is the combined contour lengths of the random coil sections linking both proteins to the surfaces. In chapter 3 a value for p similar to the literature quoted value of 0.4 nm was obtained, hence this is the value of p which was used for this purpose. For pH 7.4 a value for v_0 of 1.78 s^{-1} (S.D. +/- 0.11) was calculated, while the data from pH 4.5 observations yielded a value of 1.73 s^{-1} (+/- 0.12), with five data points for each pH. These values are very close and again suggest that the homodimers behave in the same way under forced dissociation for these two pH values.

At pH 11.2 however, a very different behaviour is observed in response to the application of force. As the retract velocity was increased, very little change in f^* was seen for the observations made with both types of cantilever, leading to the formation of a plateau in the DFS plot, i.e. the force needed to separate the dimers had no apparent dependence on the retract rate. Unfortunately, because of this the analytical approach outlined in the introduction and used to gain v_0 values for the dimers at pH 7.4 and 4.5 is not appropriate and cannot be used to estimate v_0 in this case.

At low rates of force loading a transition can occur from force-induced or far from equilibrium dissociation, to spontaneous or near-equilibrium dissociation. The

force applied to a bond by a probe diminishes with increasing distance, eventually creating a capture well. This capture well enables rebinding of the bond under force. A threshold force defines the point at which a switch is made from near-equilibrium to far from equilibrium measurements. To allow a complete severance of the bond under stress the force must rise above this threshold, which is dependent both on the stiffness of the linkage and the equilibrium constant (K_{eq}) of the bond. Far-from equilibrium measurements are made once the probe velocity is high enough to create forces greater than the threshold force (Evans 2001).

In the literature there is an account of experimental observations of the cross-over between spontaneous or near-equilibrium and force-induced bond dissociation, carried out by Simpson and colleagues (Simpson *et al.* 1999). Measurements were made of rupture forces for single protein A-IgG bonds at a range of loading rates. At high loading rates, broad distributions were observed with clear maxima. At low loading rates (≤ 27 pN nm^{-1}) the shape of the distributions changed to forces smoothly decaying from an initial maximum. The distributions observed here at pH 11.2 are very similar in appearance to those observed by Simpson *et al*, *i.e.* they consist of a decay from an initial maximum, rather than increasing towards a central maximum. As has been mentioned previously the increase in the amount of overall charge in the core-flanking *e* and *g* positions of the coiled-coil assembly with increased pH leads to a destabilisation of the helix. This destabilisation is likely to be manifested as a decrease in the characteristic lifetime of the dimer, causing a shift in the K_{eq} of the dimer. The characteristic threshold at which the crossover from near-equilibrium to force-induced dissociation is observed is dependent upon both the stiffness of the linkage and the equilibrium constant ($K_{eq}= t_{off}/t_{on}$). It therefore follows as possible that at the high pH of 11.2 the K_{eq} of the coiled-coil assemblies has shifted relative to the other pHs leading to a change in threshold. In other words a much greater probe velocity is needed to make the transition to far from equilibrium observations. Such a probe velocity is outside the range with which it is practicable to make measurements using the AFM.

In addition a stiffer linkage can also result in a higher threshold force (i.e. that at which the plateau is observed). This may account for the higher forces observed with the stiffer 'NP' type cantilevers compared with the 'Park' cantilevers,

although it must be remembered that the noise threshold is different for these cantilevers, which may also affect the forces measured. Calculating the effective linkage stiffness (combined stiffness of cantilever and protein) at the respective plateau forces for each type of cantilever gives values of 4.2 pN nm^{-1} for the 'Park' type cantilever and 9.9 pN nm^{-1} for the 'NP' type cantilever, demonstrating that the effective linkage stiffness is different for each cantilever. However, it must be borne in mind that the noise threshold is different for each type of cantilever. If the threshold force to far from equilibrium dissociation is below the measurement threshold of the cantilever then it will be this difference in noise that will account the different forces measured between these two cantilevers. Indeed it is quite likely that for all of these measurements at pH 11.2, the near-equilibrium threshold may be below, and hence masked by, the noise of the cantilever.

Interestingly, the pH 7.4 measurement made at the lowest probe retract velocity (Figure 4-5 e) also shows a steady decrease, consistent with measurements at near-equilibrium. The peak force at this probe velocity is similar to that measured at pH 11.2 with the NP cantilever, (although this may also be due to having a similar thermal noise threshold). Some additional measurements henceforth were taken using diving board shaped 'Biolever' type cantilevers (Olympus UK Ltd. London). These cantilevers are very soft (nominal k = 7 pN nm^{-1}) and have a still lower noise threshold (~ 10 pN). Histograms of rupture forces measured at probe velocities of 2000, 500 and 200 nm s^{-1} are shown in Figure 4-10. These histograms again have the decreasing distribution that would be expected with near to equilibrium measurements. As these cantilevers are so soft, the cantilevers in this case would have an effect on the loading rate (system stiffness multiplied by velocity). Therefore for the same velocity range, the loading rate is much lower, than measured with the stiffer NP cantilevers.

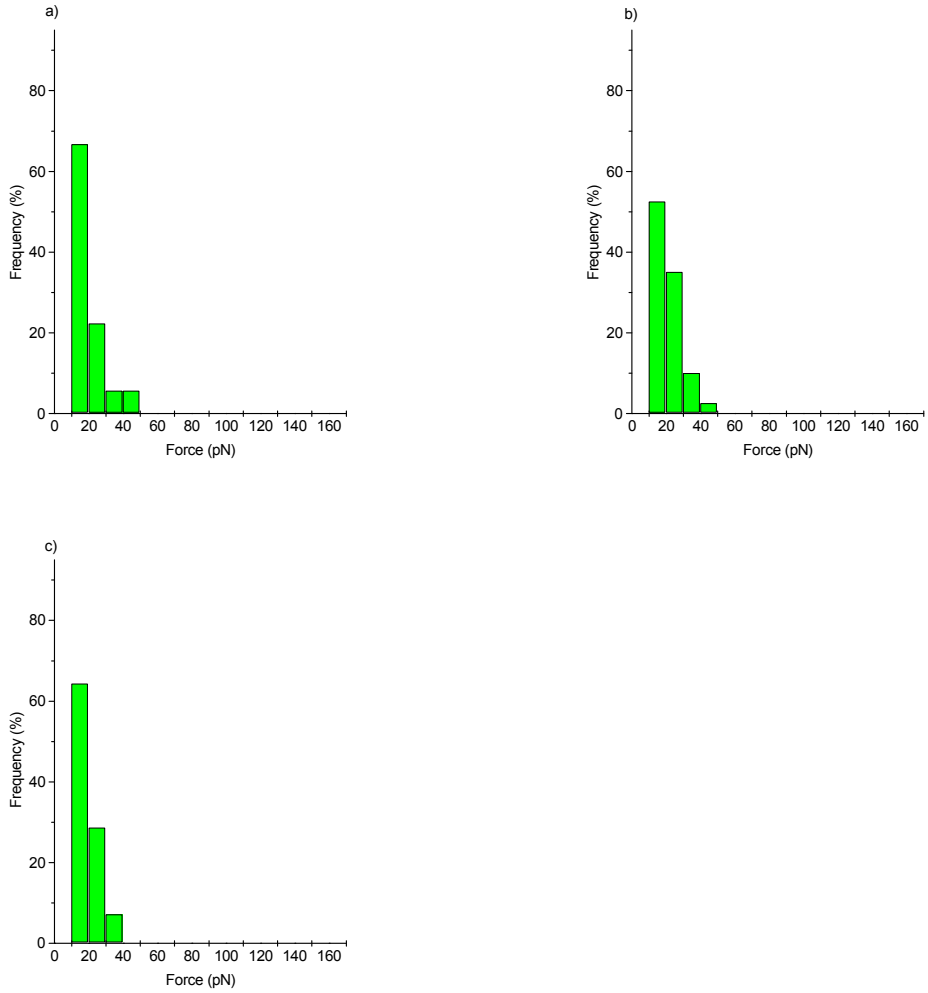

Figure 4-10: Histograms of rupture force measured using ultra soft 'Olympus' cantilevers, recorded at retract velocities of: a) 2000 nm s^{-1}; b) 500 nm s^{-1}; c) 200 nm s^{-1}. For all velocities a steady decaying distribution was seen.

4.4.2 BCys Experiments

The protein BCys has a similar structure to ACys, but instead has the basic B helix. As a result it is expected to have a pH response of an opposite character to ACys. At high pH as the lysine residues in the core-flanking regions of the coiled-coil assembly are less likely to carry a positive charge BCys homodimers were expected to be more stable than at low pH where the large proportion of positively charged lysine residues will have a destabilising repulsive effect (Petka 1997).

Unfortunately due to time constraints on the project it was not possible to carry out a full dynamic study of BCys homodimers. Instead rupture forces between BCys dimers were measured at a static probe retract velocity of 2000 nm s^{-1} at different pH values. Histograms of these rupture forces are shown in Figure 4-11. Most frequent rupture force values were obtained by the same method as described above for ACys. Differences in peak values (pH4.5: 28 pN; pH 7.4: 31 pN; pH 11.2: 33 pN) were not significant. These forces, especially at neutral and acidic pH, are also lower than for ACys homodimers at this probe velocity. This suggests that the BCys homodimers are less mechanically stable than the related ACys homodimers.

The distributions are sharp, but like ACys at pH 11.2 they decrease from an initial maximum, suggesting that the maxima of the distributions are masked by the lower noise limit of the cantilever. This would explain why such a small difference was measured between the different pHs. However, an interesting observation is that at pH 11.2 the tail of the distribution is longer than at the other pHs, suggesting a greater stability at this pH. At high pH only a relatively small proportion of the basic lysine residues occupying the core-flanking *e* and *g* positions of the coiled-coil complexes will contain positive charges, leading to a decrease in the destabilising effect of these residues at alkaline pH values.

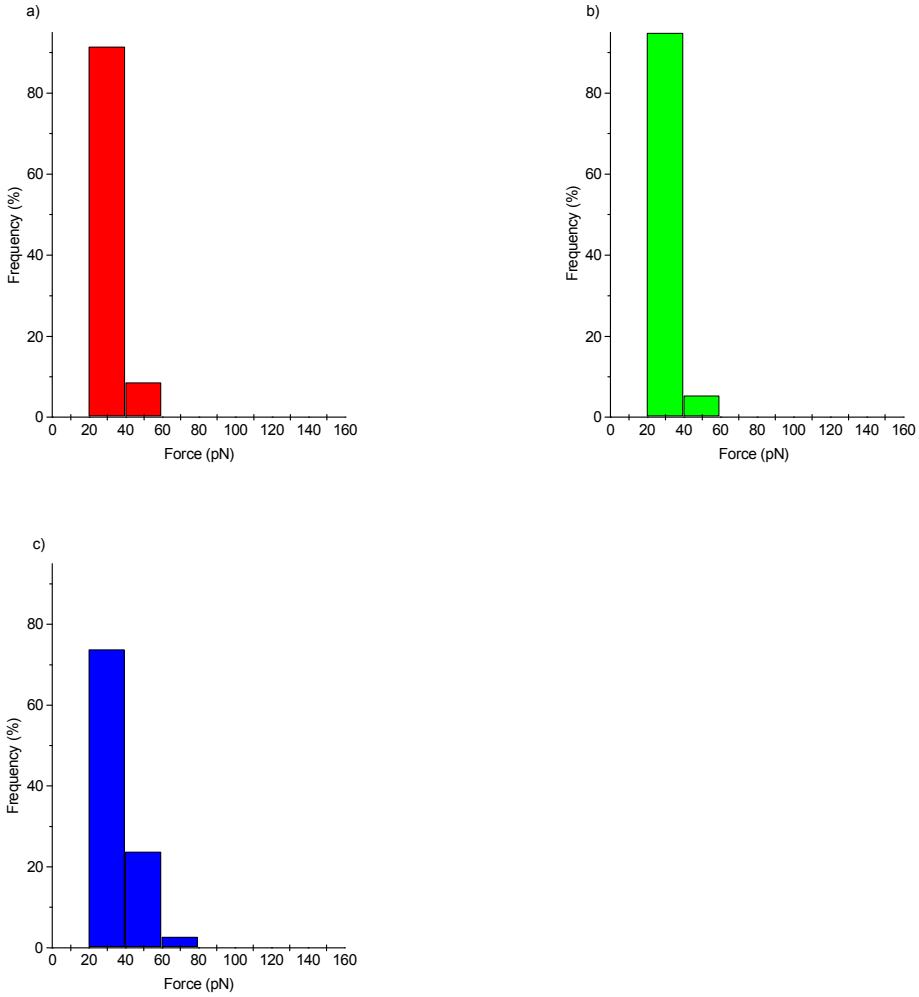

Figure 4-11: Histograms of rupture forces measured between BCys homodimers at a constant probe retract velocity of 2000 nm s^{-1} at various pH values (a) pH 4.5; b) pH 7.4; c) pH 11.2).

Previously Stevens measured the forces between BCys homodimers using a different surface preparation (Stevens 2001). While in this study the protein has been diluted on the surfaces by co-incubation with mercapto-undecanol, Stevens incubated BCys alone. Although a similar trend was seen qualitatively between peak force and pH as seen here, previously very broad distributions were observed, whereas here they are very sharp. Forces observed above the peak are indications of the presence of rupture events involving multiple connections (Williams 2003). The large decrease in width of distributions seen between the data obtained by Stevens and that observed here is likely to indicate the decrease in the observation of a multiple connections. This indicates the efficacy of the surface preparation approach used here in limiting observed interactions to single events.

4.5 Conclusions

In this chapter we have examined interactions at the heart of the coiled-coil motif, using force as a dynamic probe of their stability. It is the coiled-coil motif that is essential for the function of the responsive hydrogel proteins, as it is primarily through the association of the leucine zipper sections that the proteins associate. The single molecule approach utilised here has added complementary information at the molecular level to investigations already carried out of their macroscopic properties.

Firstly the protein ACys was probed at a range of probe velocities and at different pH values. At acidic and neutral pH their behaviour was found to be very similar. They showed a positive relationship between the most frequent rupture force and the probe velocity, as would be expected when applying force to a system far from equilibrium. As a result it was possible to analyse this data using a dynamic force approach to predict off rates for ACys dimers when under a zero force regime.

When the pH is increased to 11.2 the force at which dimers became dissociated was decreased, suggesting a decrease in their mechanical stability. In addition at pH 11.2 force was found to remain constant and did not change as probe velocity was altered. This is consistent with measurements taken at near-to equilibrium. The threshold at which near-to and far-from-equilibrium unbinding occurs is dependent upon the equilibrium constant, which can be considered as a ratio of the characteristic time scales for spontaneous dissociation and association, t_{off} and t_{on}. A decrease in the characteristic lifetime of the dimer due to destabilisation by repulsive charges in the coiled-coil at high pH will create a shift in the K_{eq} (= t_{off}/t_{on}), by altering t_{off}, and in turn a much higher probe speed will be needed to access the far-from-equilibrium part of the force spectrum. It must be remembered that the limits on probe velocity and hence loading rate of the AFM means that any force spectra obtained is merely a snapshot of part of the full spectrum. At higher probe speeds than were practicable for these experiments (> 5000 nm s^{-1}) the ACys dimers at pH 11.2 may indeed cross the threshold into far-from-equilibrium behaviour. Conversely at very low probe velocities the assemblies at neutral and acidic pH may cross this threshold into the near-equilibrium regime.

It must be remembered that due to the limited range of the dynamic force spectra obtainable by AFM that the measurements made here are possibly only a snapshot of a wider force landscape. This means that the energy barrier being probed at the retract velocities used is not necessarily the barrier to dissociation which may be observed under zero force.

The related protein BCys was also examined. The forces at which BCys homodimer complexes became dissociated were lower than those seen with ACys, suggesting that this protein is less mechanically stable. Due to time constraints it was not possible to carry out dynamic measurements over a range of probe velocities. However, the low forces measured at the relatively high rate of 2000 nm s^{-1} suggest that it would have been difficult to record data for much of the operational range of the AFM.

In this work a different surface preparation strategy was employed to previous experiments. Proteins were co-incubated with mercapto-undecanol molecules to dilute the proteins on the probe and substrate surfaces in an effort to limit the number of multiple interactions that may occur. The reduction in width compared with previous measurements, particularly with BCys, suggest that this approach was effective.

The results presented in this chapter are consistent with previous macroscopic measurements made by Petka *et* al (Petka 1997; Petka *et al.* 1998) and with the design of the peptides. ACys homodimers are less stable at high pH, where its behaviour is more fluid-like. Dimers at neutral and acidic pH are more stable with characteristically longer lifetimes. This allows hydrogel proteins containing the acidic leucine zipper helix to make more stable connections at these pHs, leading to the formation of stable gel networks. We have provided mechanical information on the dynamic response of the linkages of such networks to force, probing changes in their kinetic stability with pH. As biomaterials made using the coiled-coil motif as a mechanical linkage domain are likely to be routinely exposed to external forces in their possible applications (such as drug delivery materials, tissue engineering scaffolds etc.) then the approach used here of applying force is highly appropriate.

Chapter 5 : AFM Microcantilevers as Sensors for Detection of Changes in Viscosity and Aggregation of Proteins in Solution

5.1 Introduction

In this chapter experiments are described which employ the resonance response of AFM microcantilevers to monitor changes in the viscosity of dilute solutions of a series of pH-responsive hydrogel proteins, all of which associate via leucine zipper type domains to form coiled-coil dimers. In addition the sensitivity of the resonance of cantilevers to small changes in mass is employed to study the aggregation or association of these proteins on and or in the vicinity of the cantilever surfaces, both with plain unfunctionalised cantilevers and with cantilevers given a variety of functional coatings.

5.1.1 Use of AFM Cantilevers as Sensors

The ability of AFM microcantilever technology to study the dynamic viscosity of solutions by monitoring changes in the resonant frequency of microcantilevers has been investigated by a number of groups in recent years (Chen *et al.* 1994; Ogden *et al.* 1996; Sader 1998; Bergaud and Nicu 2000; Ahmed *et al.* 2001; Boskovic *et al.* 2002).

According to equation 5-1 taken from Ahmed *et al* (Ahmed *et al.* 2001) (originally adapted from a previous equation described by Chen *et al* (Chen *et al.* 1994)) the resonant frequency of a cantilever in a simple solution should relate to the viscosity of the solution by the following relationship:

$$\omega = 1/8\left(\left(\sqrt{9(K\eta\rho)^4 + 64\omega_0{}^2}\right) - 3(K\eta\rho)^2\right) \qquad \textit{Equation 5-1}$$

Where ω is the resonant frequency of the cantilever, ω_0 is the resonant frequency under vacuum, η is the dynamic viscosity of the solution, ρ is the density of the solution and K is a constant for a given cantilever, representing various physical properties, such as geometry, mass and material properties. Varying the viscosity of the medium in which experiments are performed is known to affect the damping of the cantilever and will consequently change its resonant frequency, with the resonant frequency increasing as the surrounding solution becomes less viscous (Chen *et al.* 1994). As a consequence, if all other factors are kept constant, then any change in resonant frequency will reflect a change in the viscosity of the surrounding fluid. An advantage of this approach is the very low volume needed when compared with conventional rheological techniques.

Typically in experiments, volumes used are as low as 50-100 μL, probing volumes that have been estimated to be as low as 1 nL around the cantilever (Boskovic *et al.* 2002). In addition, studies have been carried out which investigate the effect of the addition of mass to AFM microcantilevers on their resonant frequency to assess thickness of adsorbed films and also for utilization in the calibration of the spring constant of AFM microcantilevers (Cleveland *et al.* 1993; Sader *et al.* 1995). Consequently, by the functionalisation of microcantilevers much progress has been made in their development as highly specific biosensors (Moulin *et al.* 1999; Baller *et al.* 2000; Subramanian *et al.* 2002).

5.1.2 Proteins

The studies described here concern investigations of artificial coiled-coil containing proteins, termed $AC_{10}ACys$, $AC_{10}BCys$, L2FC3 and L2FC5, engineered to form pH-responsive hydrogel systems (Petka 1997; Petka *et al.* 1998; Guhr 2000). The structure of the protein $AC_{10}ACys$ has already been described in chapter 3, and will not be repeated here.

$AC_{10}BCys$ has a similar structure to $AC_{10}ACys$, but instead it contains an A-type (acidic) helical domain and a basic domain, B in place of the second A Both of these leucine zipper regions are based on the *jun* oncogene products (Petka 1997). The basic domain contains a large proportion of lysine residues in the core-flanking *e* and *g* positions, but is otherwise identical in structure and sequence to the A domain. As the pH is decreased the lysine residues will become more likely to carry a positive charge, and at a low enough pH lysine residues on opposite helices will repel each other sufficiently to overcome the hydrophobic attraction between the core residues. The structure for $AC_{10}BCys$ is illustrated in Figure 5-1. The A and B domains are able to dimerise to form either homodimers or heterodimers, with a greater affinity expected between the heterodimers due to a more favourable arrangement of charges. At high pH repulsion between glutamic acid residues will destabilise A-A homodimers, while conversely at low pH, repulsion between positive charges of lysine residues will destabilise interactions of B-B homodimers. As a result of the net interactions between molecules of $AC_{10}BCys$ solutions of this protein are not expected to have a significant pH dependence (Petka 1997).

The proteins L2FC3 and L2FC5 are of a different design to the $AC_{10}ACys$ and $AC_{10}Bcys$ proteins, with their leucine zipper domains based upon the *fos* oncogene products. Their sequences are listed in Figure 5-2 Both contain the same leucine zipper-type sections (two in the case of L2FC3 and three in the case of L2FC5) that can form helices upon dimerisation with another helical

Amino acid Sequence:

MRGSHHHHHHGSDDDDKWA – *Helix A* –
IGKHVAPRDTSYRDPMG – [AG$_3$PEG]$_{10}$ – ARMPTGD –
***Helix B* – IGDHVAPRDTSMGGC**

Figure 5-1: Above is shown the amino-acid sequence for the protein AC$_{10}$BCys, with a helix-loop-helix construction. The sequence [AG$_3$PEG]$_n$ is an alanine and glycine rich region repeated 10 times. Adapted from (Petka 1997; Petka *et al.* 1998).

L2FC3:

MRGSHHHHHHGSDDDDKWAS-*Helix*-
TSYRDPMG[AGAGAGPEG]$_{10}$ARMPTS-*Helix*-TSMGGC

L2FC5:

MRGSHHHHHHGSDDDDKWAS-*Helix*-
TSYRDPMG[AGAGAGPEG]$_{10}$ARMPTS-*Helix*-
TSYRDPMG[AGAGAGPEG]$_{10}$ARMPTS-*Helix*- TSMGGC

***Helix*:**

LTDTLQAETDQLEDKKSALQTEIANLLKEKEKLEFILAAY

Figure 5-2: Amino acid sequences of L2FC3 and L2FC5 proteins. Helical wheel representation of homodimers formed by F leucine zipper sequence is shown in Figure 1-5. The core *d* positions are exclusively inhabited by hydrophobic lysine residues.

section to form two-helix coiled-coils. In each protein these helical regions are spaced out by random-coil polyelectrolyte regions, incorporated to provide greater solubility (Guhr 2000). L2FC3 contains 210 amino acid residues, of which 80 are in helix forming regions and 90 are polyelectrolyte residues. The larger L2FC5 contains 354 amino acid residues, with 120 in helical regions and 180 in polyelectrolyte regions. The helical regions are acidic helices (F) consisting of 5 classic 7-residue heptad repeats which are typical of coiled-coil proteins and are described in more detail in chapter 1. As pH increases repulsive charges in the helices increases, destabilising the coiled-coil dimers. As a result these proteins are able to cross-link via the F sequences to form hydrogels in acidic pH solutions (given sufficient concentration), but are de-stabilised at higher pH and instead form viscous liquids (Guhr 2000).

5.1.3 Aims and Objectives

In the chapter presented here the effects of viscosity and added mass on the resonance of a microcantilever were employed to assess changes in the viscosity of dilute solutions of the proteins described above with changes in pH. In addition the change in resonant frequency of cantilevers immersed in different pH solutions of proteins over time was measured at concentrations well below that required for forming gels, with the aim of characterising any possible interactions between the proteins and the cantilever. Any such interactions are liable to add mass to the cantilever which will confound any attempt to measure differences in viscosity between solutions.

5.2 Materials and Methods

Proteins used in this study (Petka 1997; Petka *et al.* 1998; Guhr 2000) were provided by Prof. D.A. Tirrell (Division of Chemistry and Chemical Engineering, California Institute of Technology). All chemicals used were obtained from Sigma-Aldrich Co. Ltd (Gillingham, Dorset, UK) unless

otherwise stated. Gold was obtained from Agar (Stansted, Essex, UK). All solutions used consisted of 10 mM NaH_2PO_4, 150 mM NaCl, adjusted to the appropriate pH (4.5, 6.0, 7.4 and 11.2) using 5 M NaOH or 5 M HCl. All solutions were prepared using high purity de-ionised water (purified on an ELGA water system, Maxima HPLC, Elga Ltd, Bucks, UK; resistivity 18.2 MΩ cm). Experiments were carried out using a Molecular Force Probe (MFP) instrument (Asylum Research, Santa Barbera, CA, USA), using an Igor Pro software interface (Wavemetrics, Oregon, USA). NP type V-shaped silicon nitride cantilevers were used in all cases (Veeco, Santa Barbera CA), with a nominal spring constant of 60 pN nm^{-1}. Where experiments required, cantilevers were coated with approximately 30 nm thickness of gold using a sputter coater.

At the commencement of experiments cantilevers were allowed to equilibrate in buffer for at least 30 minutes. The buffer used was in all cases of the same pH as the subsequent protein solution to be investigated. During experiments cantilevers were immersed in 100 µl volumes of protein solution at the specified concentrations.

Resonant frequency values quoted are the fundamental resonance peak of the cantilever at ambient thermal excitation. This value was obtained from the power spectral density (PSD) curves obtained using the instrument software.

5.3 Results and Discussion

5.3.1 Measurements of Change in Viscosity of Protein Solutions with pH

In Figure 5-3 a graph is shown illustrating the relationship between cantilever resonance and solution viscosity as suggested by equation 5-1. In this graph is plotted the resonant frequency of a cantilever when placed in aqueous glycerol

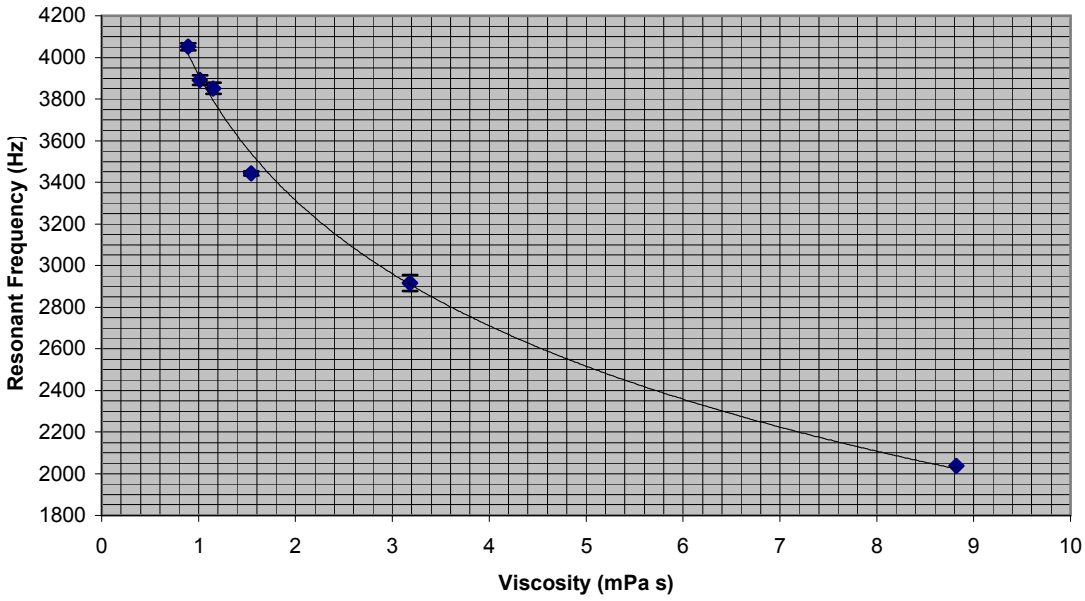

Figure 5-3: Change in resonant frequency of a standard AFM cantilever when immersed in aqueous glycerol solutions of known dynamic viscosity.

solutions of different concentration with known dynamic viscosity. It can be seen that as the viscosity is increased the resonant frequency decreases. It is possible to use this to create a calibration curve for each cantilever used to convert resonant frequency change directly into viscosity values in Pa s. However, as solutions of macromolecules often have non-linear viscosities (i.e. they are non-ideal or non-Newtonian in behaviour), this has not been done in this case, as the relationship between resonant frequency and solution viscosity for the protein solutions used in these experiments may not be adequately described by equation 5-1. However instead the resonant frequency values can be used to reflect qualitative changes in viscosity, and differences in viscosity between different samples, providing that the same cantilever is used for each measurement.

5.3.1.1 Change in Viscosity of $AC_{10}ACys$ Solutions

Three 5 μM solutions of $AC_{10}ACys$ in phosphate buffers of different pH values (pH 11.2, 7.4, 4.5) were prepared. AFM cantilevers were immersed in 50 μL volumes of the solutions, and were allowed to equilibrate for at least 15 minutes. The fundamental resonant frequency of the cantilevers was measured in each of the pH solutions and compared with values obtained for the same cantilevers when immersed in buffer solutions alone. It can be seen from Figure 5-4 that there does not appear to be any significant detectable difference between the resonant frequency in buffer and in $AC_{10}ACys$ solutions at pH 11.2 and pH 7.4. At the acidic pH 4.5, however, there does appear to be a larger difference between the buffer and protein solution, suggesting that there is likely to be an increase in solution viscosity at low pH when compared with the other pHs.

The experiment was repeated to investigate both the reproducibility of the experiment and also to further investigate the effect of protein concentration on measurements (see Figure 5-5). Two different concentrations of $AC_{10}ACys$

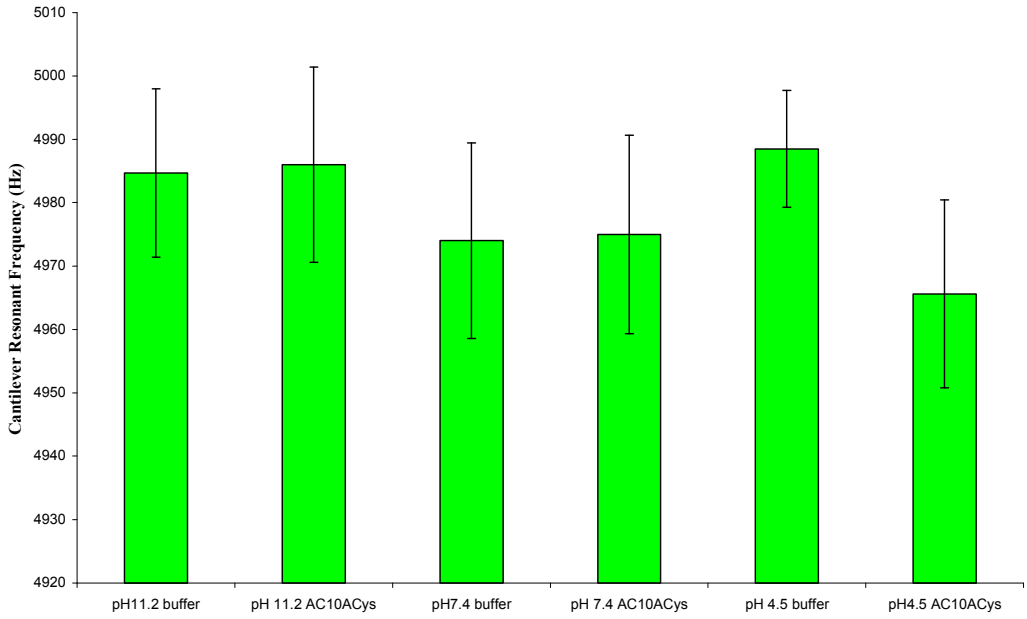

Figure 5-4: Resonant frequency of an AFM cantilever when immersed in buffer and 5 μM $AC_{10}ACys$ solutions of different pH.

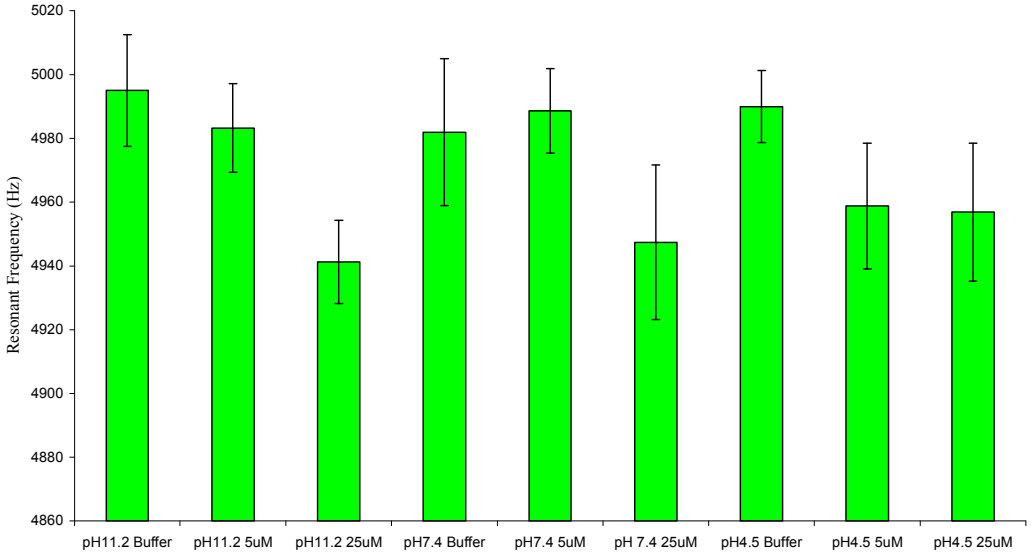

Figure 5-5: Change in cantilever resonant frequency for $AC_{10}ACys$ at two different concentrations with change in environmental pH.

were used, one at 5 μM and another at the higher concentration of 25 μM. It was expected that a higher protein concentration would yield more detectable changes in viscosity due to a better signal. Again at the 5μM concentration little difference was seen between the $AC_{10}ACys$ solution and buffer alone at pH 11.2 and pH 7.4, but there was a more appreciable difference at pH 4.5. At the higher concentration there is generally a more marked difference between the $AC_{10}ACys$ solutions and the buffer alone, suggesting that this method is able to detect a difference between solutions at different concentrations and hence of different viscosity, as it would be expected that solutions laden with more of the protein would become more viscous in a concentration dependent manner. As the mass of protein added to the solutions is very low compared with the mass of the volumes to which they were added this is not expected to be due to changes in density of the solutions rather than viscosity. The difference in cantilever resonant frequency between the pH 11.2 and pH 7.4 25 μM solutions, however, is not significant, suggesting that there is no appreciable change in viscosity of the $AC_{10}ACys$ solutions between these pH regimes. At low pH there is no apparent difference between the data recorded in lower and higher protein concentrations, and the higher concentration actually gives a slightly higher resonant frequency than at the other pH solutions.

5.3.1.2 Change in Viscosity of $AC_{10}BCys$ Solutions with pH

Solutions of the protein $AC_{10}BCys$ were prepared at concentrations of 52 μM and 104 μM and at four different pH values (pH 11.2, 7.4, 6.0 and 4.5). Measurements are displayed in Figure 5-6. There mostly appears to be a decrease in the resonant frequency at the higher concentrations when compared with the buffer, which would be expected due to the amount of dissolved protein. However, this is not apparent at pH 11.2 and is also not very marked at pH 4.5. Conversely, at pH 7.4 and 6.0 a marked increase in resonant frequency can be seen. This suggests that the solution becomes more viscous at these pH

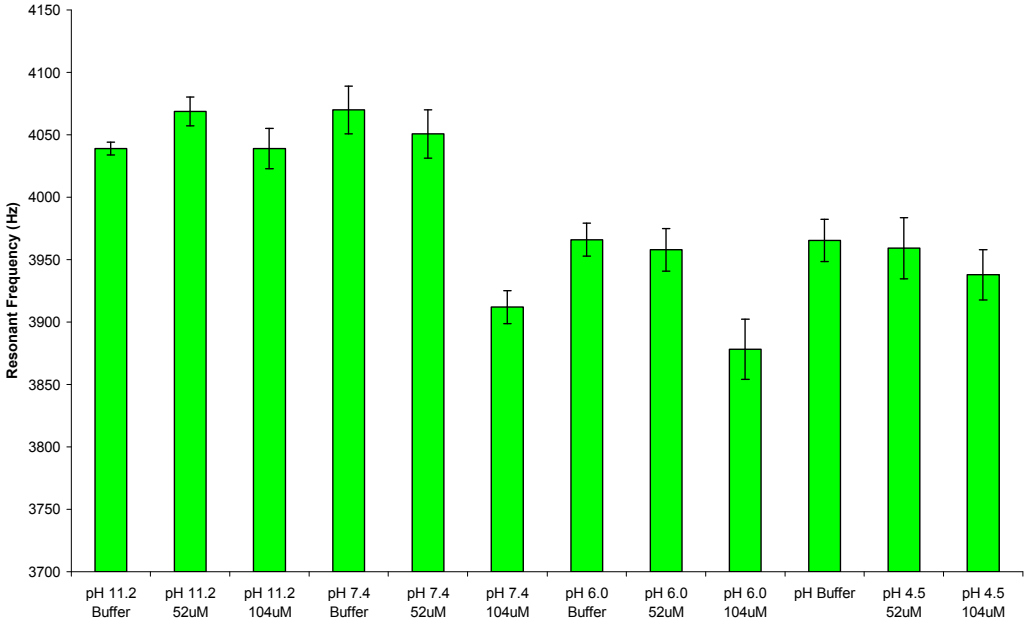

Figure 5-6: Cantilever resonance response when immersed in $AC_{10}BCys$ solutions of different concentration and pH.

levels. The A helix of the protein would be expected to be able to form stable homodimers at acidic pH (as glutamic acid residues will not be ionised) and the B helix to form stable homodimers at alkali pH (lysines will not be ionised in any great proportion) (Petka 1997). This could explain why there is no real difference in viscosity between the alkali solutions and the solution at pH 4.5. With the more neutral solutions (pH 7.4 and 6.0) the more stable heterodimers would predominate. This could explain why these solutions appeared to have the highest viscosities.

Overall it was noted that there was a general decrease in the observed resonant frequency during the experiment. It is possible that this phenomena may have been caused by protein adsorbing on the back of the cantilever, either non-specifically or by the linking of terminal cysteine residues to the reflective gold coating on the reverse side of the cantilever by thiolate bond formation with the gold. If this is borne in mind when looking at Figure 5-3, it becomes clear that it is not possible to tell how much the change in resonant frequency is due to pH-dependent changes in solution viscosity and how much is due to interactions between proteins in solution and the cantilever. Experiments which address this issue, i.e. whether protein is interacting with the cantilever, are described below (see section 5.3.2).

5.3.1.3 Investigations into the Change in Viscosity of L2FC3 and L2FC5 Solutions with pH

AFM cantilevers were immersed in solutions of L2FC3 and L2FC5 proteins at pH 6.0, 7.4 and 11.2 and their resonant frequencies measured (see Figure 5-7 and Figure 5-8). In both cases the resonant frequency was found to be significantly lower for the protein solutions when compared with buffer. In the case of the L2FC3 data, the 120 μM solutions also were found to produce lower resonant frequency values than for the lower protein concentration of 60 μM.

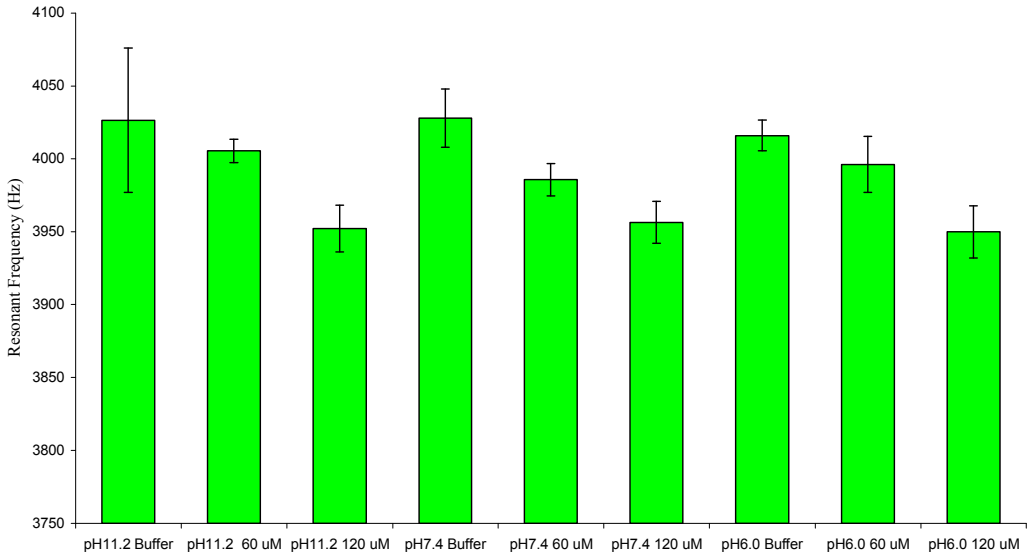

Figure 5-7: Resonant frequency change for an AFM cantilever immersed in L2FC3 solutions of different pH at concentrations of 60 and 120 µM.

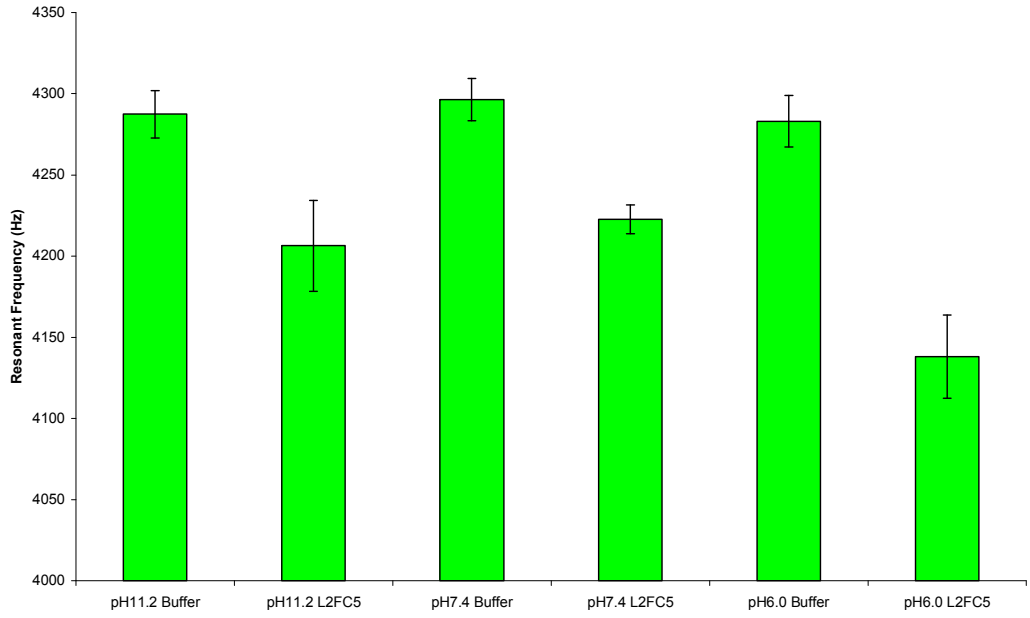

Figure 5-8: Cantilever resonance immersed in different pH solutions of L2FC5.

The observed decrease in resonant frequency with an increase in protein concentration is likely to reflect an increase in the viscosity of solutions. The decrease in resonant frequency is unlikely to be due to a change in the density of the solution because the masses of protein dissolved were very small when considered against the masses of the volumes of buffer in which they were dissolved. With regard to effects of pH, the data displayed here do not show any significant change in resonant frequency with pH for L2FC3. From the known pH-responsive behaviour of this protein it is, however, expected to be more viscous in the low pH range (Guhr 2000), but it is possible that this method is not sensitive enough to detect any changes in viscosity of solutions at these low protein concentrations.

Both of the proteins contain a terminal cysteine residue, which can readily form thiolate bonds with gold surfaces and thus would be expected to be able to bind to the reflective gold surface on the reverse (uppermost) side of standard AFM cantilevers. In addition it is also possible that the proteins can adsorb onto the bare silicon oxide surfaces of the cantilever in a non-specific manner. Once this occurs it may also be possible for the employed proteins to form aggregates or gel-like networks in the vicinity of the cantilever surface. Any significant change in the mass of the cantilever due to the adsorption or aggregation of protein onto the cantilever will also affect the resonant frequency of the cantilever, producing a confounding effect when trying to measure viscosity by the method employed above. Because of this it was decided to monitor changes in the resonance of cantilevers immersed in protein solutions as a function of time, in order to study whether protein could be binding to the cantilevers used in the viscosity experiments. Additionally any change in resonance over time due to mass-related effects will reflect the aggregation of the proteins in solution and can be used to further probe the pH-dependent behaviour of the proteins. The following section details experiments to assess time-dependent changes in the resonant frequency of cantilevers due to changes in adsorbed mass.

5.3.2 Change in the Aggregation of L2FC3 and L2FC5 with pH Using AFM Microcantilevers as Mass Sensors

Figure 5-9 shows data recorded from a single AFM cantilever following immersion in 150 μM solutions of L2FC3 of different pH values, in which the resonant frequency of the cantilever was measured at intervals of 5 minutes for one hour. Each data point represents five measurements taken consecutively (each measurement taking approximately 10 seconds). In between sets of measurements (i.e. in each pH protein solution) the cantilever was gently rinsed first in pH 11.2 buffer to cause the dissociation of any protein aggregates that may have formed on the cantilever, and then in buffer of the same pH as that of the next protein solution to be studied. It was expected that the pH 11.2 buffer solutions would dissociate coiled-coil dimers because of the number of negative charges that are be present on the core-flanking regions of the helices at high pH. Data for the change in resonant frequency is shown in Figure 5-9-a. For the solutions at pH 7.4 and pH 11.2 the resonant frequencies remain relatively constant, with only a slight decrease over time. However, at pH 6.0 the resonant frequency steadily decreases over time.

Using the change in resonant frequency of the cantilever during the experiment, compared with the initial values, it is possible to calculate the change in effective mass over this period using Equation 5-2, originally used by Cleveland *et al* (Cleveland *et al.* 1993) in the calibration of cantilevers by addition of an end loaded mass:

$$k = (2\pi)^2 \frac{M}{\left(1/\nu_1^{\,2}\right) - \left(1/\nu_0^{\,2}\right)} \qquad \textit{Equation 5-2}$$

Where k is the spring constant of the cantilever, M is the added mass (in this case a change in the effective mass of the cantilever) and υ_0 and υ_1 are the

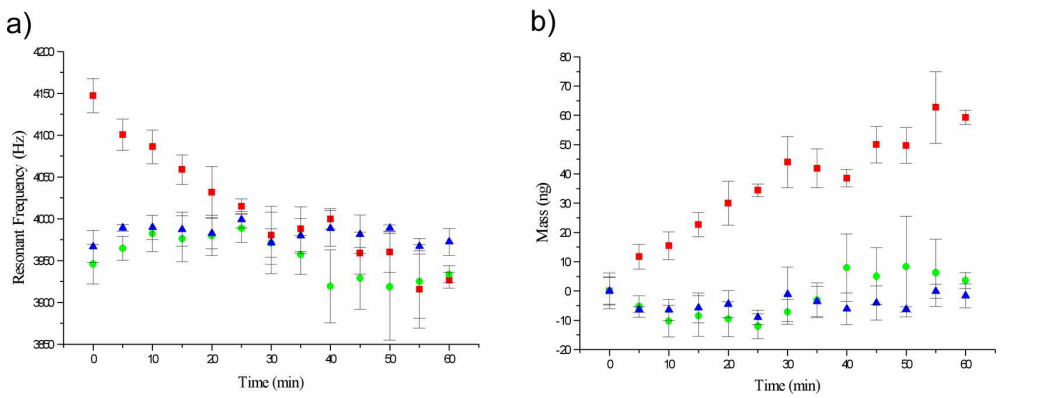

Figure 5-9: **a)** Change in resonant frequency over time of an AFM cantilever immersed in 150µM solutions of L2FC3 at different pH's (pH 11.2: ▲, pH 7.4: ♦ pH 6.0: ■). **b)** Change in mass of cantilever over time calculated from resonant frequency data used in a).

initial and loaded resonant frequencies respectively. To gain values of actual added mass a conversion factor based on the geometry of the cantilever, originally calculated by Sader (Sader *et al.* 1995), was used to take account of any added mass from the protein being evenly spread over the cantilever. For the case of the cantilevers used here mass values were divided by the correction factor of 0.24. Calculated mass for this experiment is shown in Figure 5-9-b. An estimate of the maximum mass of protein on the cantilever due to a monolayer can be made. From the crystal structure of the leucine zipper protein GCN4-p1, which has a leucine zipper type domain similar in structure to that reported in L2FC3, a cross-sectional area of 6.6 nm^2 was previously calculated for the footprint of a dimer, if arranged perpendicular to the surface (O'Shea *et al.* 1991). Using this value combined with the molecular weight of L2FC3 (20 198 Da) and an estimated total surface area of the cantilever of approximately 16 300 μm^2, it was estimated that a monolayer of L2FC3 coating both sides of the cantilever would have a maximum mass of 0.17 ng, if arranged in a closely packed layer with all coils arranged vertically away from the surface. Clearly the mass on the cantilever calculated from experimental data is several orders of magnitude greater than this value, suggesting that at the time of the final measurement for the pH 6.0 solution there are in the order of approximately 350 monolayers present, assuming that the aggregation is occurring on both sides of the cantilever.

To further investigate these observations the experiment was repeated with the cantilever surface prepared in a number of different ways. In these experiments it was also decided to use the related L2FC5 protein, as due to its greater mass (32 967 Da) it was expected to have a greater effect on the resonant frequency of the cantilever, and hence the method should be more sensitive to its behaviour. Also as there are more leucine zipper domains on each protein there are more attachment points and hence it was expected to more readily form networks.

Cantilevers were prepared in four different ways. The first set were clean uncoated silicon nitride cantilevers for direct comparison with the previous

L2FC3 data. The second set were cantilevers that had been sputter-coated with gold on both sides. This was to verify whether the protein was adhering to just the upper gold surface in the case of standard AFM cantilevers or both the gold and silicon nitride surfaces. If the protein was only adhering to the gold then presumably using a cantilever coated with gold on both sides would have double the amount of protein adhering to it. The third set of cantilevers were coated in gold on both sides before incubation with a 100 μM solution of 11-mercapto-1-undecanol (for at least one hour) in an attempt to see if the surface could be made resistant to the adsorption of the protein. This molecule was chosen because previous force spectroscopy experiments on similar proteins had not shown very little interaction between the proteins and mercapto-undecanol (see chapter 4 and chapter 7). Finally, the last set of cantilevers to be investigated were sputter-coated with gold on both sides before being incubated with a 10 μM solution of L2FC5 for at least one hour and then rinsed with pH 11.2 buffer. This was in order to pre-prepare a monolayer of protein on the cantilever surface for comparison with the second type of cantilever, to assess whether the observed effects were due to the initial binding of the protein to the cantilever.

The recorded resonant frequency data is shown in Figure 5-10. The change in the mass of the cantilevers was calculated from this data, by the same method as it was for L2FC3, and is presented in Figure 5-11. For the experiments recorded using the bare and gold-coated cantilevers fresh cantilevers were used for each set of measurements (i.e. when switching between solutions). This was to remove any effects of previous exposure of the cantilevers to protein, i.e. any effects that may have been caused by the previous adsorption of the protein onto the cantilever surface. As different cantilevers will have slightly different spring constants, which will thus have an effect on their resonance response, it is perhaps more useful to look primarily at the mass data calculated from the resonant frequencies when comparing the different pH's, as the mass data is normalised for the spring constant of the cantilevers.

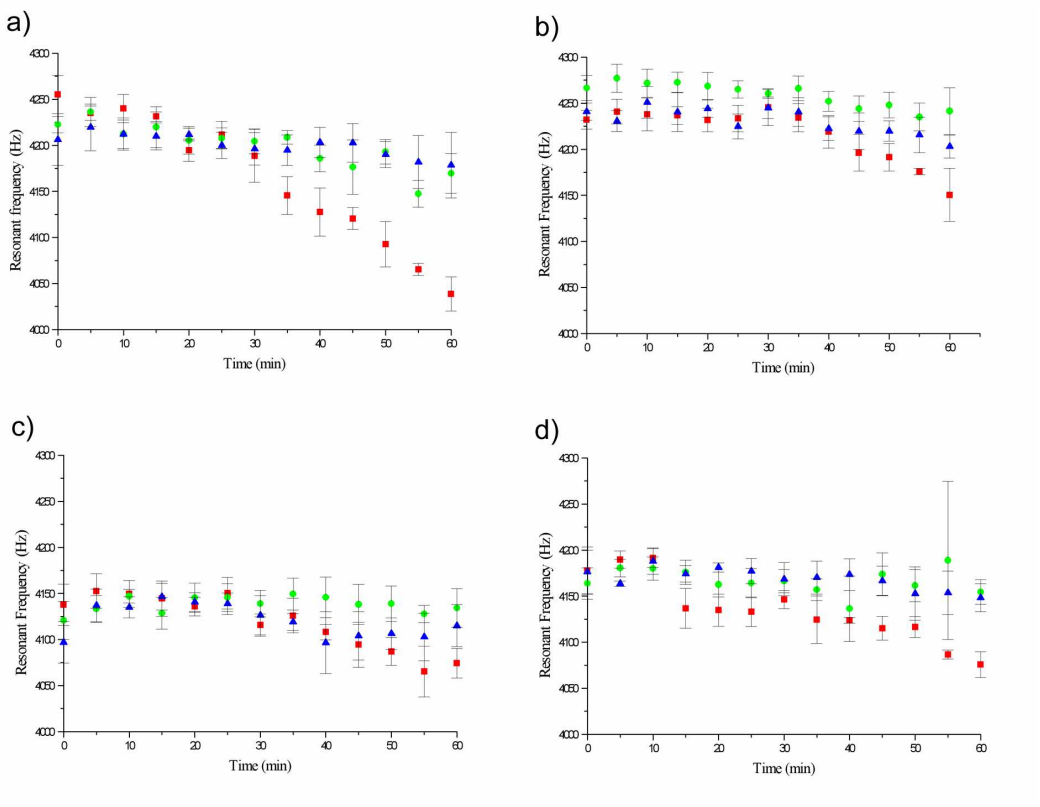

Figure 5-10: Differently functionalised cantilevers immersed in 150µM L2FC5 solutions of different pH (pH 11.2: ▲, pH 7.4: ♦ pH 6.0: ■). **a)** Uncoated, untreated cantilever. **b)** Cantilever sputter-coated on both sides with approximately 5 nm gold, but otherwise unfunctionalised. **c)** Cantilever coated with gold before being 'blocked' with a monolayer of mercapto-undecanol. **d)** Cantilever coated in gold before being pre-treated with a monolayer of L2FC5.

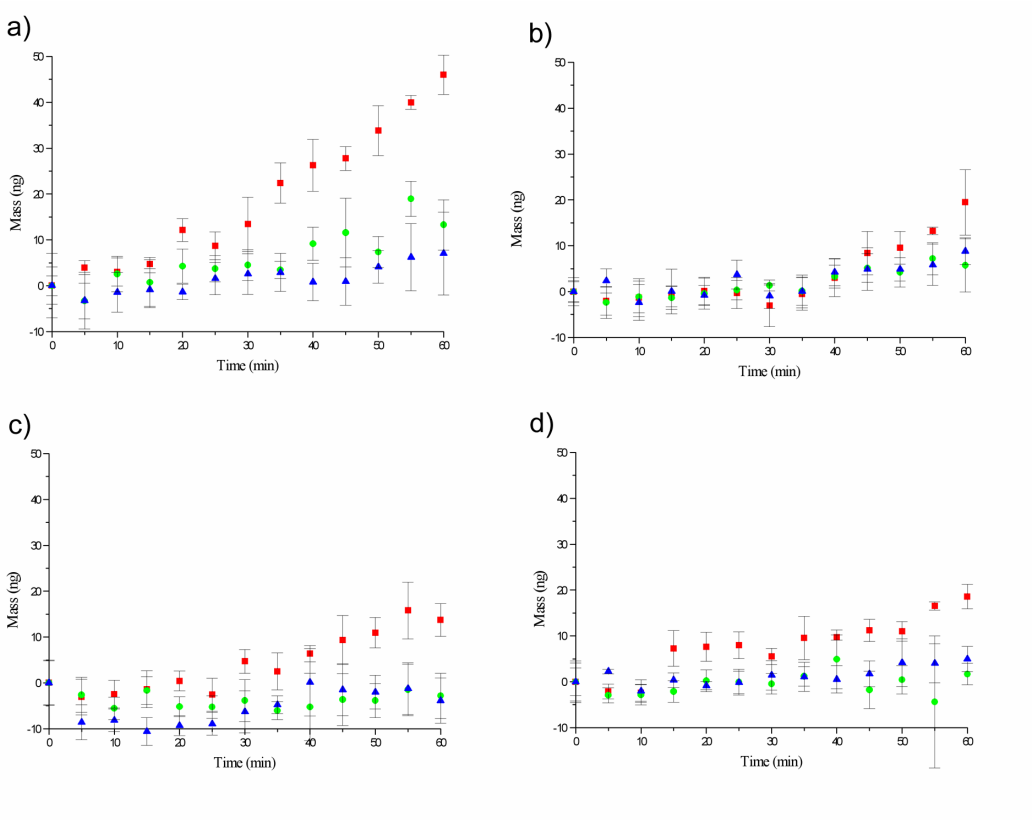

Figure 5-11: Calculated mass adsorbing to differently functionalised cantilevers at different pHs (pH 11.2: ▲, pH 7.4: ♦ pH 6.0: ■). a) Uncoated, untreated cantilever. b) Cantilever coated with gold but otherwise untreated. c) Cantilever 'blocked' with mercapto-undecanol. d) Cantilever pre-treated with monolayer of L2FC5.

When the bare untreated cantilever was used (Figure 5-10-a and Figure 5-11-a) a similar effect was observed as to when L2FC3 was investigated. The pH 6.0 solution showed an increase in mass far above that of the other two pH values studied. This is in accordance with what was expected, as at pH 6.0 L2FC5 will form more stable and hence longer-lived connections with other L2FC5 molecules. The pH 7.4 and pH 11.2 solutions, however, also showed a gradual increase in calculated mass. Generally the trend was for a greater increase in mass over time the lower the pH of the solution. This trend was repeated with the cantilevers coated in gold alone, although the magnitude of the mass increase at pH 6.0 was less than that of the uncoated cantilever. This discrepancy could be due to a more rapid adsorption to the silicon oxide surface exposed in the untreated and uncoated cantilever, or may reflect some other property not accounted for here. Again, the upper limit for mass due to a monolayer was estimated. In the case of L2FC5 this was predicted to be approximately 0.27 ng, far below the values obtained, suggesting that the observations were not the result of the formation of a monolayer alone.

Next, cantilevers which had been gold-coated on both sides before being functionalised with the mercapto-undecanol were examined, which was employed with the aim of blocking or reducing any protein binding to the gold surface. Data for these cantilevers is presented in Figure 5-10-c and Figure 5-11-c. Unfortunately, as can be seen, the attempt to block the cantilevers was unsuccessful, as the resonant frequency change at the different pH values was similar in appearance to that for the gold-coated cantilever. It is probable that the mercapto-undecanol did not sufficiently block access to the surface by the protein. It is quite possible that only a relatively small amount of protein is needed to bind to the underlying surface to allow a network to form in the vicinity of the cantilever.

However, the decrease in resonant frequency change seen between the bare untreated cantilever and cantilevers prepared by the other methods does suggest that, by the modification of the cantilever surfaces, a change in the resonance responsive behaviour of the cantilevers is brought about. This

strongly suggests that the phenomena detected is due to the surface adsorption of protein molecules to the cantilever rather than a time-dependent change in the bulk solution properties of the protein solutions.

Finally cantilevers were examined which had been pre-treated with L2FC5 to form a monolayer. This was to isolate any effects due to initial specific binding of a monolayer of L2FC5 to the gold surface. The calculated mass data (Figure 5-11-c) appears very similar to that obtained with the gold-coated, but unfunctionalised cantilevers. This demonstrates that the effects observed were therefore not due to the binding of the initial monolayer.

5.4 Conclusions

Viscosity- and mass-dependent effects on the undriven resonant frequencies of AFM microcantilevers have been used to probe the pH-dependent behaviour of responsive hydrogel proteins, both in solution and on the surface of a microcantilever. An increase in apparent viscosity was observed with increasing solution concentration, thus demonstrating the validity of this type of approach. It was not possible to detect significant differences between different pH solutions of the proteins investigated using this approach. It is a possibility that the protein concentrations employed were below the threshold of sensitivity of this method.

We further went on to assess the change of resonant frequency of the AFM cantilever as a function of time. It was found that the proteins did adsorb to the cantilever, which may confound viscosity results obtained with a bare cantilever, especially if cantilevers are immersed in protein solutions for some time, such as to allow systems to equilibrate. In previous attempts to assay changes in the viscosity of solutions of biomolecules (Ahmed *et al.* 2001) this potentially confounding effect has not been examined. In future experiments, using microcantilevers to probe changes in solutions containing biomolecules,

our experiments show that careful consideration should be given to any potential interactions that may occur between the molecules of interest and the surface of the cantilever itself.

The effect of protein adsorption and hence calculated mass increase was greater than that calculated for a monolayer alone with both L2FC3 and L2FC5, suggesting that the proteins were cross-linking to form aggregates or gel-like networks around the cantilever.

This study has provided complementary data to that obtained in previous work on these proteins (Guhr 2000) and has shown that these proteins form aggregates at different rates according to pH. In addition it has shown the importance of preparation of the cantilever before these type of viscosity experiments are carried out to ensure that results are not confounded by effects that biomolecules may have on cantilevers other than viscosity.

Chapter 6 : pH-Dependent Behaviour of Surface-Immobilised Hydrogel Proteins

6.1 Introduction

Recently, there has been much interest in the creation of environmentally-responsive or switchable surfaces (Heine and Wu 2001; Advincula *et al.* 2002; Julthongpiput *et al.* 2003; Julthongpiput *et al.* 2003; Sumerlin *et al.* 2003; Luzinov *et al.* 2004) for a variety of applications, including chromatography and the separation of compounds (Kobayashi *et al.* 2001), the control of cell adhesion to surfaces (Chao *et al.* 1998; Tsuda *et al.* 2004), biosensors (Chao *et al.* 1998), cross-linking of nano-particles (Stevens *et al.* 2004) and the control of fluid transport through membranes (Zhang and Ito 2001).

In this chapter the pH-dependent properties of two different surface-immobilized coiled-coil containing proteins, termed L2FC7and BCys, are examined using the mechanical and optical techniques of QCM-D, DPI and SPR. The amino acid sequences for these proteins are shown in Figure 6-1.

L2FC7 was *de novo* designed to form a reversible hydrogel (Guhr 2000). L2FC7 is an approximately 45 kDa protein containing four leucine zipper-based 'helix' domains which are capable of dimerising to form coiled-coil structures. In between the coiled-coil domains are random-coil polyelectrolyte regions responsible for granting a high degree of water solubility to the protein. Within the coil forming regions the core-flanking (*e* and *g*) positions are populated to a large extent by glutamic acid residues (pK_a 4.4). Under high

L2FC7:

MRGSHHHHHHGSDDDDKWAS-*Helix*-TSYRDPMG[AGAGAGPEG]$_{10}$ ARMPTS-*Helix*- TSYRDPMG[AGAGAGPEG]$_{10}$ ARMPTS-*Helix*-TSYRDPMG[AGAGAGPEG]$_{10}$ ARMPTS-*Helix* TSMGGC

Helix:
LTDTLQAETDQLEDKKSALQTEIANLLKEKEKLEFILAAY

BCys:

MRGSHHHHHHGSDDDDKWA-*Helix*-IGHDHVARPRDTSMGGC

Helix:
SGDLKNKVAQLKRKVRSLKDKAAELKQEVSRLENEIEDLKAK

Figure 6-1: Amino acid sequences for L2FC7 and BCys. Like all leucine zipper type domains the core *d* position is inhabited exclusively by leucine (L) residues. The core-flanking *e* and *g* positions are inhabited by mostly potentially charged residues, most notably lysine (K). The residues positioned on the outer parts of the coiled-coil are also mainly polar residues.

pH conditions a large proportion of these residues at the interface will be negatively charged, and the resultant repulsive electrostatic forces will overcome the favourable hydrophobic attractions between side chains in the core of the coiled-coil, destabilising the coiled-coil interactions. Conversely at lower pH conditions there will be less repulsive negative charges and so the coiled-coil dimers will be more stable. As a result of this the L2FC7 protein cross-links at low pH regimes to form a hydrogel (on the macroscale), whereas at high pH it forms a viscous liquid.

The BCys protein is a truncated form of a tri-block hydrogel protein and has already been described in detail. BCys contains a single leucine zipper domain, with a short 'tail' section at its carboxy-terminal end, terminating in a cysteine residue. The leucine zipper section is basic and previous studies have shown it to homo-dimerise to form coiled-coil structures preferentially at high pH regimes (Petka 1997; Stevens 2001). Previously Stevens *et al* has examined the behaviour of surface-immobilised monolayers of the protein ACys when exposed to changes in pH using QCM-D (Stevens *et al.* 2004). In this study the related protein BCys will be treated in a similar manner, but with additional measurements using DPI, to attempt to assess its behaviour and compare with the previous ACys studies.

To investigate the physical properties of the functionalised surfaces under dynamic pH environments, and their ability to associate with additional hydrogel proteins in solution, the complementary optical and mechanical techniques of dual polarisation interferometry (DPI) and quartz crystal microbalance with dissipation monitoring (QCM-D) have been employed. DPI consists of a pair of wave-guides through which light, polarised in two planes perpendicular to each other, is passed. It is the uppermost wave-guide which constitutes the sensor surface, and as biomolecules either are deposited on this surface or change their physical characteristics, the resultant change in refractive index at the wave-guide interface causes a change in the interference between the light passing through both wave-guides. By monitoring the resultant shift in interference pattern, film thickness and refractive index can be

directly measured, and from these values layer mass and density can be calculated (Sauerbray 1959; Cross and Ren 1999; Cross *et al.* 2003; Cross *et al.* 2004). In the complementary technique of QCM-D, a gold-coated quartz crystal is used as the sensor platform. Changes in the resonant frequency of the crystal are used to detect changes in adsorbed mass (Sauerbray 1959). In parallel the damping (or dissipation, a dimensionless quantity) of the crystal oscillations is also monitored, which can provide information about the mechanical properties of the adsorbed layers (Voinova *et al.* 1999).

6.2 Materials and Methods

All buffers used were solutions of 10mM NaH_2PO_4, 150mM NaCl, with pH adjusted using 5M NaOH. All solutions were prepared using high purity de-ionised water (ELGA water system, Maxima HPLC, Elga Ltd, Bucks, UK; resistivity 18.2MΩ cm).

6.2.1 Dual Polarisation Interferometry (DPI)

DPI experiments were performed on an Ana Light Bio200 dual polarisation interferometer using an amine-functionalised FAR-100 chip (Farfield Sensors Ltd., Salford, UK). The running buffer was pH 7.4 10 mM sodium phosphate, 150 mM sodium chloride, with a flow rate of 100 µl per minute, unless otherwise stated. Prior to immobilisation, sensor surfaces were twice washed with 80% w/w ethanol then de-ionised water. The sensor was calibrated using high purity water and 80% ethanol solutions of known refractive index (1.3 and 1.359 respectively). Protein L2FC7 and BCys were both immobilised via the coupling of the terminal cysteine residue to the amine surface with the hetero-bifunctional cross-linker Sulfo-GMBS (N-[g-Maleimidobutyryloxy] sulfosuccinimide ester) (Pierce, Rockford Il.), which contains both a maleimide group and an N-hydroxysuccinimide (NHS) ester group. To achieve this two of

the three flow channels within the instrument were rinsed with 10 mM Sulfo-GMBS (in pH 7.4 buffer), before rinsing with buffer alone. A 10 μM solution of protein (also in pH 7.4 buffer) was then applied to only one of these channels, leaving the other channel with linker alone, to act as a negative control. Data from the control channel (channel one) was subtracted from this channel to account for changes due to bulk solution differences. Data was analysed using "Resolver" and "Interpreter" software packages (Farfield Sensors Ltd., Salford, UK). The sample chamber was a continuous flow cell attached to a syringe pump with a flow rate of 100 μl minute^{-1} unless otherwise stated. The chamber was kept at a constant temperature of 20.0°C throughout all experiments.

During protein-binding experiments, 5 μM solutions of the proteins suspended in phosphate buffer were exposed to the already functionalised sensor surface and the flow shut off for the duration of exposure of protein to the surface. This was to economise on the limited supply of protein available for the experiments. Flow was then continued as before with buffer to flush protein solutions out of the chamber.

6.2.2 Quartz Crystal Microbalance with Dissipation Monitoring (QCM-D)

QCM-D experiments were carried out on a Q-Sense D300 QCM-D using a standard gold-coated quartz sensor crystal (Q-Sense AB, Sweden). The QCM-D crystals used had a fundamental resonant frequency of 4.9 MHz and a mass sensitivity of the order of 5 ng cm^{-3} in a liquid environment. Changes in resonant frequency (Δf) and dissipation (D) were measured simultaneously at the third, fifth and seventh overtones. For simplicity the results presented in this study show the data from the third overtone only, normalised to that of the fundamental mode by dividing the frequency data by the overtone number. L2FC7 and BCys were both immobilised by direct attachment to the gold substrate by incubating 10 μM solutions of protein (in pH 7.4 buffer) with the

sensor surface. The protein becomes attached to the gold sensor surface by the direct thiol coupling of its terminal cysteine residue side chain. All samples were introduced as a volume of approximately 1.5 ml via an axial flow chamber, which included a T-loop, where the sample was thermally equilibrated at 23.0 °C for at least two minutes before injection of 0.5 ml into the sample chamber.

6.2.3 Surface Plasmon Resonance (SPR)

SPR measurements were all carried out on a Biacore 3000 instrument (Biacore, Uppsala, Sweden). A flow rate of 5 μl min^{-1} was used throughout. A gold-coated sensor (sensor chip Au, Biacore) was used for immobilisation of protein.

6.3 Results and Discussion

6.3.1 pH-Dependent Behaviour of a Surface-Immobilised Protein Hydrogel

6.3.1.1 Deposition of Protein Monolayers.

6.3.1.1.1 DPI

The raw traces for both polarizations obtained during addition of linker and protein to the DPI sensor are shown in Figure 6-2. A 10 mM solution of the Sulfo-GMBS linker was allowed to flow over the sensor surface (at the beginning of the trace), which was observed as an abrupt initial increase in the signal, before returning to running buffer at t = 2 minutes. At approximately t = 8 minutes a 10 μM solution of the L2FC7 protein in pH 7.4 buffer was allowed to flow over the surface until no further increase in the deposited film thickness

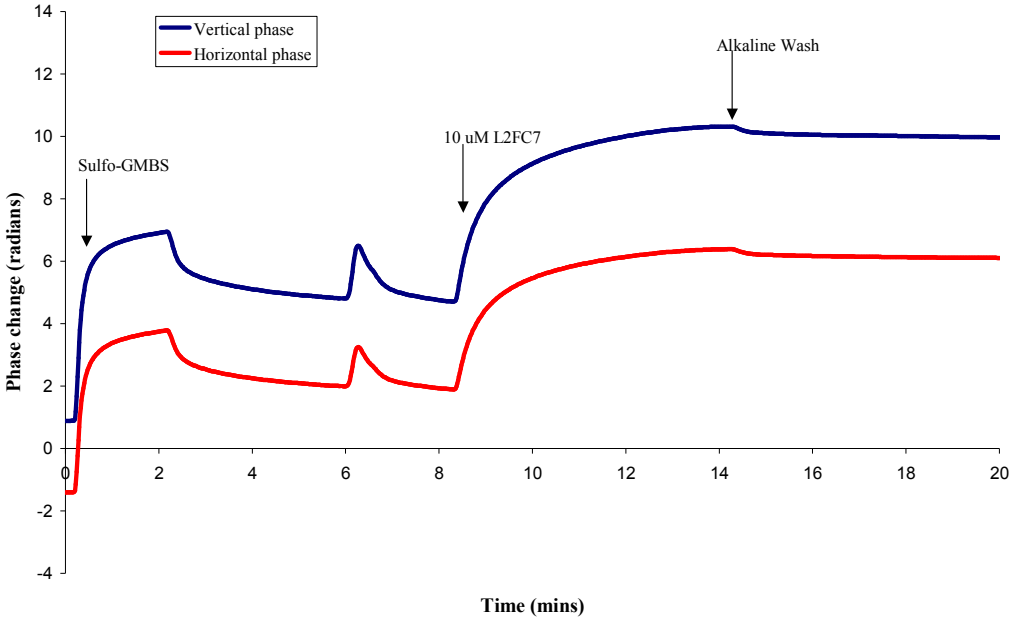

Figure 6-2: Addition of monolayer of L2FC7 onto DPI sensor. Both the vertically and horizontally polarized signals are shown. To the amine-functionalised sensor was added a solution of the linker Sulfo-GMBS, which was then rinsed with buffer before the addition of a 10μM solution of L2FC7. The adsorbed layer of protein was then washed with pH11.2 sodium phosphate buffer to dissociate any protein not covalently attached. The small peak in the traces after approximately six minutes is an artefact of a change in flow rate at this point and does not correspond to an injection into the flow chamber.

was observed. To economise on limited stocks of protein flow rate was reduced to 50 µl min^{-1} for duration of protein adsorption. After 14 minutes the protein layer was then washed with pH 11.2 buffer to destabilise interactions between any coiled-coil aggregates which may have formed and thus dissociate any protein not covalently bound to the sensor surface. At high pH the large number of negative charges due to the glutamic acid residues within the coiled-coil domains has a destabilising effect on the interaction of the dimers, due to electrostatic repulsion, leading to increased dissociation. When buffer was allowed to flush excess protein out of the sample chamber, some protein was released initially, as evinced by a decrease in the thickness of the layer, but after the repeated washes with the alkaline solution, film thickness stabilized. It should also be noted that the exposure to high pH solution would have hydrolysed any maleimide groups that had not interacted with L2FC7 already (Ishikawa *et al.* 1983), preventing further attachment of protein to the Sulfo-GMBS layer during later protein adsorption studies.

Data for the initial washed layer thickness for the protein is summarised in Table 6-1. The layer of L2FC7 had a mass of approximately 2.3 ng mm^{-2}. Using the molecular weight of L2FC7 of 45kDa and Avogadro's number (6.022×10^{23}) it is possible to calculate the average surface coverage of the protein, assuming monolayer coverage, which yields an average footprint of 1 L2FC7 molecule per 59 nm^2.

6.3.1.1.2 QCM-D

Prior to the attachment of protein to the QCM-D surface, a series of blank measurements were obtained with each of the different buffers to be used throughout the experiment. The range of resonant frequency shifts (Δf) across the range of buffers used was less than 2 Hz; while the maximal shift in dissipation (D) was 0.6×10^{-6}, representative of the slight density differences between the experimental solutions resulting from differences in dilution caused by pH adjustment.

Layer	RI	Thickness (nm)	Mass (ng/mm^2)
GMBS	1.47	1.41	1.02
L2FC7	1.43	4.60	2.30

Table 6-1: Summary of layer data for L2FC7 surface adsorption in DPI experiments. Protein layer data is cumulative, based on Sulfo-GMBS and L2FC7 combined.

The Δf (blue trace) and D data (yellow trace) obtained from the adsorption of L2FC7 to the sensor surface is shown in Figure 6-3. Prior to the adsorption of protein, the sensor crystal was incubated with the pH 7.4 buffer until a steady baseline was obtained. A 5 μM solution of L2FC7 protein in pH 7.4 buffer was then added at time, t = 1 minute. When the frequency response had reached a plateau at -64 Hz after approximately 35 min, which suggested that little or no more protein was binding to the surface, the surfaces were washed with 0.1M NaOH repeatedly to dissociate any L2FC7 complexes, and hence remove any protein not directly attached to the surface. The Δf was reduced to -58Hz after this step.

Using the Sauerbray relationship, the adsorbed layer of L2FC7 was estimated to have a mass of 11.50 ng mm^{-2}. Again, using Avogadro's number, surface coverage of the protein on the sensor was calculated to be 1 molecule of L2FC7 per 6.6nm^2.

Using the QCM-D values obtained at face value, the layer immobilised on the Au QCM-D sensor would seem to be approximately nine times more compact than that on the DPI sensor. This would imply that the surface arrangement is quite different for the surfaces used with the two techniques. The denser molecules within the monolayer in the case of the QCM-D surface would have less conformational freedom than the monolayer on the DPI surface. A cross sectional area for the dimer of 7.1 nm^2 (i.e. 4.6 nm^2 per molecule) has previously been estimated for a similar coiled-coil domain orientated perpendicular to the surface (Stevens *et al.* 2004), based on the crystal structure of the GCN4-p1 protein complex (O'Shea *et al.* 1991). This value, obtained from the QCM-D, is also approximately half as dense on the surface as the figure calculated for maximal theoretical coverage in this study. Thus the molecules of L2FC7 would not be packed in an ordered vertical arrangement, but would be much more likely to be in a disordered array.

However, the calculated value can only be used as an approximation, as the adsorbed layer under observation does not fit the criteria mentioned previously

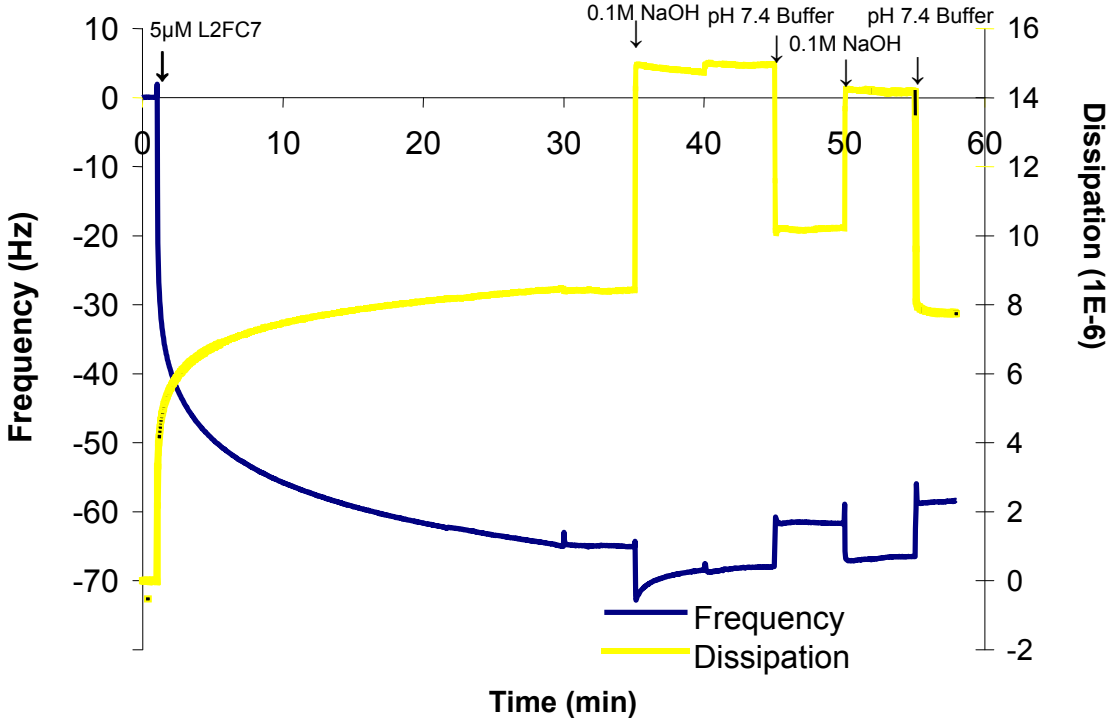

Figure 6-3: Deposition of L2FC7 into a monolayer on gold. As protein adsorbs frequency decreases due to addition of mass onto surface and dissipation increases due to addition of a soft visco-elastic layer.

necessary for compliance with the Sauerbray equation, leading to a quite possibly sizeable error. If a shift in the D signal of greater than 10^{-6} per 5 Hz shift in frequency is achieved, then the adsorbed film on a QCM-D sensor is too soft to function as a fully coupled oscillator (Q-Sense 2005). In other words if the dissipation is greater than this then its effect on Δf will make direct calculation of mass unreliable. For the layer observed here the D shift is greater than this demonstrating that the mass of the layer obtained from the Sauerbray equation will only give approximate values. In addition, because the QCM-D technique is sensitive to hydration associated with the adsorbed layer, while optical techniques are not, this will cause a larger estimate of mass for the QCM-D technique when compared with optical techniques such as DPI and SPR (Höök *et al.* 2002). This point is particularly relevant as the hydrogel proteins are expected to be well hydrated. Even though the surfaces used and associated attachment strategies in the two techniques are chemically different, the amount of protein bound to each would not be expected to be greatly different as both bind via the covalent coupling of carboxy-terminal thiol groups. To test, therefore, whether the difference in coverage for the DPI and QCM-D experiments was due to the detection of the hydration of the protein layer an estimate of the mass of bound water can be made for DPI data and compared with the QCM-D data. The volume fraction (v_f) of the protein in the adsorbed layer can be estimated using equation 6-1, where ρ_L is the density of the protein layer. This value can then be used to make a calculation for the mass of the layer including its relative hydration (equation 6-2).

$$v_f = \rho_L / 1.3 \qquad \textit{Equation 6-1}$$

$$M_L = M_P + (1 - v_f) \times Th \qquad \textit{Equation 6-2}$$

Where M_L is the mass of the layer (mass of protein plus water), M_P is the mass of protein in the layer and Th is the thickness of the layer The value 1.3 in *equation 6-1* is the density of a packed protein layer obtained from the

literature (Höök *et al.* 2002; Voros 2004). This gives a value of 0.384 for the volume fraction and an estimated mass for the protein layer including hydration of 3.24 ng mm^{-2}, more than twice the 'dry' protein mass value (1.02) and which is closer to the value obtained from the QCM-D data.

6.3.1.2 Effect of pH Challenge on Protein Monolayers

L2FC7 monolayers formed during the above experimental steps on the DPI were subsequently exposed to injections of pH-adjusted solutions of pH 4.5, 6.0, 9.5 and 11.2. In between each injection the sample chamber was returned to the pH 7.4 running buffer. The calculated changes for the thickness and density of the monolayer for each pH condition, relative to the thickness and density observed in pH 7.4 buffer (taken as baseline) are shown in Figure 6-4. It can be seen that as the pH was adjusted from an alkaline to an acidic regime, the thickness of the layer decreased, whilst being accompanied by a concomitant increase in layer density.

The pH of the buffer environment surrounding a monolayer of L2FC7 immobilised onto a QCM-D sensor chip was also similarly altered (Figure 6-5). The Δf signal increased as pH was adjusted from basic to acidic. This may indicate a decrease in the mass of the monolayer. However, as all of the protein is expected to be covalently attached to the surface no material should be released from the surface, i.e. this reduction in mass would not be expected to be due to release of protein. As indicated previously the technique of QCM-D is sensitive to the presence of water associated with bound monolayers, either as hydration shells of the proteins, trapped within the protein layer or hydrodynamically coupled to the layer (Höök *et al.* 2002; Stevens *et al.* 2004). This makes it probable that the observed Δf is due to the dehydration of the protein layer as the L2FC7 proteins associate. As an optical technique the DPI data is, however, not sensitive to mass changes due to water bound to adsorbed layers (Höök *et al.* 2002), and net change in mass recorded by the DPI (thickness multiplied by density) was negligible.

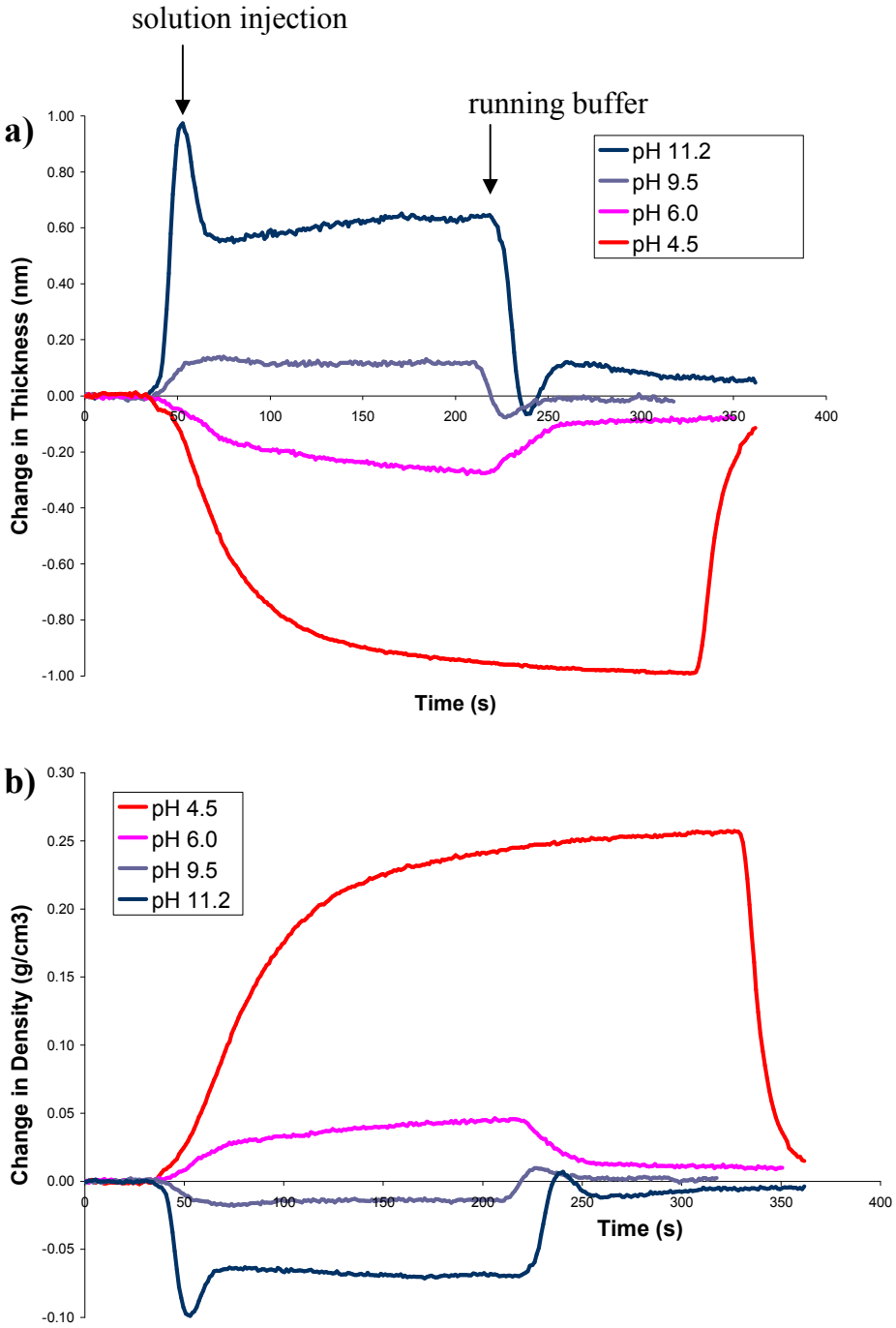

Figure 6-4: Change in a) thickness and b) density of monolayers of L2FC7 in different pH solutions. Values are relative to that at pH7.4, which is the baseline. Note that because at pH 4.5 thickness and density took longer to stabilize, surfaces were maintained at this pH for longer than at other pH values (approx 330 s).

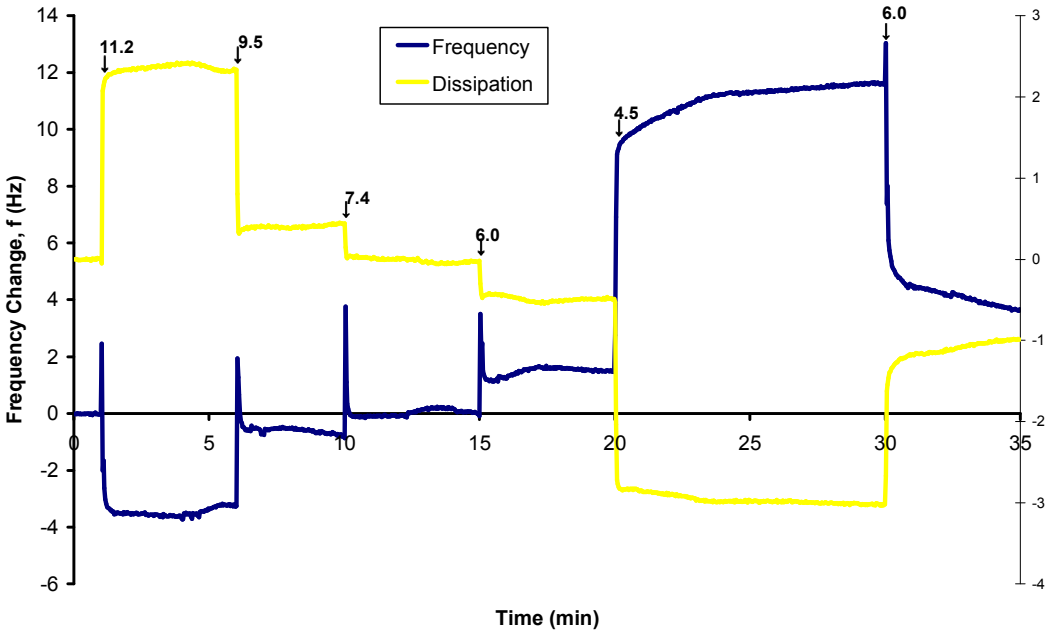

Figure 6-5: Frequency and dissipation change measured for L2FC7 protein immobilized on a gold-coated QCM-D crystal. Numbers on the graph refer to pH of buffers injected onto the monolayer at the points indicated by the arrows. pH 7.4 buffer was used for a baseline with all other frequency and dissipation values relative to this pH.

The behaviour of the QCM dissipative signal also mirrors that of the Δf signal, being highest at pH 11.2, decreasing with pH and reaching its lowest measured point at pH 4.5. As the dissipation signal is due to interactions between the viscous and elastic properties of the layer, as well as the thickness and mass of the layer (Voinova *et al.* 1999; Voinova *et al.* 2002) the changes in D seen are most likely due to the layer becoming 'stiffer' and/or thinner (as shown by DPI) as the pH is decreased.

The data observed by both the DPI and QCM-D can best be explained by the relative dehydration of the layer under acidic conditions, which arises due to an increase in the stability of the coiled-coil aggregates at low pH. As the coiled-coil dimers form, the proteins themselves will become more compact due to the switch of the leucine-zipper domains from random coil to helical conformations, and also because as they associate with neighbouring proteins attached to the surface, or associate with other domains on the same protein, they will be impaired from extending away from the surface. At low pH the glutamic acid residues in the core-flanking *e* and *g* positions of the coiled-coil dimers are protonated and hence the coiled-coil domains are more stable. In contrast at pH 11.2, when these residues become de-protonated, the coiled-coil complexes become less stable due to electrostatic repulsion between charged glutamic acid side chains. Consequently under such conditions a diffuse layer consisting of proteins in a loosely-associated, predominantly random coil conformation will most likely exist. These findings are consistent with previous work, both with a simpler coiled-coil-based system immobilised on a surface (Stevens *et al.* 2004), as well as with the same (Guhr 2000) or similar, but related, systems in solution (Petka *et al.* 1998).

The frequency changes observed with QCM-D as the environment was changed to and from the pH 4.5 buffer show a biphasic response, consisting of an almost instantaneous change in Δf and D, followed by a more gradual change over the next four minutes. This most likely represents a re-ordering of the monolayer at pH 4.5 to a conformation that is different to those existing at other pHs. In addition to the helical sections, glutamic acid residues are found

in abundance in the polyelectrolyte linker regions primarily responsible for the water solubility of the protein (Petka *et al.* 1998). As glutamic acid side-chains have a pK_a of 4.4, in the pH 4.5 buffer only approximately 50% of them will retain their negative charge. As a result the putative re-ordering of the monolayer may be due to a more gradual loss of solubility and dehydration of the protein.

6.3.1.3 Binding of Protein from Solution to Functionalised Surfaces

Figure 6-6 shows the change in thickness and density of monolayers, obtained by DPI, when exposed to 5 μM solutions of L2FC7 in pH 6.0, 7.4 and 11.2 for a duration of 40 minutes each. Exposure to pH 11.2 buffer, which should cause dissociation of coiled-coil dimers, always returned values to close to those of a monolayer, suggesting that changes observed were due to protein in solution non-covalently attaching to proteins in the monolayer and not to the underlying surface. The observed increase in mass is greater at pH 6.0 than at pH 7.4, which in turn is greater than at pH 11.2, a trend also consistent with the change in thickness. This, we propose, is also due to the increased stability of the coiled-coil dimers at acidic pH. At pH 11.2 some of the increase in thickness may be due to the change in thickness of the underlying monolayer. Conversely at pH 6.0 the increase in thickness due to protein association with the monolayer may be reduced to an extent by the established compacting of the monolayer that occurs when exposed to this pH.

Frequency change data for the addition of L2FC7 protein to the monolayer on the QCM-D sensor is shown in Figure 6-7. The sensor was first allowed to equilibrate in pH 6.0 buffer until a steady baseline was reached. At time, t = 1 min a 5 μM solution of L2FC7 in pH 6.0 buffer was added. This solution was allowed to incubate with the monolayer for 30 min before rinsing with pH 6.0 buffer for five minutes, and was then rinsed with 0.1M NaOH solution to dissociate any proteins that may be interacting, before again rinsing with pH 6.0 buffer. This was repeated with the pH 7.4 and 11.2 solutions and buffers. In all cases the frequency was found to decrease, suggesting that mass was

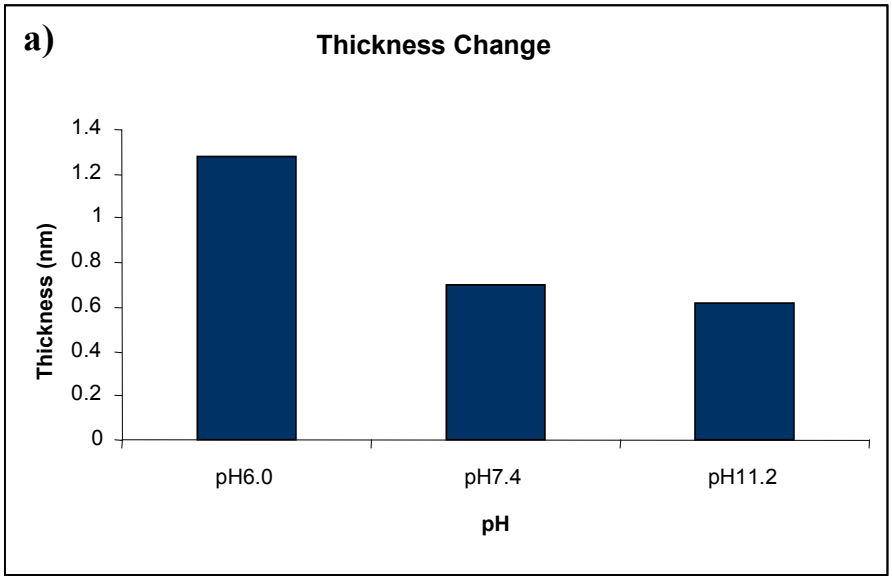

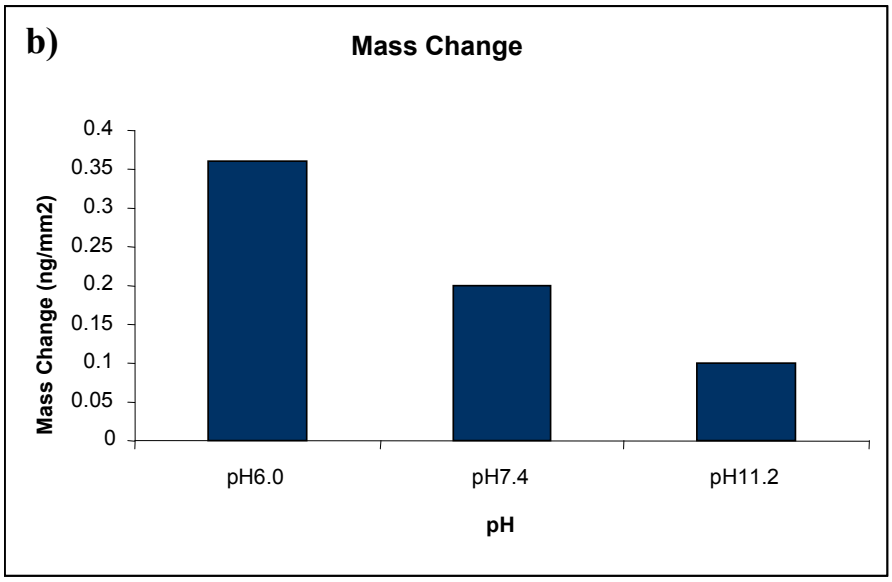

Figure 6-6: Change in a) thickness and b) mass of a monolayer of L2FC7 on exposure to 10μM solutions of L2FC7 of differing pH.

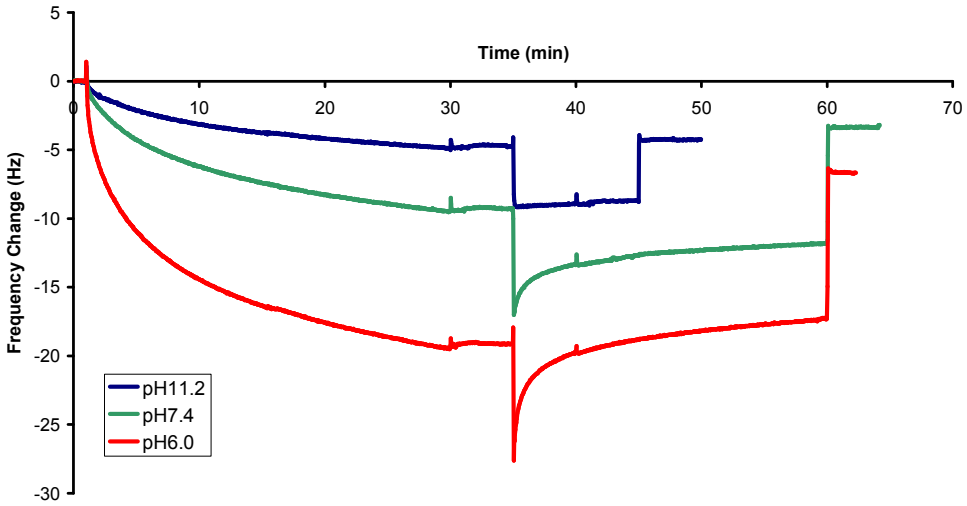

Figure 6-7: Change in QCM-D frequency due to adsorption of L2FC7 to monolayer with solutions of differing pH. After an alkaline wash (0.1M NaOH) majority of the freshly adsorbed mass is removed suggesting that observed mass increases were due to interaction with monolayer and not with the underlying surface.

added to the sensor crystal. At pH 6.0 (Δf of -20Hz after 30 min) the frequency was found to decrease at a faster rate than at pH 7.4 (Δf of -8Hz after 30 min), which in turn decreases at a faster rate than pH 11.2 (Δf of -4Hz after 30 min). Taking into account the Δf changes previously observed with monolayers due to pH alone then pH 7.4 and 11.2 have a net Δf of -8 Hz and pH 6.0 Δf is -18 Hz.

This trend follows closely the mass change trend seen with the DPI data. After the 0.1 M NaOH wash, Δf returned almost to the original values in the case of pH 6.0 and pH 7.4; indication that the observations largely represent protein adsorbing to the monolayer of L2FC7. The residual Δf values retained after the experiment may represent some of the protein being too tightly bound to be dissociated in the time frame of the wash, or some small amount of adherence to the underlying gold surface.

6.3.2 pH-Responsive Behaviour of an Alkali Stable Leucine Zipper Protein

6.3.2.1 Deposition of Monolayers of BCys on Surfaces

6.3.2.1.1 Dual Polarisation Interferometry

The protein BCys was deposited on the DPI sensor surface following the same protocol as previously described for L2FC7. Traces for the raw data showing both plane polarisations are shown in Figure 6-8. After sensor calibration a 10 mM solution of Sulfo-GMBS was allowed to flow over the sensor surface for approximately two minutes. The sensor was then rinsed with pH 7.4 solution. A 10 μM solution of BCys in pH 7.4 sodium phosphate solution was then allowed to flow over the surface of one sensor channel until a plateau in the

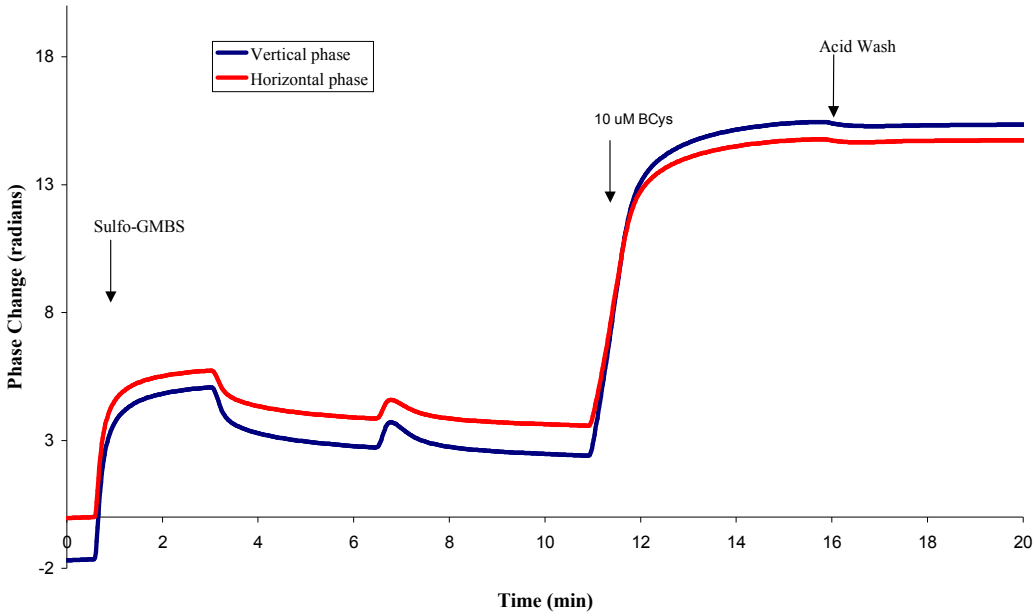

Figure 6-8: Raw phase change data for the addition of the monolayer of BCys to the DPI sensor surface. The peak apparent after approximately 6 min is an artefact due to change of flow rate at this point (100 to 50 µl min^{-1}).

trace was reached, i.e. no more protein was being deposited upon the surface. The other sensor channel was left with Sulfo-GMBS alone, to act as a control. The sensor surface was then rinsed twice with the acidic pH 4.5 solution in order to dissociate any protein non-covalently bound. At acidic pH the large number of positive charges carried by the lysine residues in the leucine zipper regions of the BCys proteins should destabilise any coiled-coil assemblies leading to their dissociation.

Data for the thickness of the deposited layer of the Sulfo-GMBS linker and BCys attached to the surface via Sulfo-GMBS is summarised in Table 6-2. Values presented are taken at pH 7.4 immediately after rinsing with buffers. The layer on the surface has an average thickness of 5.7 nm, with a mass of 4.1 ng mm^{-2}. As with L2FC7 it is possible to calculate the average surface coverage of protein using Avogadro's number along with the molecular weight of BCys (approx 8.5 kDa), assuming coverage of a monolayer was achieved. This yields an average surface coverage for each molecule of BCys of 4.6 nm^2. This value is the same as that estimated for the cross sectional area of the closely related acidic protein ACys of 4.6 nm^2 (O'Shea *et al.* 1991; Stevens *et al.* 2004), suggesting that maximal surface coverage has been achieved.

6.3.2.1.2 Quartz Crystal Microbalance

Graphical representations of the Δf and D signals obtained during deposition of protein on the QCM-D sensor surface are shown in Figure 6-9. Before introduction of protein to the sensor surface the pH 7.4 buffer was introduced into the sample chamber until a steady baseline was achieved. Data recording was started and left running for one minute to provide a baseline for later comparison. At t =1 min a 10 μM solution of BCys in pH 7.4 sodium phosphate solution was added to the sample chamber. This initially lead to a rapid decrease in the Δf value which slowed down and started to reach a plateau after approximately 10 min. A maximum Δf value was observed at this point of -33 Hz. At t = 30 min the surface was rinsed with pH 7.4 solution,

Layer	RI	Thickness (nm)	Mass (ng/mm^2)
GMBS	1.48	1.22	0.98
BCys	1.47	5.73	4.10

Table 6-2: Summary of deposition of GMBS linker and protein BCys onto DPI sensor surface. The data for the protein layer includes quantities due to the presence of the linker.

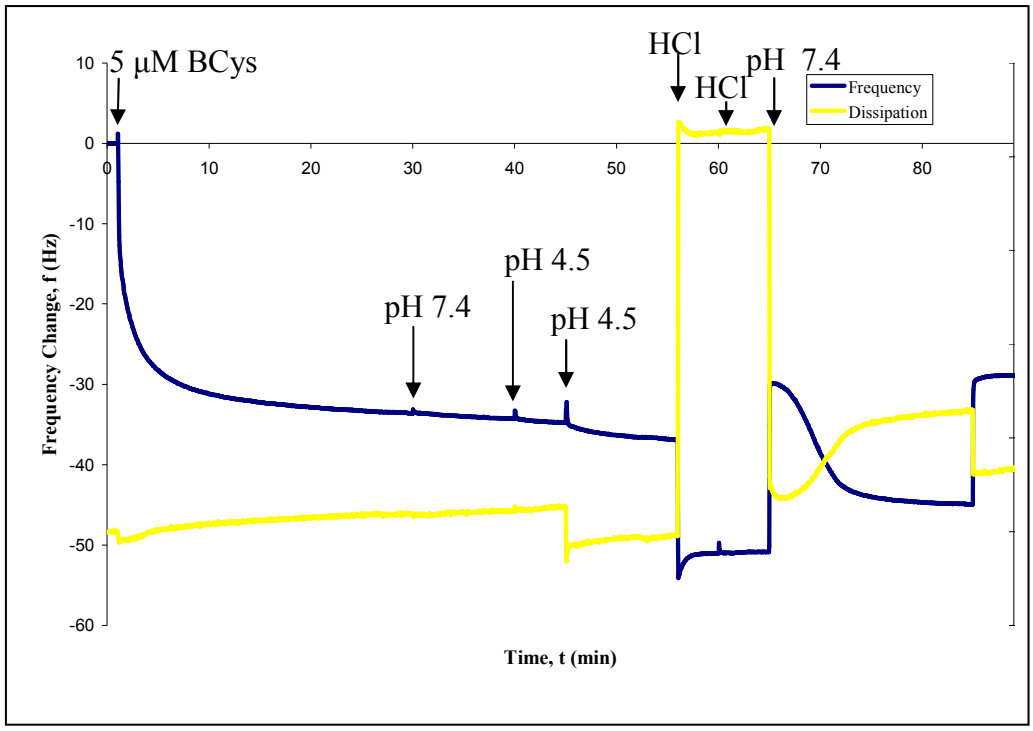

Figure 6-9: Frequency (blue trace) and dissipation (yellow trace) data for immobilization of a monolayer of BCys onto a gold-coated QCM-D sensor crystal by direct thiol linkage.

which did not lead to any noticeable change in the Δf trace.

Two washes of pH 4.5 buffer were introduced at t = 40 min and t = 45 min. This was in order to dissociate any non-covalently-bound protein from the surface. However, this did not lead to an increase in the Δf value, which would indicate a loss of mass from the surface commensurate with the dissociation of weakly bound protein, although a decrease in D was measured suggesting an increase in the rigidity of the layer.

To further ensure that any non-covalently attached protein was removed from the layer it was decided to introduce two washes of 0.1 M HCl, which would be expected to have a greater effect on the dissociation of coiled-coil assemblies. These were introduced at t = 56 and t = 60 min. Introduction of the HCl solution caused an immediate shift in both Δf and D signals, although this will largely be due to the difference in the bulk solution properties, such as density, of the HCl compared with the phosphate solutions, rather than caused by changes in the layer. During the period of exposure to HCl there is an increase in the Δf signal, suggesting that mass was lost from the sensor surface. At t = 65 and 85 min the sample chamber was flushed out with washes of pH 7.4 solution to remove any HCl from the sample. During the first of these pH 7.4 washes an unusual behaviour was observed, where the Δf signal decreased over time, mirrored by an increase in D. It is possible that this is due to a re-ordering of the protein layer as it comes out of the extreme of pH caused by exposure to the HCl. It is quite possible that there is still some HCl present in the sample chamber, at least in the film deposited on the sensor, as when the further wash of pH 7.4 solution is applied the Δf and D signals reached a stable plateau.

The Δf value measured subsequent to washes of the proteins layer is approximately -27 Hz, suggesting that some mass was lost from the surface during the acid washes. An approximate mass for this layer can be calculated from the Sauerbray relationship for this Δf value of 1.7 ng mm^{-2}. From this value a footprint for the average space taken up by a single BCys molecule of

8.5 nm^2 can be estimated. This value is close to that calculated for the immobilisation of BCys on the DPI sensor, suggesting that the layers formed are comparable, and would be expected to show similar behaviour. The higher refractive index for the BCys layer compared with that for L2FC7 obtained for the DPI experiment suggests that the layer is much denser. This would suggest that there is a much greater volume fraction for the protein layer. This means that the BCys layer is most likely less hydrated than for L2FC7, and would explain why there is a much closer correlation between the values for the surface concentration of protein in the layer of BCys for DPI and QCM-D than was obtained with the L2FC7 experiments.

6.3.2.1.3 Surface Plasmon Resonance

To gain further insight into the formation of monolayers of BCys onto a gold surface similar to that of the QCM-D crystal the complementary technique of surface plasmon resonance (SPR) was employed. For this experiment pH 7.4 solution was used as a running buffer with the flow rate set at 5 μl min^{-1}. Figure 6-10 shows the change in the SPR trace as protein was allowed to bind to the sensor surface. The pH 7.4 solution was allowed to flow through the sample chamber for 60 s before the introduction of a 10 μM solution of BCys (pH 7.4) was introduced at point A. This was followed by an abrupt increase in sensor response indicating an addition of mass to the gold sensor surface, which then started to reach a plateau indicating that the surface was becoming saturated with little further increase in mass. After 1000 s a 0.1 M HCl solution was introduced (point B). The low pH of this solution promotes an increase in the number of lysine residues carrying positive charges and hence destabilise any dimers of BCys, allowing any protein not directly attached to the underlying gold surface to dissociate. After 1600 s (point C) the sample chamber was again flushed with pH 7.4 solution. However, the immediate abrupt increase in the response of the sensor at this point was most likely due

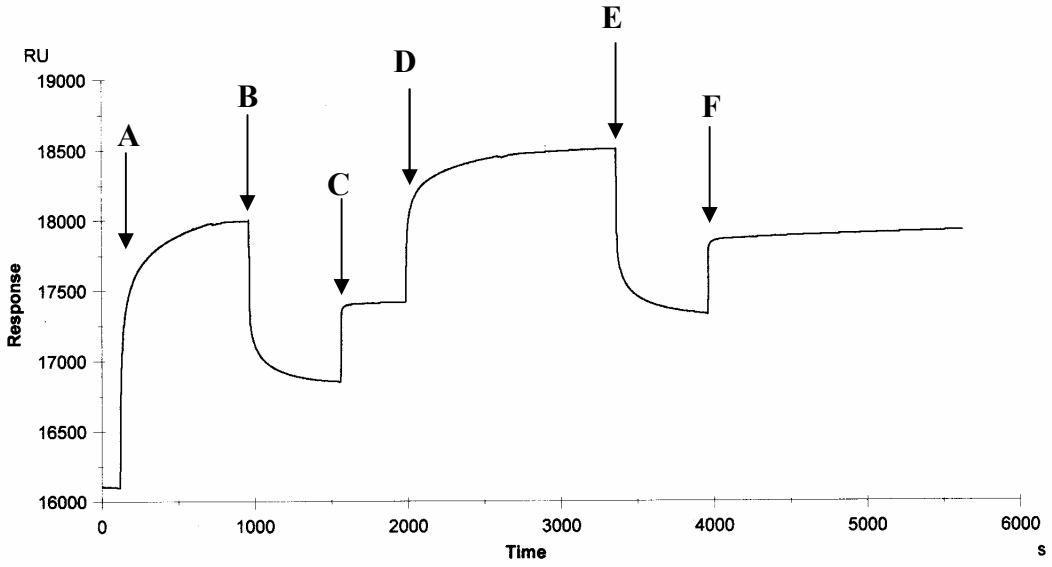

Figure 6-10: The adsorption of BCys in solution onto a gold-coated SPR sensor chip. Changes in sensor response is related to change in mass attached to the surface (RU). Protein is introduced (A,D), before a rinse with 0.1 M HCl (B,E) and a return to pH 7.4 running buffer (C,F).

to the change in the bulk properties of the solution surrounding the sensor and not a change in mass on the sensor. The response at this point is higher than at the start of the experiment by approximately 1250 response units (RU), indicating that the mass on the sensor had increased during the adsorption phase. To ensure that good monolayer coverage was achieved, this cycle was repeated with 10 μM of BCys injected at point D, followed by a rinse with 0.1 M HCl at point E before returning to pH 7.4 running solution at point F. Here a further increase in response is seen indicating that further protein attachment occurred, with a cumulative increase in sensor response of 1750 RU. For protein adsorption, 1000 RU is the equivalent of a surface concentration of 1 ng mm^{-2} (Davis and Wilson 2000). This gives a final surface coverage of protein of 1.8 ng mm^{-2} here. This value is identical to the value obtained with the QCM-D on an identical surface, suggesting that the observed differences between the QCM-D and DPI experiments are mostly due to surface coverage differences.

Given that QCM-D is sensitive to hydration within the layer it would be expected that the value obtained by QCM-D would be greater than obtained by SPR, but this is not the case here. However, it must be borne in mind that the Sauerbray equation used to calculate mass deposited on the QCM-D does not accurately account for visco-elastic layers and hence values obtained with it in this thesis can only be considered to be approximations.

6.3.2.2 Effect of pH Challenge on Monolayers of BCys

Monolayers of BCys attached to the DPI sensor, as described above, were exposed to injections of solutions with pH values of 4.5, 6.0, 9.5 and 11.2. Between each injection the surface was re-exposed to the running solution at pH 7.4. The calculated changes in both thickness and density for the layers relative to that at pH 7.4 are shown in Figure 6-11. For the first 100 s of each trace the monolayer is in the pH 7.4 running solution to give a baseline. At a time of 100 s a solution of another pH was then allowed to flow into the sample

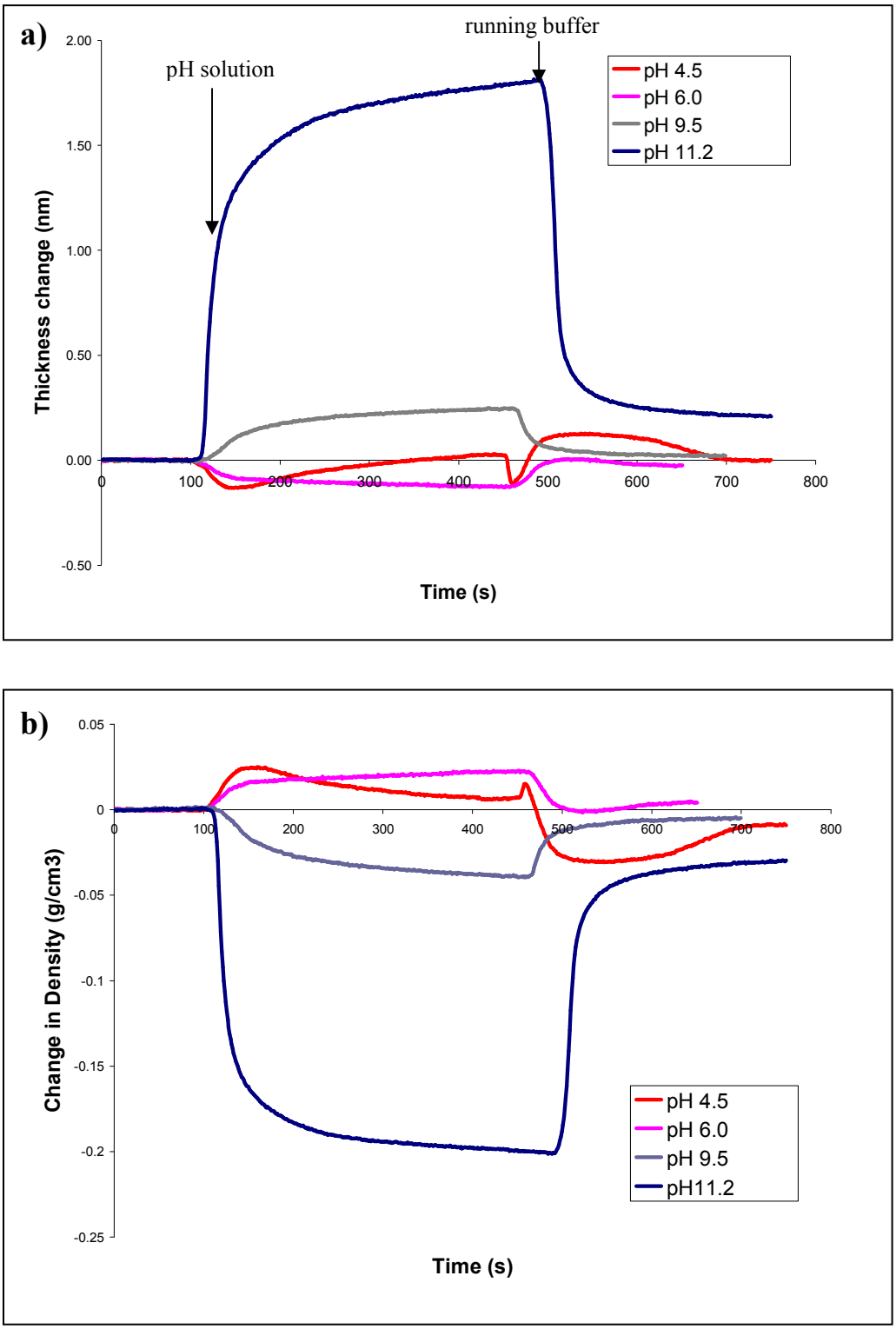

Figure 6-11: Change in a) thickness and b) density of monolayers of BCys in different pH solutions. The values presented here are relative to the thickness and density at pH 7.4.

chamber for approximately a further 400 s before returning to the pH 7.4 running solution. As the pH was increased the monolayer was observed to undergo an increase in thickness. This was matched by a complimentary decrease in the density of the layer. At pH 4.5 the layer is relatively thin and dense while at pH 11.2 the layer is thicker and more diffuse, with a gradation of these effects at intermediate pH values.

As well as many polar residues, BCys contains a large number of hydrophobic residues, with 2 out of every 7 residues in the leucine zipper domains being hydrophobic. At low pH values when little or no coiled-coil assemblages are present these hydrophobic residues may associate to cause a collapse of the layer. Polymers with hydrophobic sections in water have a tendency to collapse into irregular, blob-like structures which may consist of a single unit or several units depending upon the relative sequence of hydrophobic and hydrophilic sections (Allegra and Ganazzoli 1997; Lee *et al.* 2002; Lee and Vilgis 2002b). It is quite possible that the hydrophobic residues in BCys may associate in this manner when not assembled into coiled-coil units, leading to a relatively compressed layer. As pH was increased and the leucine zipper sections assembled into coiled-coils, the height may increase slightly, leading to the small increase in height detected between the acidic pHs and pH 7.4. At the pH of 9.5 most of the BCys proteins in the layer are likely to be associated, but the layer thickness continues to increase, reaching a maximum at pH 11.2. As well as the leucine zipper regions, BCys also contains an amino-terminal random coil section, containing a number of polar residues. As the pH is increased in the alkali region, the sum of charges carried by amino acid side chains in this section will result in a significant net negative charge of -3.5 per molecule at pH 11.2, based upon the proportion of each side chain that will be charged at this pH. As has been seen from the work in chapter 3 and in the literature (Li and Witten 1995) an overall charge on a random coil chain will cause a more elongated conformation to be adopted. This could result in the elongation of this amino terminal section of the BCys protein to become more elongated at high pH and to an increasing extent as pH increases.

A more complex behaviour was observed when the surfaces were exposed to a pH transition from 7.4 to 4.5. Initially there was a decrease in thickness accompanied by an increase in density of the layer. This then subsides, returning to close to the original value. As the pH 7.4 solution returns to the chamber there is an initial spike in the thickness and density traces followed by a change to a layer that is thicker and less dense before returning to the baseline. This behaviour is quite different to that observed at the next pH of 6.0 where, the thickness of the layer decreased slightly relative to at pH 7.4, with a concurrent increase in density of the layer. This behaviour was maintained steadily until the pH was returned to 7.4, whereupon there was a rapid and uncomplicated return to the baseline.

In addition as pH was changed to 4.5 there was a small mass change (Figure 6-12). The mass initially underwent a rapid increase, followed by slower, steadier increase which mimicked the steady increase observed in the thickness trace. As the monolayer underwent this transition there was quite a significant change in the charge of the protein, with a much greater number of positive charges being present. As such, it is quite possible that the change in mass is due to the exchange of ionic species within the layer as there would be expected to be an exchange of sodium ions (with a molecular weight of 23) with heavier chloride ions (molecular weight 35.5) as the layer changes its relative charge. It is therefore likely that the observed behaviour as the layer shifts from pH 7.4 to 4.5 and then back again is the result of a rearrangement of the proteins in the layer from a relatively ordered structure with some coiled-coil content, to a less ordered but relatively compact layer, with an associated mass change as associated sodium ions within this layer are replaced by chloride and phosphate ions.

In contrast, as the layer returned to pH 7.4 from pH 11.2 there was an immediate but incomplete return towards its original pH 7.4 level, followed by a slower decrease. If the layer at pH 11.2 consists of proteins that are almost completely in tightly ordered coiled-coil states, diffusion of the lower pH solution may be relatively slow, causing a delay in the time taken for the layer

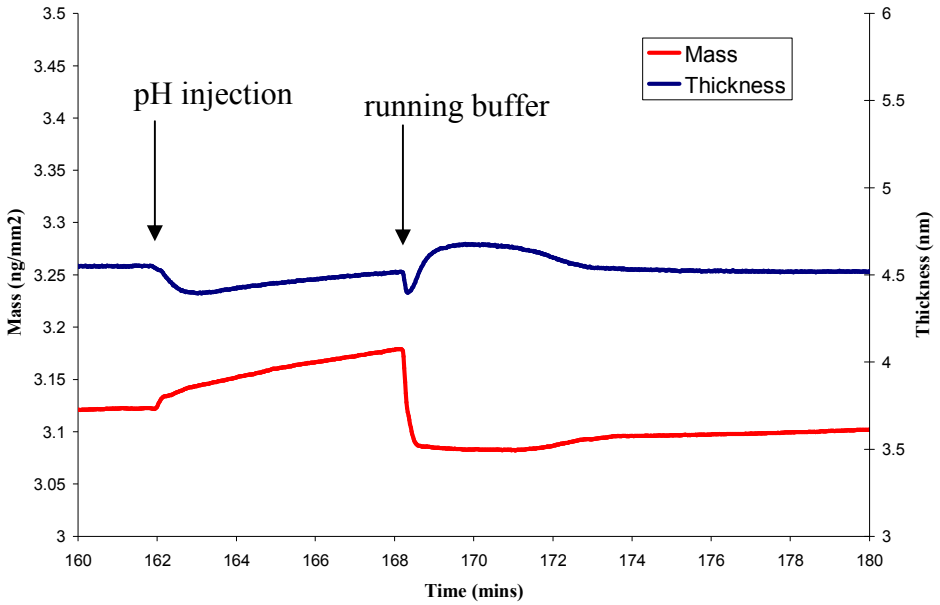

Figure 6-12: Mass change observed in BCys monolayer when undergoing transition to and from pH 4.5. Here pH 4.5 is injected into the sample chamber at 162 min, followed by a return to pH 7.4 running solution at 168 min.

to return to its pH 7.4 state.

The pH of the solution surrounding the BCys monolayer immobilised onto the QCM-D sensor was altered in a similar manner (
Figure 6-13). As the pH was adjusted there was a shift in both the Δf and D traces, although the magnitude of these shifts was much less than that observed with the L2FC7 protein. As the pH was increased an increase in D and a decrease in Δf was observed. This would suggest that the layer was more rigid at a low pH. The change in Δf also indicates a probable gain in the mass of the layer, which is most likely due to an increase in the hydration of the layer. The drop in average density of the layer seen in the DPI experiments is also suggestive of a decreasing volume fraction of the protein layer, indicating a greater proportion of fluid in the layer.

In studies by Stevens (Stevens *et al.* 2004) on the related protein of ACys, using the QCM-D technique, a similar trend to that observed here in Δf and D was observed (although the magnitudes of the shifts seen here with BCys are less than was observed with ACys). This was attributed to the proteins at low pH being associated in a rigid, compact, and ordered layer due to the leucine zipper sequences in the proteins being associated as coiled-coil assemblies. As the pH was raised the leucine zippers became less associated and more hydrated, leading to an increase in the D signal and a decrease in Δf. With the protein BCys this is an unlikely explanation as BCys was designed to form coiled-coil structures with a pH dependency opposite to that of ACys. It is already established that BCys forms more stable coiled-coil dimers at high pH than at low pH (Petka 1997). Again the results cannot entirely be explained solely by changes in the association of the leucine zipper sections of the molecule. However, both the zipper section and the amino-terminal sections of the proteins may change their relative amounts of hydration with pH. It is possible that for BCys the zipper section loses hydration as coiled-coil structures form with increasing pH, but at the same time the amino-terminal tail may be increasingly hydrated as it becomes more extended due to an overall negative charge. If this is the case then for BCys the hydration of the

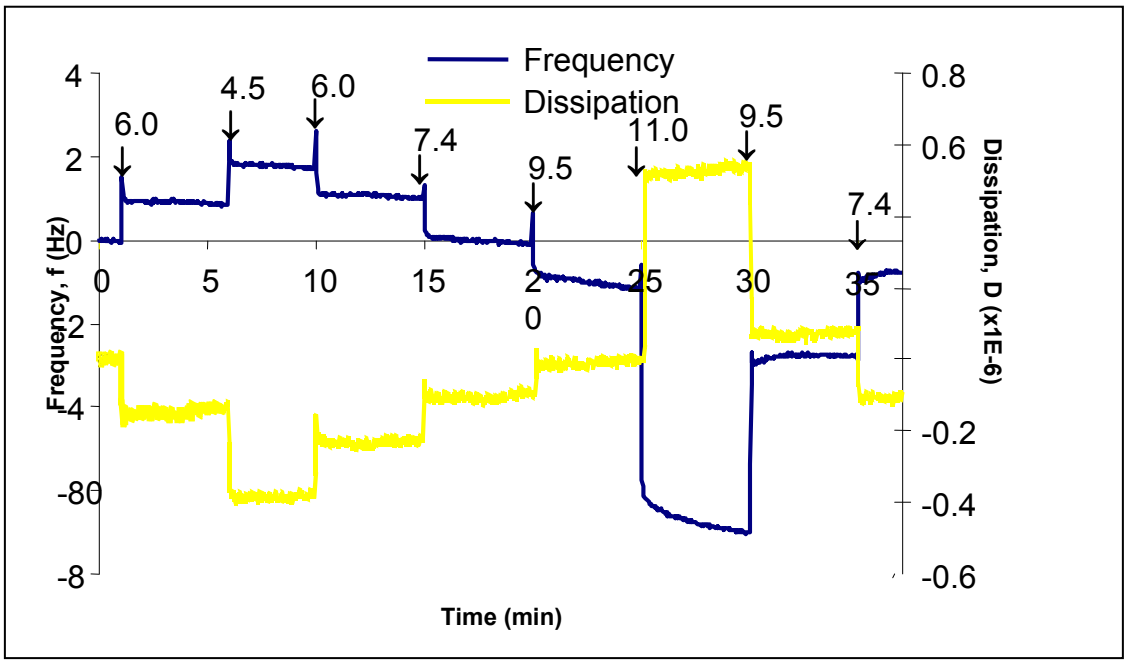

Figure 6-13: Change in frequency and dissipation of BCys monolayers exposed to different pH environments detected by QCM-D. Numbered arrows mark the injection of a different pH solution into the sample chamber.

leucine zipper portion of the layer and the hydration of the amino-terminal layer have pH dependencies that run contrary to each other, whereas for ACys they are in accord. It must be emphasised that it is this amino-terminal section of the protein which will form the interface between the protein layer and bulk solution, and so changes in this part of the protein may have a significant effect on measurements taken. This could explain why the Δf and D shifts for BCys are observed to be much less than for ACys, with a maximum shift across the range of measurements of 8 Hz, whereas Stevens obtained total shifts of 20 Hz with ACys.

Together the data suggests that as pH increases from a low to high regime, the average thickness of the layer increases, as it changes from consisting of partially collapsed and disordered layers to a thicker more ordered layer of associated leucine zippers, with a secondary layer consisting of the amino-terminal sections of the proteins extending into the solution. As this change occurs the average protein density drops. The leucine zipper sections will become less hydrated as they associate, but this will be countered by the association of water in the more diffuse upper layer.

6.3.2.3 Effect of pH on Adsorption of BCys Proteins to BCys Monolayers

BCys monolayers attached to a DPI sensor chip as described above were exposed to 5 μM solutions of BCys with different pH values. Figure 6-14 shows the change in thickness and density of these monolayers when exposed to the protein solutions for 40 minutes. Between exposures to the protein solutions the monolayers were rinsed with pH 4.5 buffer and then 0.1 M HCl to dissociate any protein not covalently associated with the layer. However, while these acid washes did reduce the mass of the layers, they were not returned completely to their original values. This suggests that some of the solution protein associating with the layer was very tightly bound. The observed

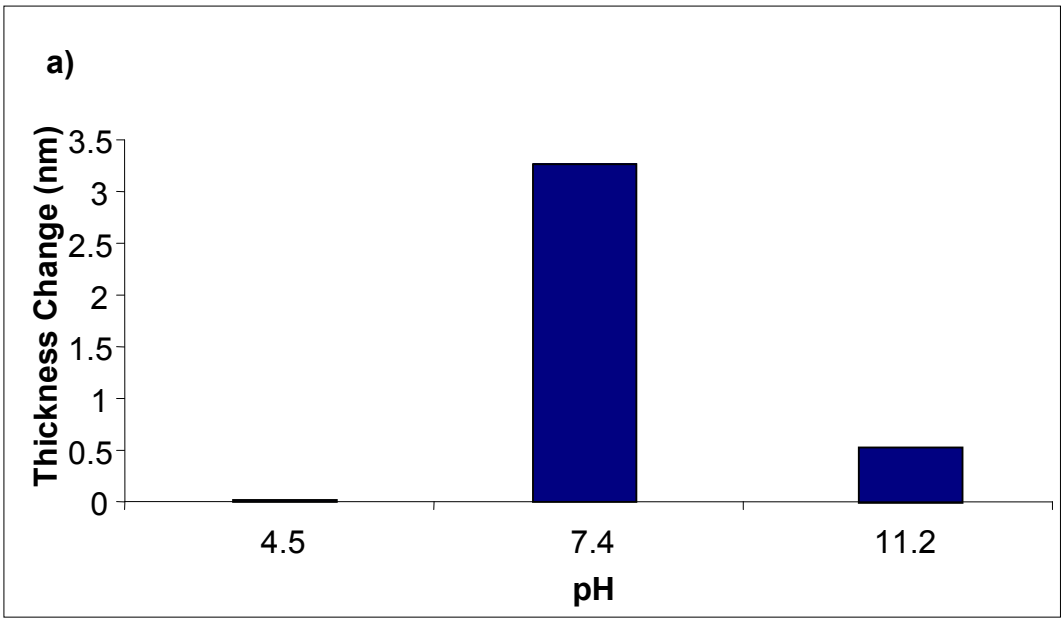

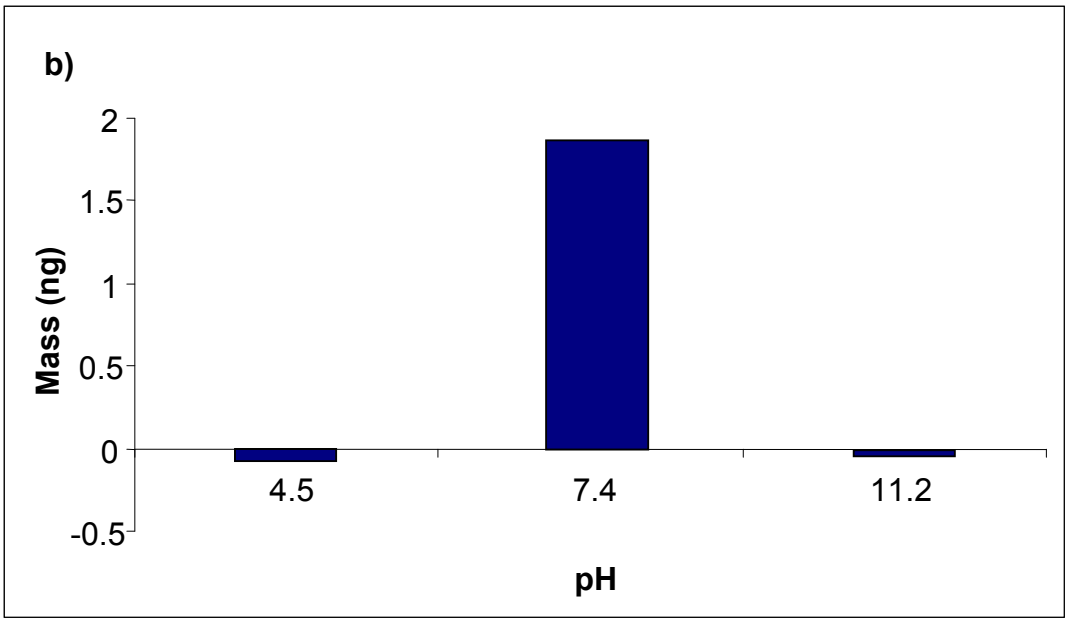

Figure 6-14: Change in a) thickness and b) mass of a monolayer of BCys on addition of different pH solutions of 10μM BCys as measured by DPI.

increase in both thickness and mass is significantly greater at pH 7.4 than for either pH 4.5 or pH 11.2 indicating that more protein became associated with the layer at this pH. At an acidic pH it would not be expected that many coiled-coil structures would be present due to their low stability at this pH, which is what is indicated by the results here. However, at pH 11.2 there was also no increase in the mass of the layer. This can be explained by the tight packing of the monolayer, which would leave individual proteins in close proximity to their neighbours. As the pH is increased to pH 11.2 they are most likely to form coiled-coil assemblies with their neighbours preventing protein in solution from interacting with the layer.

In Figure 6-15 are shown the Δf traces for a QCM-D sensor crystal with an attached monolayer of BCys when exposed to BCys protein in solutions of different pH. The surface was allowed to equilibrate with pH 7.4 buffer until a steady baseline was achieved. At time, t = 1 min a 10 μM solution of BCys was injected into the sample chamber. At t = 30 min the chamber was flushed with a solution of 0.1 M HCl for 5 min before returning to pH 7.4 solution. This was repeated with at pH 4.5 and 11.2. The change in Δf was larger at pH 7.4 (-11 Hz) than at either pH 4.5 (-9 Hz) or pH 11.2 (-1 Hz), indicating that at pH 7.4 there was the largest increase in mass. However, unlike the observation made for the DPI measurements, the pH 4.5 Δf is much greater than at pH 11.2. Again the most likely explanation for the lack of mass increase at pH 11.2 is the density with which the proteins are seeded on the surface. As the pH is changed to one which most favours the formation of coiled-coil assemblies adjacent BCys proteins are most likely to associate with their neighbours before there is a chance for proteins in solution to interact with the layer.

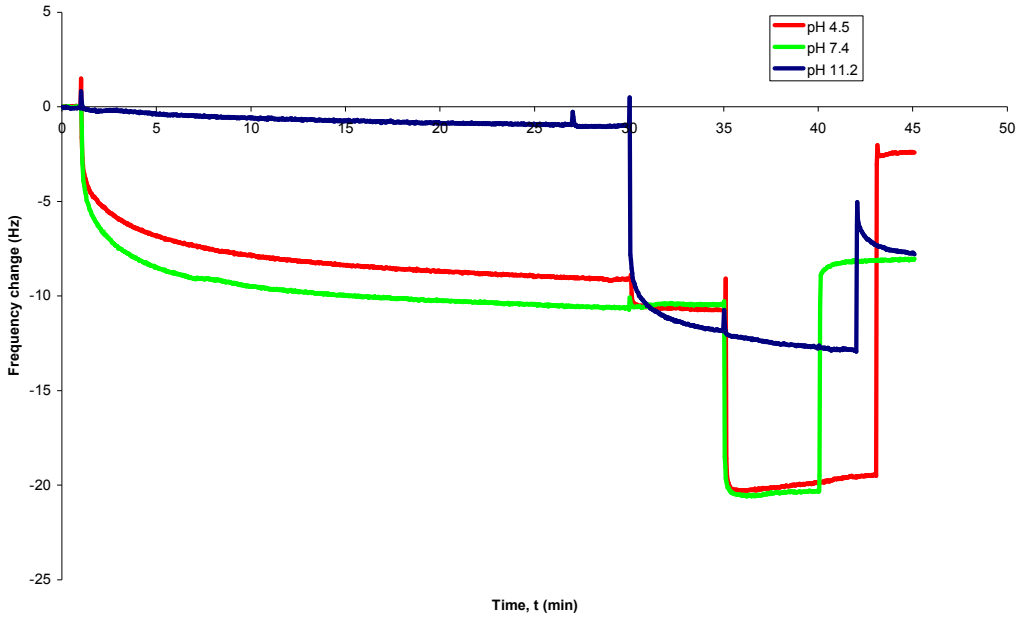

Figure 6-15: Change in frequency of a QCM-D crystal in response to the association of BCys proteins in solution at different pH values to a monolayer of BCys attached to the sensor.

6.4 Conclusions

6.4.1 L2FC7 Summary

The L2FC7 protein, previously known to form a pH-responsive gel in solution, has been immobilized as a monolayer to the glass- and gold-based sensor surfaces of a DPI and QCM-D respectively. We have thus created surfaces responsive to changes in the pH of the surrounding environment. A molecular footprint of 59 nm^2 for the L2FC7 protein on glass and an apparent footprint of 6.6 nm^2 on the gold surface was established. The differences between the layers observed with the two techniques is most likely due to differences in the way mass changes are detected in the techniques here, and to limitations in the way mass change was calculated for the QCM-D technique, as well as differences in the immobilisation strategy between the two techniques.

We have studied the behaviour of the monolayers when exposed to solutions of different pH both with and without L2FC7 protein in solution. At acidic pH the monolayers were thinner, denser and stiffer than at neutral or alkaline pH. This was concluded to be due to the increased association of proteins via coiled-coil forming domains, due to the decrease in electrostatic repulsion between glutamic acid residues in the core-flanking regions of the coiled-coils as pH was lowered. Under alkaline conditions the layers were relatively diffuse, more fluid like and increasingly hydrated as the constituent proteins become predominantly dissociated due to the large number of repulsive negative charges carried by the molecules.

When solutions of L2FC7 at different pH were exposed to these monolayers protein bound to the surface-immobilised proteins in a pH-dependent manner.

As the pH was decreased the amount of protein that could be adsorbed to the layer was increased, due to the increasing stability of association between the helical coiled-coil-forming domains and an increase in the number of links between the proteins in solution and those immobilised to the surface.

6.4.2 BCys Summary

Monolayers of the protein BCys were also immobilised on a variety of surfaces. Footprints for each surface were very similar, with a slightly more concentrated coverage on the glass DPI sensor surface. The optical and mechanical techniques of SPR and QCM-D had close agreement when BCys was immobilised on a gold surface, suggesting that the greater coverage on the DPI sensor was largely a result of the different immobilisation strategy employed.

When monolayers of BCys were challenged with different pH environments it was found that the layers became thicker and more diffuse as the pH increased. At the same time the frequency and dissipation responses obtained by QCM-D suggested that the layer became less rigid and more hydrated at high pH. A model for the changes in the layer was suggested where at low pH, as the proteins are dissociated, the layer is partially collapsed from association of hydrophobic residues. As the pH is increased, coiled-coil structures assemble, creating a more ordered layer, which is most likely more rigid and less hydrated than at lower pH. At the same time the amino-terminal random coil section of the protein becomes more extended as it increases in charge, causing it to become less rigid and more hydrated. The QCM-D data observed is a net result of the two sub-layers of the monolayer, leading to a net increase in hydration and loss of rigidity.

When monolayers were exposed to BCys proteins in solutions of different pH mass increases were the most pronounced at neutral pH. At high pH when it

would be expected for most coiled-coil dimers to form, the close proximity of adjacent proteins in the monolayer probably cause them to associate with each other before proteins in solution have time to significantly interact with the layer. One possible way to test the validity of this in future work is to repeat this experiment using a surface with protein coverage of lower density.

6.4.3 General Conclusions

The two proteins studied in this chapter have shown very different responses to pH challenge. The monolayers of the acidic protein L2FC7 became thicker, less dense and more hydrated, and less rigid as the leucine zipper regions became dissociated. Conversely, for the basic BCys protein the layer became thinner and denser as its leucine zipper domain became predominantly dissociated. The difference is hypothesised to be the much greater proportion of hydrophobic residues in the BCys protein, which will cause the layer to undergo a partial collapse. The greater part of the L2FC7 protein is occupied by poly-electrolyte spacers which are very hydrophilic, and would therefore not be expected to precipitate.

In this chapter pH-responsive surfaces have been demonstrated, created from molecules designed as responsive protein-based hydrogels. In addition the complementarity of the techniques of DPI and QCM-D when monitoring the behaviour of biomolecular films has been demonstrated. An improved understanding of the behaviour of such proteins at surfaces has implications for a wide range of applications where the coiled-coil motif has potential to grant environmental responsiveness.

Chapter 7 : The Investigation of a more Complex Coiled-coil Architecture

7.1 Introduction

In this chapter are detailed experiments in which a spectrum of force is used to probe the stability of coiled-coil assemblies with a more complex architecture than those previously examined in this thesis. The coiled-coils examined in this chapter consist of three sub-units, which combine to form two-helix leucine zippers. This system, termed the 'belt and braces' is a peptide-based linker system originally designed *de novo* in the laboratory of Woolfson *et al* (Ryadnov *et al.* 2003; Ryadnov and Woolfson 2003), designed for mediating the assembly of nanoparticles. It consists of a three peptide assembly of proteins labelled Bn, Bc and A. In particular it has been successfully used to direct the ordered aggregation of gold nanoparticles (Ryadnov *et al.* 2003). Here the nanoparticles were functionalised with Bn and Bc. When the protein A was added to solution the nanoparticles assembled into networks with an even 7 nm distance between each other, corresponding to the length of the protein assembly in helical form. This is a coiled-coil system of more complex architecture than that studied earlier in this thesis, and nothing is currently known about the mechanical properties of these structures. For any nanostructures which may be exposed to external forces their response to mechanically applied force can be important. The purpose of the experiments described in this chapter is to use force to probe the stability of the belt and braces linker system under mechanical stress at the single molecule level.

7.1.1 The 'Belt and Braces' System.

The protein system examined in this chapter consists of three proteins. These are termed Bn, Bc (the 'braces') and A (the 'belt'). The two brace proteins are able to combine with the belt to form a two-stranded leucine zipper assembly. In Figure 7-1 the amino acid sequences for these proteins are shown. The brace proteins Bn and Bc consist of 24 and 23 amino acid residues each, while the belt protein A contains 42 amino acids. At the amino-terminal end of Bn and the carboxy-terminal end of Bc is contained a three-residue GGC sequence, which can allow easy attachment to surfaces via the terminal cysteine residue.

When assembled, the resulting coiled-coil consists of six heptad repeats, with three being formed by Bn-A and three by Bc-A. All of the *a* sites consist of isoleucine and all of the *d* sites are leucine, which favours the formation of a two-stranded zipper assembly, over other possible assemblages (Woolfson and Alber 1995).

7.1.2 Aims and Objectives

In chapter 4 a dynamic force approach was used to probe the stability of a leucine zipper-type coiled-coil assembly. In this chapter a similar approach will be used to probe that of a leucine zipper of more complex architecture. It is the aim of the work detailed in this chapter to determine the stability of the belt and braces assembly under a regime of increasing force, and hence to infer information about the unloaded dissociation kinetics of the assembly and the response to force of the linkage. For the making of nanostructures which may be exposed to mechanical stresses of some form it is useful to have knowledge of the mechanical properties of the linkages between particles.

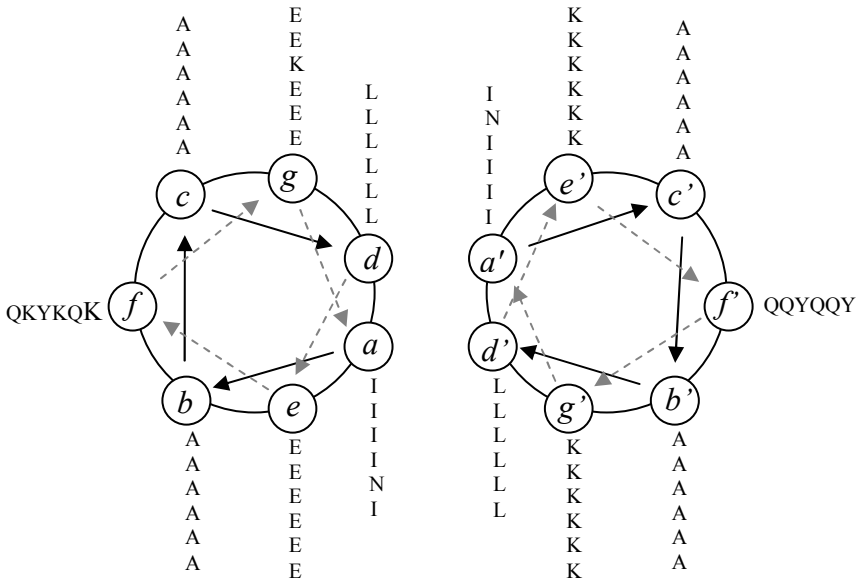

A ac-IAALEKEIAALEQEIAALEKEIAALEYENAALEKEIAALEQE-am

Bn ac-CGGIAALKQKIAALKQKIAALKYK//AALKQKNAALKQKIAALKYKGGC-am **Bc**

Figure 7-1: Diagrammatic representation of the Belt and Braces assembly. At the top is a helical wheel diagram representing the assembled leucine zipper, with Bn and Bc on the left and A on the right hand side. Note that the core-flanking (*e* and *g*) positions are all glutamic acid for the braces and lysines for the belt. These opposite charges of these regions are designed to increase the stability of this assembly. At the bottom is illustrated how the proteins fit together. The // represents the division between Bn and Bc, halfway along the length of A.

7.2 Materials and Methods

Unless otherwise stated, all chemicals used in this work were obtained from Sigma-Aldrich ltd. (Gillingham, Kent). Proteins A, Bn and Bc (Ryadnov *et al.* 2003) were a kind gift from Dr Dek Woolfson (University of Sussex). Proteins were produced by peptide synthesis on a Pioneer Peptide Synthesis System (PE Applied Biosystems, CA).

All measurements were taken in 10 mM MOPS buffer adjusted to pH 7.0 with 1 M NaOH. In the previous experiments with ACys and BCys (as described in chapter 4) proteins were co-incubated on the surfaces with mercapto-undecanol, both to limit the number of interactions seen, and hence keep multiple interactions to a minimum, as well as to help reduce non-specific interactions between surfaces. This approach was again used here, but because Bn and Bc have a much shorter non-helical section attached to the surfaces (three amino acids each), the shorter molecule of mercapto-propanol was used instead.

Gold surfaces were prepared by using the template-stripped gold method (Hegner *et al.* 1993) to create a clean flat gold surface on glass. Surfaces were then functionalised by incubation overnight with a 200 μM solution of mercapto-propanol and 2 μM of Bn protein in 75% v/v ethanol. Surfaces were then rinsed with several washes of high purity de-ionised water and buffer, before allowing to incubate with a (10 μM) solution of protein A for at least two hours, before again rinsing with buffer solution.

Cantilevers used were MCLT-AUHW type (Veeco, Santa Barbera) with nominal spring constants of approximately 12 pN nm^{-1}. AFM cantilevers were sputter-coated with 30 nm thickness of gold on both sides prior to functionalisation. Gold-coated cantilevers were incubated overnight in a 200

μM solution of mercapto-undecanol and a 2 μM solution of Bc protein in 75 % v/v ethanol. All measurements were carried out using a MFP-1D molecular force probe (Asylum Research Inc. Santa Barbera CA.) with an Igor Pro software interface (Wavemetrics Inc., Lake Oswego OR. USA). AFM cantilevers were calibrated and spring constants calculated during each experiment from their ambient thermal excitation spectra (Hutter and Bechhoefer 1993) as detailed in chapter 2. Force curves were rectified to show force versus probe sample separation, before measuring rupture force and extension.

7.3 Results and Discussion

To assess whether specific Bn-A-Bc interactions were being measured a system of several control measurements was first performed between a Bc-and mercapto-undecanol-functionalised probe and gold surfaces coated with various functionalities, as illustrated in Figure 7-2. Firstly the probe was allowed to interact with a surface coated with a monolayer of mercapto-undecanol alone. This was to assess whether any interactions could occur between the protein Bc and mercapto-undecanol; or between mercapto-undecanol on the probe with mercapto-undecanol on the surface. Typical force curves obtained from this set-up are shown in Figure 7-3: a). Secondly the probe was allowed to enter contact with the surface functionalised with both protein Bn and mercapto-undecanol. Examples of typical force curves are shown in Figure 7-3: c). From these two regimes less than 0.5% of force curves exhibited any signs of being specific interactions, i.e. generated force curves with a characteristic curved shape in the retract region. The majority of force curves showed no interaction at all, with a small number of curves exhibiting underlying ‘non-specific’ interactions between the underlying surfaces, where no stretching is in evidence. The final set of control measurements involved the interaction of the probe with a surface containing the Bn protein with an excess of the cross-linking protein A in solution. This should to a large extent block

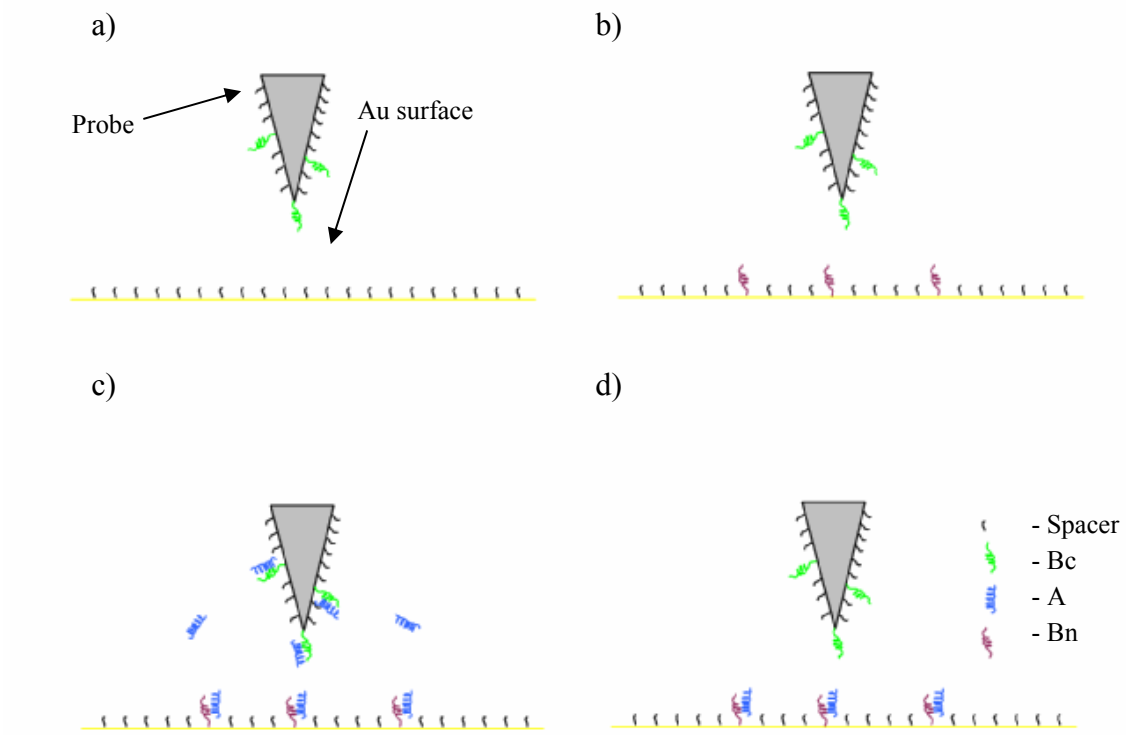

Figure 7-2: Schematic of the experimental set-up. Protein Bn is covalently attached to the surface via a thiol linkage, while the protein Bc is attached to the cantilever. Proteins on both the cantilever and the substrate are diluted on their respective surfaces by the presence of mercapto-undecanol. Sections a), b) and c) represent the different control set-ups, while d) shows the set-up for measurements of the full Bc-A-Bn complex.

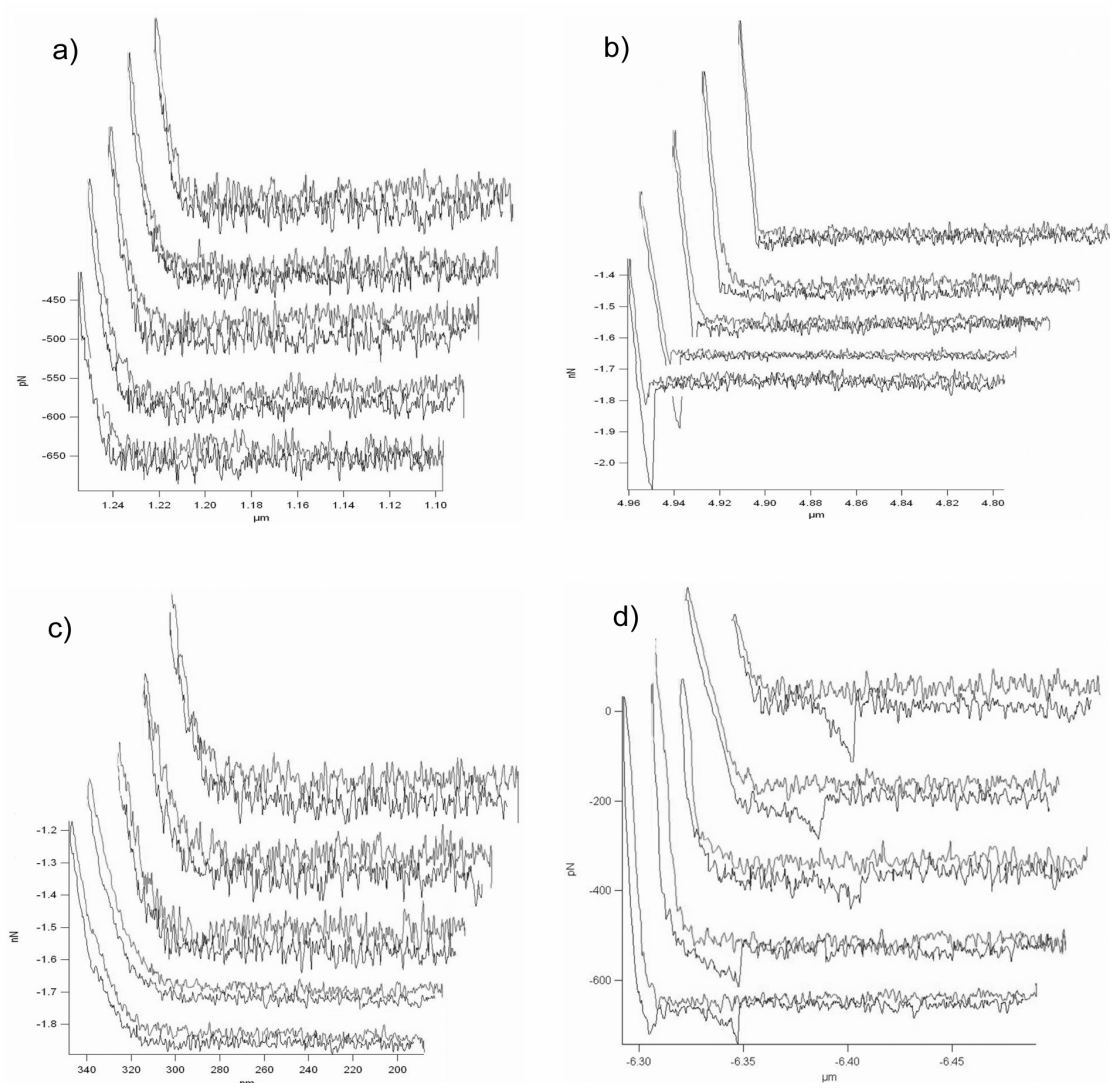

Figure 7-3: a) Force distance curves obtained from interactions of a cantilever probe covered with protein Bc versus a surface covered with mercapto-undecanol alone. b) Force curves from probe coated with Bc against a surface coated with Bn in the absence of cross-linking protein A. c) Curves obtained with probe coated in Bc and surface coated with Bn with an excess of protein A in solution. d) Force curves obtained with a probe coated with Bc, and a surface functionalised with Bn and A proteins showing specific stretching events.

most specific Bc-A-Bn interactions from occurring by the presence of A proteins attached to both the Bc and Bn proteins before the probe and surface are allowed to enter into contact. The proportion of specific interactions seen with this experimental set-up was approximately 2%. In the experimental measurements where a Bc-coated probe was allowed to interact with a Bn-A functionalised surface approximately 10% of force curves exhibited specific interactions. This demonstrates that the majority of force curves identified as representing specific interactions of the Bc-A-Bn complex are not from another source, e.g. direct interactions between Bc and Bn or between protein and the mercapto-undecanol spacer. Examples of curves demonstrating specific interactions from this set-up are shown in Figure 7-3: d).

In Figure 7-4 histograms of rupture forces are shown for force curves taken at three different retract velocities: 3000, 2000 and 500 nm s^{-1}. In order to determine the peak (modal) rupture force, each measured rupture force was assumed to be the centre of a Gaussian distribution with width equal to the cantilever noise. These distributions were then all summed and the peak of the resulting distribution determined and used as the modal force. This methodology is described in greater detail in chapter 4 and this eliminates the influence of arbitrary binning size on peak force when determining the mode directly from histograms. Peak rupture forces determined in this way were 40, 46 and 51 pN for retract rates of 500, 2000 and 3000 pN nm^{-1} respectively, indicating a positive relationship between force and retract speed. In Figure 7-5 are plotted obtained f^* values against probe retract rate on a logarithmic scale.

The model described by equations 4-7 and 4-8 was fitted to the data by the methodology outlined in chapter 4, to allow the determination of the unloaded dissociation rate and the force scale. For the fit to the data the additional parameters of contour length, L_c, and persistence length, p, are required. Proteins Bn and Bc are both attached to surfaces via a three residue non-leucine zipper section. Assuming a length per residue of 0.38 nm, this gives a total L_c of 2.3 nm. For the p length a value of 0.4 nm was used. This is the value most frequently quoted in the literature for random coil sections of

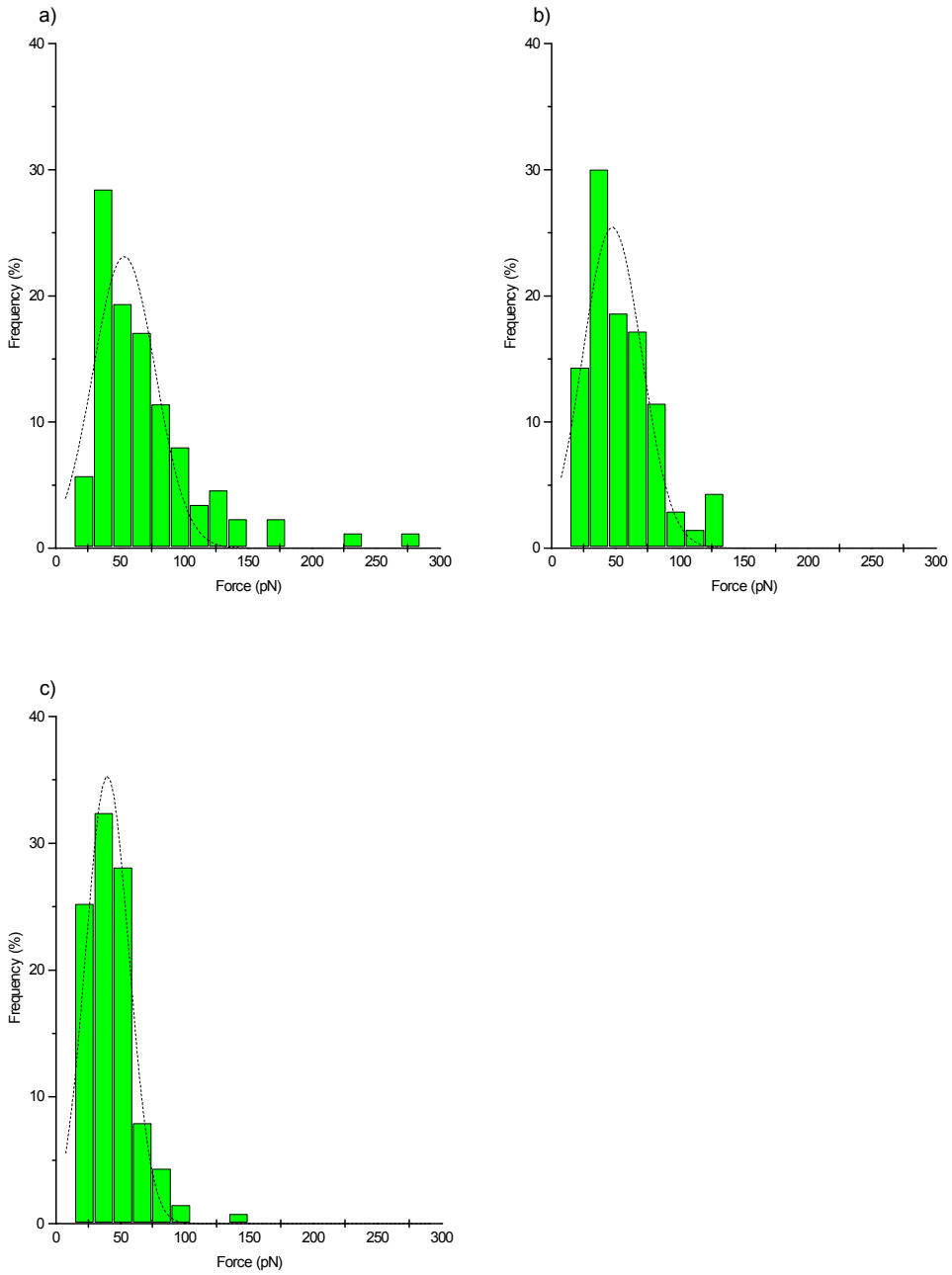

Figure 7-4: Histograms obtained from rupture forces for interactions between the Bn-A-Bc complex at three different retract velocities: a) 3000 nm s^{-1}; b) 2000 nm s^{-1}; c) 500 nm s^{-1}.

proteins (Rief *et al.* 1997; Zhou 2001). The optimal fit to the data is shown in Figure 7-5 as a smooth line. As can be seen the fit passes through the data reasonably well, suggesting a reliable fit, despite the low number of data points. Unfortunately due to time restrictions on the project it was not possible to obtain more measurements, widening the range of probe velocities. From this fit to the data a value for the unloaded dissociation rate, V_0 was obtained of 1.80 s^{-1} (standard deviation +/- 0.96 s^{-1}). This value is remarkably similar to the V_0 value obtained in chapter 4 for ACys at neutral and acidic pH of 1.78 s^{-1}. The values obtained for f_β and x_β were 4.14 pN (+/- 0.47) and 0.99 nm (+/- 0.1) respectively. These values are also fairly close to those obtained with ACys. This indicates that features of the energy landscape for these proteins as revealed by dynamic force spectroscopy, such as distance to primary energy barriers are very similar. Given the very different design approaches for these two types of leucine zippers, this may be a result of coincidence, rather than a common feature of the motif.

Although the connections between Bc and Bn with A are similar, consisting of three heptads each, there is a difference in their respective affinities, with the Bc-A interaction being less stable than the Bn-A interaction (Ryadnov *et al.* 2003). It is not possible to make the distinction from the data obtained here between a rupture event at the Bc-A assemblage or Bn-A. If there was a large separation in the affinity of the two connections then it would be expected that a bimodal distribution of forces would be apparent. This is not seen in the histograms of force data shown here. It must therefore be concluded that either both are rupturing at very similar force values with similar dynamic force behaviour, or that one interaction is so much more stable than the other that its rupture is a rare event.

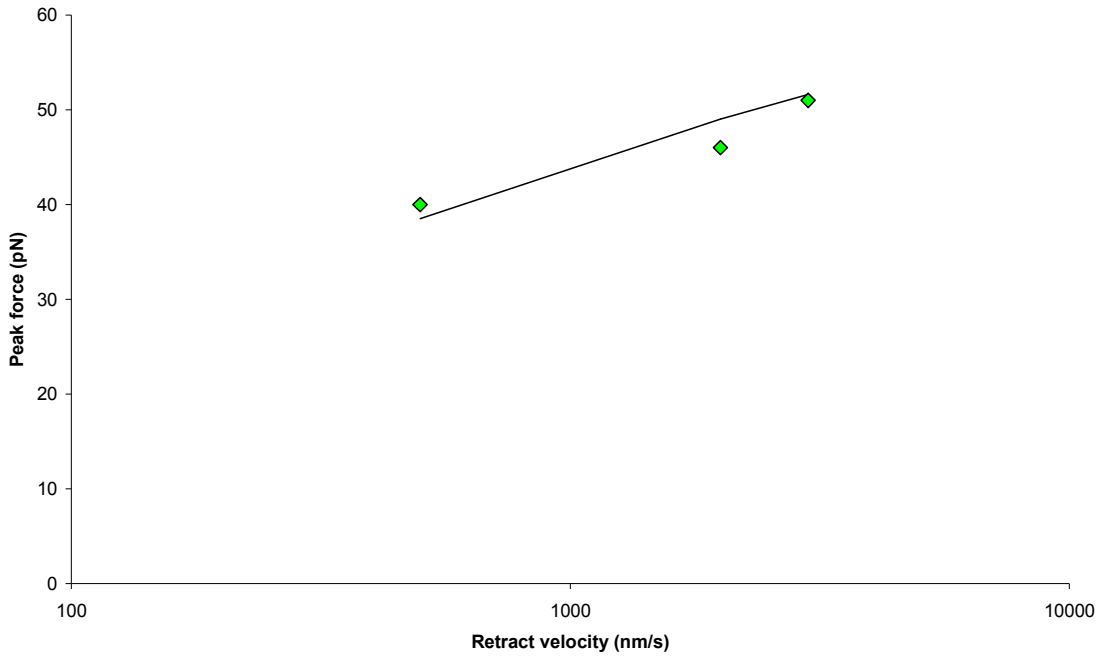

Figure 7-5: Plot of f* against log (probe retract velocity) for Bn-A-Bc complexes. Points shown here are the peak forces from the distributions shown in Figure 7-4. The smooth line represents equation 4-7 fitted to the data.

7.4 Conclusions

In this chapter we have used force as a probe to examine the non-covalent interactions of a coiled-coil assembly of a more complicated architecture than that previously examined. A series of control measurements were made which demonstrate that specific interactions involving the entire Bc-A-Bn complex were being measured. Interactions occurred only in the presence of all three, and were inhibited from occurring when measurements were made with an excess of protein A in solution.

Rupture forces were measured at a range of retract speeds and this data has been used to calculate off rates at zero loading. However, the experiments here must be considered as preliminary experiments, as it was not possible to obtain data from the full range of practicable retract rates obtainable by AFM. If any further experiments on this system, it would broaden the force spectrum and hence allow more reliable calculations of off rates, force scale etc.

The measurements carried out in this section have produced data for unloaded off rates and force scales which are consistent with measurements taken earlier on another leucine zipper assembly (chapter 4), ACys. However, due to the different design approaches between the systems, this similarity is likely to be serendipitous and not reflect any fundamental properties of the leucine zipper motif (Petka 1997; Petka *et al.* 1998; Ryadnov *et al.* 2003).

Chapter 8 : General Conclusions

Previously a series of environmentally-responsive protein hydrogel systems were created, utilising the assembly of leucine zipper sequences as cross-linking domains. As outlined in Chapter 1 these systems are known to undergo reversible transitions in their physical behaviour, switching between viscous liquids and gels, in response to changes in environmental factors such as pH, temperature and solution concentration. The pH-dependent transition is due to the change in ionisation of amino acid side-chains in regions flanking the hydrophobic cores of the coiled-coils, and was of primary interest in this work.

Whilst the bulk properties of these systems are relatively well characterised, little data previously existed at the molecular scale. The primary aim of the work presented in this thesis was to generate data at the single molecule and mesoscale levels to gain a better understanding of how properties at this more fundamental level relate to those previously observed at the macroscopic level.

The first study undertaken was that with the simplest experimental architecture, to probe the mechanical compliance of single molecules of the hydrogel proteins $AC_{10}ACys$ and $AC_{28}ACys$ and how this altered with a change in solution pH. Of particular interest was the entropic elasticity of the protein molecules. Changes in stiffness of the molecules can be related to changes of charge in the protein chains which has implications both for the swelling of hydrogels and their behaviour on surfaces. In addition any change in stiffness due to a change in pH would have implications for DFS experiments undertaken later, as changes in stiffness of protein linking the leucine zipper sections to surfaces can have a profound effect on the rate of loading of force onto bonds of interest. As the proteins examined are probed singly they are

expected to be in a random coil configuration when extended, therefore mathematical models which describe polymer chains with no ordered secondary structure were considered most appropriate for analysing the force curves. For this reason the WLC model was selected as it has previously been found to describe random coil proteins well, with persistence length of the order of 0.4 nm (Rief *et al.* 1997; Zhou 2001). For both proteins studied persistence lengths were very close to this literature-quoted value.

In addition, examination of the maximum extension lengths observed showed that at pH 4.5 the mean extension was less than that observed at pH 7.4 and 11.2. This was observed with both AC_{10}ACys and AC_{28}ACys. This can be attributed to the negative charges found on these protein molecules at the pH values studied, particularly the polyelectrolyte spacer region, which increases with pH. This would be expected to cause the proteins to more readily accept an elongated conformation. It would be expected that such a change would also cause an increase in the *p* of the proteins, but no such pH-dependent shift in *p* values was observed. This change was not observed, and it was concluded that this may have been too subtle an effect to be observed from the obtained data.

The data generated by this first study has implications of two sorts. Firstly it is consistent with the swelling observed in hydrogels formed with these proteins (Petka 1997), suggesting that the polyelectrolyte spacer molecules become more elongated as pH increases and they become increasingly hydrated. Secondly it had implications for the experiments described in chapter 4 and 7 which use force to probe single molecular bonds between these proteins. The compliance of the protein to force has a significant effect on the rate at which force is applied to the dimers.

In the second study described in this thesis, in chapter 4, force was used to probe the kinetic stability of dimers of coiled-coils. For this work the proteins ACys and BCys were used, each of which contain a single leucine zipper motif. It is the coiled-coil motif that forms the association domain between the hydrogel proteins examined in this thesis and is thus essential for their

function. Homodimers of the protein ACys were loaded with force at a range of rates and environmental pH values. At all of the retract velocities studied, the force at which the dimers became dissociated was significantly greater at pH 4.5 and pH 7.4 than at pH 11.2, suggesting greater stability at low and neutral pH values than at alkaline pH. A positive relationship was observed between rupture force and retract velocity at pH 4.5 and pH 7.4, suggesting that these measurements were probing the system far from equilibrium i.e. rather than spontaneous dissociation occurring the force applied was accelerating the dissociation kinetics of the dimers. As a consequence it was possible to use a dynamic force spectroscopy based analysis, allowing estimation of off rates and f_β. At pH 11.2 the rupture force remained constant and did not vary with retract velocity, an observation which is consistent with force applied to a system close to equilibrium i.e. the characteristic lifetime of the bonds was comparable to the time over which the bond was being probed. As the threshold at which bonds switch between close-to and far-from-equilibrium is dependent upon the equilibrium constant, K_{eq}, then it was hypothesised that between pH 7.4 and 11.2 an increase in the off rate for the bond had occurred.

The related protein BCys was also examined using forces at a single velocity, with rupture forces much lower than for the same velocity with ACys, suggesting that BCys homodimers are less mechanically stable than ACys homodimers.

The results of this study are consistent with previous observations (Petka 1997; Petka *et al.* 1998), suggesting that at high pH, acidic leucine zipper dimers are less stable and hence more fluid like than at lower pH, leading to the ability to form more stable gel networks at low pH which dissociate to viscous fluids with increasing pH. Conversely, the opposite behaviour is observed with hydrogels utilising the basic leucine zipper as a dimerisation domain. As far as the authors are aware this is the first time that the coiled-coil motif has been probed at the single molecule level using a spectrum of loading rates and hence demonstrates that this methodology is effective in the study of the kinetic stability of this motif. This has provided information about the mechanical

behaviour of coiled-coils in solution, and their dynamic response to force. As biomaterials which may be made using coiled-coil motifs as linkages are likely to be routinely exposed to external forces, the observation of their behaviour in response to force is therefore highly appropriate.

In chapter 5 the resonance response of thermally oscillating AFM cantilevers was adopted as a probe to study the viscosity of fluid containing hydrogel proteins and also their association at different pH values. A correlation was noticed between resonant frequency of cantilevers and protein concentration, suggesting that increases in solution viscosity were being monitored. However, it was not possible to detect differences between protein solutions of different pH, possibly due to limitations on the sensitivity of this method. Observations were also made of the association of proteins onto and in the vicinity of the cantilever, due to mass-dependent effects on their resonance response. This was observed to vary with pH, in a manner consistent with their design (Guhr 2000). This observation demonstrates that much care must be taken, in any future attempts to measure changes in viscosity by such an approach to ensure that interactions between cantilevers and the solution do not create erroneous results.

The work detailed in this chapter provided some complimentary information on the behaviour of various hydrogel proteins in solution. The technique used represents rheology on a much smaller scale than conventional rheological methods allow, consequently requiring much smaller volumes for experiments. The work carried out in this chapter provides an increase in the development of this technique and has demonstrated the importance of the careful preparation of cantilevers before measurements using AFM cantilevers as probes.

In chapter 6, pH-responsive switchable surfaces were created using the proteins BCys and L2FC7. These surfaces were then examined using the complementary optical and mechanical techniques of DPI and QCM-D. The surfaces functionalised with a monolayer of BCys were found to become thinner and denser and more rigid at low pH, and became thicker and less rigid

at high pH. A model for the behaviour of the layer was postulated where at low pH as the proteins are unassociated, the layer is partially collapsed due to the hydrophobic association of amino acid residues within each protein. As the pH is increased coiled-coil structure begin to assemble resulting in the creation of a more ordered and thicker layer. At the same time the amino-terminal random coil section will become more extended as it increases in charge, becoming less rigid and more hydrated.

The hydrogel protein L2FC7 was also immobilised as a monolayer onto surfaces and exposed to challenge with different pH solutions. At acidic pH monolayers were thinner, denser and stiffer than at neutral or alkaline pH values. It was concluded that this was due to the increased association of leucine zipper sections of the proteins to form coiled-coil structures, in turn the result of a lower proportion of glutamic acid residues carrying charge and hence less destabilising repulsion between the helices. In addition, as pH increased the polyelectrolyte spacer sections of each protein will carry greater proportion of negative charges, which would be expected to result in an elongation and subsequent increase in hydration as the molecule becomes extended. This is also consistent with observations of the mechanical extension of single hydrogel proteins as detailed in chapter 3, and related to the swelling of hydrogels formed from these proteins (Petka 1997).

The optical and mechanical techniques of DPI and QCM-D were employed in a complimentary manner in this chapter, which allowed comparison between them. This allowed comparisons between parameters such as thickness and density as generated by DPI with changes in rigidity and mass of the layer as assessed by QCM-D. Together these measurements made the interpretation of the behaviour of the protein monolayers more straightforward than from one technique alone. For example, simple models already exist to allow the interpretation of frequency and dissipation change data obtained by QCM-D into parameters such as viscosity and density as well as more accurate data for changes in the mass of viscoelastic materials (Voinova *et al.* 1999; Höök *et al.* 2001; Höök *et al.* 2002; Voinova *et al.* 2002); however they were not sufficient

to allow interpretation of the data gathered in this work in such terms. With the development of more sophisticated models it may be possible to combine Δf and D values along with parameters of thickness obtained from optical techniques such as DPI or elipsometry to gain this further quantitative information.

Finally in chapter 7, a series of preliminary measurements were described using a coiled-coil-forming system of a more complex architecture than those previously examined. A series of control measurements demonstrated that specific interactions were being examined of an assembly of three proteins forming a two-stranded coiled-coil. Although only a small range of retract rates was examined, values for off rates and f_β were consistent with those obtained previously between homodimers of ACys.

In summary, this thesis describes a range of approaches utilized in the examination of a series of proteins containing the coiled-coil motif as the primary functional domain. Starting at the single molecule level and scaling up to the mesoscale, the behaviour of hydrogel-forming proteins has been assessed, particularly with respect to the interactions of the coiled-coil-forming domains. Studies have concentrated on the change of physical characteristics of these proteins and their assemblies as pH has been altered. We have thus been able to connect behaviour of these proteins at the molecular scale to bulk properties of solutions and materials formed from them. With the increasing use of the coiled-coil motif as a cross-linking domain in the use of biomaterials it is increasingly important to be able to connect the behaviour of such materials to the behaviour of the coiled-coil motif at the molecular scale, to gain further insight into the mechanistics behind their behaviour. It will be interesting in the future to see the development of techniques in conjunction with each other in a complimentary manner to solve these problems, both for this motif and also for more complex protein structural motifs which may also be utilised in the creation of biomaterials.

Chapter 9 References

Advincula, R., Zhou Q. G., Park M., Wang S. G., Mays J., Sakellariou G., Pispas S. and Hadjichristidis N. (2002). "Polymer brushes by living surface initiated polymerization on flat silicon (SiOx) and gold surfaces: homopolymers and block copolymers." Langmuir **18**(22): 8672-8684.

Ahmed, N., Nino D. F. and Moy V. T. (2001). "Measurement of solution viscosity by atomic force microscopy." Review of Scientific Instruments **72**(6): 2731-2734.

Akey, D. L., Malashkevich V. N. and Kim P. S. (2001). "Buried polar residues in coiled-coil interfaces." Biochemistry **40**: 6352-6360.

Allegra, G. and Ganazzoli F. (1997). "Polymer dynamics in solution." Faraday Transactions **93**(14): 2341-2353.

Allen, S., Chen X., Davies J., Davies M. D., Dawkes A. C., Edwards J. C., Roberts C. J., Sefton J., Tendler S. J. B. and Williams P. M. (1997). "Detection of antigen-antibody binding events with the atomic force microscope." Biochemistry **36**: 7457-7463.

Allison, D. P., Hinterdorfer P. and Han W. (2002). "Biomolecular force measurements and the atomic force microscope." Current Opinion in Biotechnology **13**: 47-51.

Anselmetti, D., Fritz J., Smith B. and Fernandez-Busquets X. (2000). "Single molecule DNA biophysics with atomic force microscopy." Single Mol. **1**: 53-58.

Baller, M. K., Lang H. P., Fritz J., Gerber C., Gimzewski J. K., Drechsler U., Rothuizen H., Despont M., Vettiger P., Battiston F. M., Ramsteyer J. P., Fornaro P., Meyer E. and Guntherodt H.-J. (2000). "A cantilever array based artificial nose." Ultramicroscopy **82**: 1-9.

Bell, G. I. (1978). "Models for the specific adhesion of cells to cells." Science **200**: 618-627.

Bergaud, C. and Nicu L. (2000). "Viscosity measurements based on experimental investigations of composite cantilever beam eigenfrequencies in viscous media." Review of Scientific Instruments **71**(6): 2487-2491.

Binnig, G., Quate C. F. and Gerber C. (1986). "Atomic force microscope." Physical Review Letters **56**(9): 930-933.

Boskovic, S., Chon J. M. W., Mulvaney and Sader J. E. (2002). "Rheological measurements using microcantilevers." Journal of Rheology **46**(4): 891-899.

Bosshard, H. R., Durr E., Hitz T. and Jelesarov I. (2001). "Energetics of coiled-coil folding: the nature of the transition states." Biochemistry **40**: 3544-3552.

Bouchiat, C., Wang M. D., Allemand J.-F., Strick T., Block S. M. and Croquette V. (1999). "Estimating the persitence length of a worm-like chain molecule from force-extension measurements." Biophysical Journal **76**: 409-413.

Branden, C. T. and Tooze J. (1991). Introduction to Protein Structure, Garland Publishing Inc.

Bravo, A., Serrano-Herass G. and Salas M. (2001). "A single amino acid substitution within a coiled-coil motif changes the assembly of a 53-amino acif protein from two-dimensional sheets to filamentous structures." Journal of Biological Chemistry **276**(24): 21250-21256.

Burkhard, P., Kammerer R. A., Steinmetz M. O., Bourenkov G. P. and Aebi U. (2000). "The coiled-coil trigger site of the rod domain of cortexillin I unveils a distinct network of interhelical and intrahelical salt-bridges." Structure **223**: 8.

Burkhard, P., Stretefeld J. and Strelkov S. V. (2001). "Coiled-coils: a highly versatile protein folding motif." Trends in Cell Biology **11**(2): 82-88.

Burnham, N. A. and Colton R. J. (1989). "Measuring the nanomechanical properties and surface forces of materials using an atomic force microscope." Journal of Vacuum Science Technology **7**(4): 2906-2913.

Bustamante, C., Marko J. F., Siggia E. D. and Smith S. (1994). "Entropic elasticity of lambd-phage DNA." Science **265**: 1599-1600.

Bustamante, C., Smith S. B., Liphardt J. and Smith D. (2000). "Single-molecule studies of DNA mechanics." Current Opinion in Structural Biology **10**: 279-285.

Camesano, T. A. and Wilkinson K. J. (2001). "Single molecule study of xanthan conformation using atomic force microscopy." Biomacromolecules **2**: 1184-1191.

Chao, H. M., Bautista D. L., Litowski J., Irvin R. T. and Hodges R. S. (1998). "Use of a heterodimeric coiled-coil system for biosensor application and affinity purification." Journal of Chromatography B **715**: 307-329.

Chen, G. Y., Warmack R. J., Thundat T., Allison D. P. and Huang A. (1994). "Resonance response of scanning force microscopy cantilevers." Review of Scientific Instruments **65**(8): 2532-2537.

Clarke, J. and Williams P. M. (2005). Unfolding Induced by Mechanical Force. Protein Folding Handbook. Part 1. J. Buchner and T. Kiefhaber, Wiley-VCH**:** 1111-1142.

Clausen-Schaumann, H., Seitz M., Krautbauer R. and Gaub H. E. (2000). "Force spectroscopy with single bio-molecules." Current Opinion in Chemical Biology **4**: 524-530.

Cleveland, J. P., Manne S., Bocek D. and Hansma P. K. (1993). "A nondestructive method for determining the spring constant of cantilevers for scanning force microscpy." Review of Scientific Instruments **64**(2): 403-405.

Cohen, C. and Parry D. A. D. (1994). "Alpha-helical coile coils: more facts and better predictions." Science **263**: 488-489.

Crick, F. H. C. (1953). "The packing of alpha-helices: simple coiled-coils." Acta Crystallographa **6**: 689-698.

Cross, G. H., Reeves A., Brands S., Swann M. J., Peel L. L., Freeman N. J. and Lu J. R. (2004). "The metrics of surface adsorbed small molecules on the Young's fringe dual-slab waveguide interferometer." Journal of Physics D: Applied Physics **37**: 74-80.

Cross, G. H., Reeves A. A., Brand S., Poppelwell J. F., Peel L. L., Swann M. J. and Freeman N. J. (2003). "A new quantitative optical biosensor for protein characterisation." Biosensors and bioelectronics **19**: 383-390.

Cross, G. H. and Ren Y. (1999). "Young's fringes from vertically integrated slab waveguides: applications to humidity sensing." Journal of Applied Physics **86**(11): 6483-6488.

Danilowicz, C. B., Coljee V., Bouzig C., Conroy R. S., Lubensky D., Sarkar A., Nelson D. R. and Prentiss M. (2003). "Single Molecule DNA Unzipping Under Constant Force Using Magnetic Tweezers." Biophysical Journal **84**(2): 301A.

Davis, T. M. and Wilson W. D. (2000). "Determination of the refractive index increments of small molecules for correction of surface plasmon resonance data." Analytical Biochemistry **284**: 348-353.

DeGrado, W. F., Summa C. M., Pavone V., Nastri F. and Lombardi A. (1999). "De novo design of structural proteins and metalloproteins." Annual Review of Biochemistry **68**: 779-819.

Dragan, A. I. and Privalov P. L. (2002). "Unfolding of a lecuine zipper is not a simple two-state transition." Journal of Molecular Biology **321**: 891-908.

Dunn, M. J. (1987). "Electrophoresis in polyacrylamide gels." ACS Symposium Series **335**: 20-32.

Efimov, A. V. (1999). "Complemetary packing of alpha-helices in proteins." FEBS Letters **463**: 3-6.

Evans, E. (1998). "Energy landscapes of biomolecular adhesion and receptor anchoring at interfaces explored with dynamic force spectroscopy." Faraday Discussions **111**: 1-16.

Evans, E. (2001). "Probing the relation between force-lifetime-and chemistry in single molecular bonds." Annual Review of Biophysics and Biomolecular Structure **30**: 105-128.

Evans, E., Leung A., Hammer D. and Simon S. (2001). "Chemically distinct transition states govern rapid dissociation of single L-selectin bonds under force." Proceedings of the National Academy of Sciences USA **98**: 3784-3789.

Evans, E. and Ritchie K. (1997). "Dynamic strength of molecular adhesion bonds." Biophysical Journal **72**: 1541-1555.

Friedsam, C., Wehle A. K., Kuhner F. and Gaub H. E. (2003). "Dynamic single-molecule force spectroscopy: bond rupure analysis with variable spacer length." Journal of Physics: Condensed Matter **15**: S1709-S1723.

Gibson, C. T., Watson G. S. and Myra S. (1996). "Determination of the spring constants of probes for force microscopy/spectroscopy." Nanotechnology **7**: 259-62.

Glover, J. N. M. and Harrison S. C. (1995). "Crystal structure of the heterodimeric bZIP transscription factor C-Fos-C-Jun bound to DNA." Nature **373**: 257-261.

Gosse, C. and Croquette V. (2002). "Magnetic Tweezers: Micromanipulation and Force Measurement at the Molecular Level." Biophysical Journal **82**(6): 3314-3329.

Guhr, K. I. (2000). Controlling the responsive behaviour of genetically enginered block copolymerhydrogels through molecular architecture, University of Massachusetts Amherst.

Harbury, P. B., Zhang T., Kim P. S. and Alber T. (1993). "A switch between two-, three-, and four stranded coiled-coils in GCN4 leucine zipper mutants." Science **262**: 1401-1407.

Hegner, M., Wagner P. and Semenza G. (1993). "Ultralarge atomically flat template-stripped Au surfaces for scanning probe microscopy." Surface Science **291**: 39-46.

Heine, D. and Wu D. T. (2001). "A switchable polymer layer: chain folding in end-charged polymer brushes." Journal of Chemical Physics **114**(12): 5313-5321.

Hodges, R. S. (1996). "De novo design of alpha-helical proteins: basic research to medical applications." Biochemical Cell Biology **74**: 133-154.

Höök, F., Kasemo B., Nylander T., Fant C., Sott K. and Elwing H. (2001). "Variations in coupled water, viscoelastic properties, and film thickness of a Mefp-1 protein film during adsorption and cross-linking: a quartz crystal microbalance with dissipation monitoring, ellipsometry, and

surface plasmon resonance study." Analytical Chemistry **73**: 5796-5804.

Höök, F., Voros J., Rodahl M., Kurrat R., Boni P., Ramsden J. J., Textor M., Spencer N. D., Tengvall P., Gold J. and Kasemo B. (2002). "A comparitive study of protein adsorption on titanium oxide surfaces using in situ elipsometry, optical waveguide lightmode spectroscopy, and quartz crystal microbalance / dissipation." Colloids and Surfaces B: Biointerfaces **24**: 155-170.

Hu, J. C. (2000). "A guided tour in protein interaction space: coiled-coils from the yeast proteome." Proceedings of the National Academy of Sciences USA **97**(24): 12935-12936.

Hutter, L. and Bechhoefer J. (1993). "Calibration of atomic force microscope tips." Review of Scientific Instruments **64**(7): 1868-1873.

Ibarra-Molero, B., Zitzewitz J. A. and Matthews C. R. (2004). "Salt bridges can stabilize but do not accelerate the folding of the homodimeric coiled-coil peptide GCN4-p1." Journal of Molecular Biology **336**: 989-996.

Ibbarra-Molero, B., Makhatadze G. I. and Matthews C. R. (2001). "Mapping the energy surface for the folding reaction of the coiled-coil peptide GCN4-p1." Biochemistry **40**: 719-731.

Ikai, A., Idiris A., Sekiguchi H., Arakawa H. and Nishida S. (2002). "Intra- and intermolecular mechanics of proteins and polypeptides studied by AFM: with applications." Applied Surface Science **188**: 506-512.

Ishikawa, E., Imagawa M., Hashida S., Yoshitake S., Hamaguchi Y. and Ueno T. (1983). "Enzyme-labelling of antibodies and their fragments for enzyme immunoassay and immunohistochemical staining." Journal of Immunoassay **4**(3): 209-327.

Julthongpiput, D., Lin Y. H., Teng J., Zubarev E. R. and Tsukruk V. V. (2003). "Y-shaped amphiphilic brushes with switchable micellar surface structures." Journal of the American Chemical Society **125**(51): 15912-15921.

Julthongpiput, D., Lin Y. H., Teng J., Zubarev E. R. and Tsukruk V. V. (2003). "Y-shaped polymer brushes: nanoscale switchable surfaces." Langmuir **19**(19): 7832-7836.

Kammerer, R. A., Schultess T., Andwehr R., Lusitg A., Engel J., Aebi U. and Steinmetz M. O. (1998). "An autonomous folding unit mediates the assembly of two-stranded coiled-coils." Proceedings of the National Academy of Sciences USA **95**: 13419-13424.

Kapoor, M., Thomas C. J., Bachhawat-Sikder K., Sharma S. and Surolia A. (2003). "Exploring kinetics and mechanism of potein-sugar recognition by surface plasmon resonance." Methods in Enzymology **362**: 312-329.

Kavourides, N. (2003). Single molecule investigations of coiled-coil proteins. School of Pharmacy, University of Nottingham.

Kobayashi, J., Kikuchi A., Sakai K. and Okano T. (2001). "Aqueous chromatography utilizing pH-/temperature responsive polymer stationary phases to seperate ionic bioactive compounds." Analytical Chemistry **73**(9): 2027-2033.

Kohn, W. D., Kay C. M. and Hodges R. S. (1997). "Salt effects on protein stability: two-stranded alpha-helical coiled-coils containing inter- or intrahelical ion pairs." Journal of Molecular Biology **267**: 1039-1052.

Kramers, H. A. (1940). "Brownian motion in a field of force and the diffusion model fo chemical reactions." Physica (Utrecht) **7**(4): 284-304.

Kreplat, L., Doucet J. and Briki F. (2001). "Unraveling double stranded alpha-helical coiled-coils: an X-ray diffraction study on hard keratin fibers." Biopolymers **58**: 526-533.

Krylov, D., Barchi J. and Vinson C. (1998). "Inter-helical interactions in the leucine zipper coiled-coil dimer: pH and salt dependence of coupling energy between charged amino acids." Journal of Molecular Biology **279**: 959-972.

Lee, N. and Vilgis T. A. (2002). "Single-protein force spectroscopy: sequence dependence." Europhysics Letters **57**(6): 817-823.

Lee, N.-K., Johner A. and Vilgis T. A. (2002a). "Single chain stretching of block copolymers under different solvent conditions." Macromolecules **35**: 6043-6054.

Lee, N.-K. and Vilgis T. A. (2002b). "Single chain force spectroscopy - reading the sequence of HP protein models." The European Physical Journal B **28**: 451-465.

Lee, W. F. and Shieh C. H. (1999). "pH-thermoreversible hydrogels. II. Synthesis and swelling behaiours of N-isopropylcrylamide-co-acylic acid-co-sodium acrylate hydrogels." Journal of Applied Polymer Science **73**(10): 1955-1967.

Levy, R. and Maaloum M. (2002). "Measuring the spring constant of atomic force microscope cantilevers: thermal fluctuations and other methods." Nanotechnology **13**: 33-37.

Li, H. and Witten T. A. (1995). "Fluctuations and persistence length of charged flexible polymers." Macromolecules **28**(17): 5921-5927.

Lu, S. M. and Hodges R. S. (2004). "Defining the minimum size of a hydrophobic cluster in two-stranded alpha-helical coiled-coils: effects on protein stability." Protein Science **13**: 714-726.

Lupas, A. (1996). "Coiled-coils: new structures and new functions." Trends in Biochemical Sciences **21**: 375-382.

Luzinov, I., Minko S. and Tsukruk V. V. (2004). "Adaptive and responsive surfaces through controlled reorganization of interfacial polymer layers." Progress in Polymer Science **29**(7): 635-698.

MacArthur, I. (1943). "Structure of alpha keratin." Nature **152**: 38.

Makarov, D. E. and Wang Z. (2002). "On the interpretation of force extension curves of single protein molecules." Journal of Chemical Physics **116**(17): 7760-7765.

Markland, P., Zhang Y. H., Amidon G. L. and Yang V. C. (1999). "A pH and ionic strength responsive polypeptide hydrogel: synthesis, characterisation, and preliminary protein release studies." Journal of Biomedical Materials Research **47**(4): 595-602.

Marti, D. N., Jelesarov I. and H.R. B. (2000). "Interhelical ion pairing in coiled-coils: solution structure of a heterodimeric leucine zipper and determination of pKa values of glu side-chains." Biochemistry **39**: 12804-12818.

McClain, D. L., Woods H. L. and M.G. O. (2001). "Design and characterisation of a heterodimeric coiled-coil that forms exclusivewly with an antiparallel relative helix orientation." Journal of the American Chemical Society **123**: 3151-3152.

McGrath, K. P., Fournier M. J., Mason T. L. and Tirrell D. A. (1992). "Genetically directed syntheses of new polymeric materials - expression of artificial genes encoding proteins with repeating (alagly)3proglugyl elements." Journal of the American Chemical Society **114**(2): 727-733.

McGrath, K. P. and Kaplan D. L. (1993). Material Research Society Symposium Proceedings **292**(83).

Merkel, R., Nassoy P., Leung A., Ritchie K. and Evans E. (1999). "Energy landscapes of receptor ligand bonds explored with dynamic force spectroscopy." Nature **397**: 50-53.

Moll, J. R., Ruvinov S. B., Pastan I. and Vinson C. (2001). "Designed heterodimerizing lecine zippers with a range of PIs and stabilities up to 10^{-15} M." Protein Science **10**: 649-655.

Moreau, V. H., da Silva A. C., Siloto R. M. P., Valente A. P., Leite A. and Almeida F. V. L. (2004). "The bZIP region of the plant transcription factor opaque-2 forms stable homodimers in solution and retains its helical structure upon subunit dissociation." Biochemistry **43**: 4862-4868.

Moulin, A. M., O'Shea S. J., Badly R. A., Doyle P. and Welland M. E. (1999). "Measuring surface induced conformational changes in proteins." Langmuir **15**: 8776-8779.

Naik, R. R., Kirkpatrick S. M. and Stone M. O. (2001). "The thermostability of an alpha-helical coiled-coil protein and its potential use in sensor applications." Biosensors and Bioelectronics **16**: 1051-1057.

Nguyen-Duong, M., Koch K. W. and Merkel R. (2003). "Surface Anchoring Reduces the Lifetime of Single Specific Bonds." Europhysics Letters **61**(6): 845-851.

Oakley, M. G. and Hollenbeck J. J. (2001). "The design of antiparallel coiled-coils." Current Opinion in Structural Biology **11**: 450-457.

Ogden, P. I., Chen G. Y., Steele R. A., Warwick R. J. and Thundat T. (1996). "Viscous drag measurements using micro-fabricated cantilevers." Applied Physics Letters **68**(26): 3814-3816.

Ortiz, C. and Hadziioannou G. (1999). "Entropic elasticity of single polymer chains of poly(methacrylic acid) measured by atomic force microscopy." Macromolecules **32**: 780-787.

O'Shea, E. K., Rutkowski R., Kim P. S. and Alber T. (1991). "X-ray Structure of the GCN4 Leucine Zipper, A Two-Stranded, Parallel Coiled-coil." Science **254**: 539-544.

Pagel, K., Seeger K., Seiwert B., Villa A., Mark A. E., Berger S. and Koksch B. (2005). "Advanced approaches for the characterization of a de novo designed antiparallel coiled-coil." Organic and Biomolecular Chemistry **3**: 1189-1194.

Petka, W. A. (1997). Reversible Gelation of Genetically Engineered Macromolecules. Amherst, University of Massachusetts.

Petka, W. A., Harden J. L., McGrath K. P., Wirtz D. A. and Tirrell D. A. (1998). "Reversible hydrogels from self-assembling artificial proteins." Science **281**: 389-391.

Q-Sense (2005).

Rief, M., Gautel M., Oesterhelt F., Fernandez J. M. and Gaub H. E. (1997). "Reversible unfolding of individual titin immunoglobulin domains by AFM." Science **276**: 1109-1113.

Rief, M. and Grubmuller H. (2002). "Force spectroscopy of single biomolecules." ChemPhysChem **3**: 255-261.

Rief, M., Pascual J., Saraste M. and Gaub H. E. (1999). "Single molecule force spectroscopy of spectrin repeats: low unfolding force in helix bundles." Journal of Molecular Biology **286**: 553-561.

Rivetti, C., Walker C. and Bustamante C. (1998). "Polymer chain statistics and conformational analysis of DNA molecules with bends or sections of different flexibility." 1998 **280**: 41-59.

Rodahl, M., Höök F., Fredriksson C., Keller C. A., Krozer A., Brzezinski P., Voinova M. V. and Kasemo B. (1997). "Simultaneous frequency and

dissipation factor QCM measurements of biomolecular adsorption and cell adhesion." Faraday Discussions **107**: 229-246.

Rodahl, M. and Kasemo B. (1996). "On the measurement of thin liquid overlayers with the quartz crystal miccrobalance." Sensor and Actuators A **54**: 448-456.

Ryadnov, M. G., Ceyhan B., Niemeyer C. M. and Woolfson D. N. (2003). ""Belt and braces": a peptide-based linker system of de novo design." Journal of the American Chemical Society **125**(31): 9388-9394.

Ryadnov, M. G. and Woolfson D. N. (2003). "Engineering the morphology of a self-assembling protein fibre." Nature Materials **2**: 329-322.

Sader, J. E. (1995). "Parallel beam approximation for v-shaped atomic force microscopy cantilevers." Review of Scientific Instruments **66**(9): 4583-4586.

Sader, J. E. (1998). "Frequency response of cantilever beams immersed in viscous fluids with applications to the atomic force microscope." Journal of Applied Physics **84**(1): 64-76.

Sader, J. E. (2002). "Surface stress induced deflections of cantilever plates with applications to the atomic force microscope: V-shaped plates." Journal of Applied Physics **91**(11): 9354-9361.

Sader, J. E., Chon J. W. N. and Mulvaney P. (1999). "Calibration of rectangular atomic force microscopy cantilevers." Review of Scientific Instruments **70**(10): 3967-3969.

Sader, J. E., Larson I., Mulvaney P. and White L. R. (1995). "Method for the calibration of atomic force microscopy cantilevers." Review of Scientific Instruments **66**(7): 3789-3798.

Sauerbray, G. Z. (1959). Physics **155**: 206-222.

Simpson, D. A., Strigle M., Hohenadl M. and Merkel R. (1999). "Statistical breakage of single protein A-IgG bonds reveals crossover from spontaneous to force-induced dissociation." Physical Review Letters **83**(3): 652-655.

Skolnick, J., Kolinski A. and Mohanty D. (1999). "De novo predictions of the quaternary structure of leucine zippers and other coiled-coils." International Journal of Quantum Chemistry **75**: 165-176.

Stevens, M. M. (2001). Atomic force microscopy studies of biomolecular adhesion and mechanics. School of Pharmacy, University of Nottingham.

Stevens, M. M., Allen S., Davies M. C., Roberts C. J., Schacht E., Tendler S. J. B., VanSteenkiste S. and Williams P. M. (2002). "The development, characterisation, and demonstration of a versatile immobilization strategy for biomolecular force measurements." Langmuir **18**: 6659-6665.

Stevens, M. M., Allen S., Sakata J. K., Davies M. C., Roberts C. J., Tendler S. J. B., Tirrell D. A. and Williams P. M. (2004). "pH-dependent behaviour of surface-immobilised artificial leucine zipper proteins." Langmuir **20**: 7747-7752.

Stevens, M. M., Flynn N. T., Wang C., Tirrell D. A. and Langer R. (2004). "Coiled-coil peptide based assembly of gold nanoparticles." Advanced Materials **16**(11): 915-918.

Stryer, L. (1988). Biochemistry, W. H. Freeman and Co.

Subramanian, A., Oden P. I., Kennel S. J., Jacobson K. B., Warmack R. J., Thundat T. and Doktycz M. J. (2002). "Glucose biosensing using an enzyme-coated microcantilever." Applied Physics Letters **81**(2): 385-387.

Sumerlin, B. S., Lowe A. B., D.B. T. and McCormick C. L. (2003). "Aqueous properties of pH-responsive AN diblock acrylamido copolymers synthesized via aqueous RAFT." Macromolecules **36**(16): 5982-5987.

Suzuki, K., Yamada T. and Tanaka T. (1999). "Role of the buried glutamate in the alpha-helical coiled-coil domain of the macrophage scavenger receptor." Biochemistry **38**: 1751-1756.

Tang, A., Wang C., Stewart R. J. and Kopecek J. (2001). "The coiled-coils in the design of protein-based constructs: hybrid hydrogels and epitope displays." Journal of Controlled Release **72**(1-3): 57-70.

Trepat, X., Grabulosa M., Buscemi L., Rico F., Fabry B., Freberg J. J. and Farre R. (2003). "Oscillatory Magnetic Tweezers Based on Ferromagnetic Beads and Simple Coaxial Coils." Review of Scientific Instruments **74**(9): 4012-4020.

Tskhovrebova, L., Trinick J., Sleep J. A. and Simmons R. M. (1997). "Elasticity and unfolding of single molecules of the giant muscle protein titin." Nature **387**: 308-313.

Tsuda, Y., Kikuchi A., Yamato M., Sakurai Y., Umezu M. and Okano T. (2004). "Control of cell adhesion and detachment using temperature and thermoresponsive copolymer grafted culture surfaces." Journal of Biomedical Materials Research Part A **69A**(1): 70-78.

Voinova, M. V., Jonson M. and Kasemo B. (2002). "'Missing mass' effect in biosensor's QCM applications." Biosensors and bioelectronics **17**: 835-841.

Voinova, M. V., Rodahl M., Jonson M. and Kasemo B. (1999). "Viscoelasticacoustic response of layered polymer films at fluid solid interaces: continuum mechanics approach." Physica Scripta **59**: 391-396.

Walsh, S. T. R., Cheng H., Bryson J. W., Roder H. and DeGrado W. F. (1999). "Solution structure and dynamics of a de novo designed three-helix bundle protein." Proceedings of the National Academy of Sciences USA **96**: 5486-5491.

Wang, C., Kopecek J. and Stewart R. J. (2001). "Hybrid hydrogels cross-linked by genetically engineered coiled-coil block proteins." Biomacromolecules **2**: 912-920.

Williams, P. M. (2003). "Analytical descriptions of dynamic force spectroscopy: behaviour of multiple connections." Analytica Chimica Acta **479**: 107-115.

Woolfson, D. N. and Alber T. (1995). "Predicting Oligomerization states of coiled-coils." Protein Science **4**: 1596-1607.

Xu, Q., Zou S., Zhang W. and Zhang X. (2001). "Single molecule force spectroscopy on carrageenan by means of AFM." Macromol.Rapid.Commun. **22**: 1163-1167.

Yadav, M. K., Redman J. E., Leman L. J., Alvarez-Gutierrez J. M., Zhang Y., Stout C. D. and Ghadiri M. R. (2005). "Structure based engineering of internal cavities in coiled-coil peptides." Biochemistry **44**: 9723-9732.

Yang, Y., Schulz D. and Steiner C. A. (1999). "Physical gelation of hydrophobically modified polyelectrolytes. 1. homogeneous gelation of alkylated poly[acrylamide-co-sodium acrylate]." Langmuir **15**: 4335-4343.

Yu, Y., Monera O. D., Hodges R. S. and Privalov P. L. (1996). "Ion pairs significantly stabilize coiled-coils in the abscence of electrolyte." Journal of Molecular Biology **255**: 367-372.

Yu, Y. B. (2002). "Coiled-coils: stability, specificity, and drug delivery potential." Advance Drug Delivery Reviews **54**: 1113-1129.

Zhang, H. A. and Ito Y. (2001). "pH control of transport through a porous membrane self-assembled with a poly(acrylic acid) loop brush." Langmuir **17**(26): 8336-8340.

Zhang, W. and Zhang X. (2003). "Single molecule mechanochemistry of macromolecules." Progress in Polymer Science **28**: 1271-1295.

Zhou, H.-X. (2001). "Loops in proteins can be modelled as worm-like chains." Journal of Physical Chemistry B **105**: 6763-6766.

Zhou, M., Bently D. and Ghosh I. (2004). "Helical supramolecules and fibers utilizing leucine zipper-displaying dedrimers." Journal of the American Chemical Society **126**: 734-735.

Acknowledgements

I would like to begin by thanking all of the academics within LBSA for their support and advice. I would particularly like to thank Stephanie Allen for her advice and encouragement and for having the patience to proofread this thesis; Phil Williams for much-needed advice on interpreting data from force experiments; and Clive Roberts for his advice on the work included in chapters 5 and 6.

In addition I would also like to thank Dr Jill Sakata and Prof. David Tirrell (CALTECH) for the kind donation of the hydrogel proteins used in chapters 3 to 6. I would also like to thank Dr Dek Woolfson (University of Sussex) for letting me use the 'belt and braces' proteins examined in chapter 7. I would also like to thank Kathryn Chapman, Marcus Swann and Farfield Sensors Ltd. (Salford, United Kingdom) for the use of their instrument for the DPI measurements included in chapter 6 and for very useful help and advice to accompany it. I would like to thank the EPSRC for funding my work.

I would also like to thank my friends in the LBSA, in no particular order: Trev, Liz, Perkins, Gibbo, James B, Sarah, Chris A and everyone else for making the dark days a little brighter and the pub a little blurrier.

Finally, and most of all, I would like to thank Mum, Luke, Matt, Rachel, Alex and Ellie.

Publications

"Method to Determine the Spring Constant of Atomic Force Microcantilevers" C.T. Gibson, D.J. Johnson, C.J. Anderson, C. Abell, T. Rayment; Review of Scientific Instruments 2004; 75 (2)

"The pH-dependent Behaviour of a Surface-immobilised Responsive Protein Hydrogel." D.J. Johnson, P.M. Williams, C.J. Roberts, S.J.B. Tendler, M.C. Davies, S. Allen. *In Preparation*

"Detection of the pH-responsive Behaviour of a Coiled-coil Protein Hydrogel Using an AFM Microcantilever Detector" D.J. Johnson, P.M. Williams, C.J. Roberts, S.J.B. Tendler, M.C. Davies, S. Allen. *In Preparation*

Conference Presentations

Protein Dynamics and Function Meeting, University of Leicester, January 2005. Poster presentation: "pH-dependent Behaviour of a Surface-immobilised Responsive Protein Hydrogel".

5th International Conference on Biological Physics, Chalmers University of Technology, Gothenburg, August 2004. Oral presentation: "Molecular Investigations of pH-responsive Hydrogel Proteins".

UKSPM, University of Nottingham, March 2003. Poster presentation: "Detection of the pH-responsive Behaviour of Artificial Coiled-coil Proteins".